Mechanically Active Heterogeneous Polymer Matrix Composites

by

Meng Wang

A Dissertation Presented in Partial Fulfillment
of the Requirements for the Degree
Doctor of Philosophy

Approved October 2019 by the
Graduate Supervisory Committee

Matthew Green, Chair
Alexander Green
Jeffery Yarger

ARIZONA STATE UNIVERSITY

December 2019

ABSTRACT

An evolving understanding of elastomeric polymer nanocomposites continues to expand commercial, defense, and industrial products and applications. This work explores the thermomechanical properties of elastomeric nanocomposites prepared from bisphenol A diglycidyl ether (BADGE) and three amine-terminated poly(propylene oxides) (Jeffamines). The Jeffamines investigated include difunctional crosslinkers with molecular weights of 2,000 and 4,000 g/mol and a trifunctional crosslinker with a molecular weight of 3,000 g/mol. Additionally, carbon nanotubes (CNTs) were added, up to 1.25 wt%, to each thermoset. The findings indicate that the Tg and storage modulus of the polymer nanocomposites can be controlled independently within narrow concentration windows, and that effects observed following CNT incorporation are dependent on the crosslinker molecular weight.

Polymer matrix composites (PMCs) offer design solutions to produce smart sensing, conductive, or high performance composites for a number of critical applications. Nanoparticle additives, in particular, carbon nanotubes and metallic quantum dots, have been investigated for their ability to improve the conductivity, thermal stability, and mechanical strength of traditional composites. Herein we report the use of quantum dots (QDs) and fluorescently labeled carbon nanotubes (CNTs) to modify the thermomechanical properties of PMCs. Additionally, we find that pronounced changes in fluorescence emerge following plastic deformation, indicating that in these polymeric materials the transduction of mechanical force into the fluorescence occurs in response to mechanical activation.

Segmented ionenes are a class of thermoplastic elastomers that contain a permanent charged group within the polymer backbone and a spacer segment with a low glass transition temperature (Tg) to provide flexibility. Ionenes are of interest because of their synthetic versatility, unique morphologies, and ionic nature. Using phase changing ionene-based nanocomposites could be extended to create reversible mechanically, electrically, optically, and/or thermally responsive materials depending on constituent nanoparticles and polymers. This talk will discuss recent efforts to utilize the synthetic versatility of ionenes (e.g., spacer composition of PTMO or PEG) to prepare percolated ionic domains in microphase separated polymers that display a range of thermomechanical properties. Furthermore, by synthesizing two series of ionene copolymers with either PEG or PTMO spacers at various ratios with 1,12-dibromododecane will yield a range of ion contents (hard contents) and will impact nanoparticle dispersion.

ACKNOWLEDGMENTS

I would like to thank my advisor, Prof. Matthew D. Green, for his guidance, encouragement, and support over the course of my graduate career. I am grateful to work under his supervision; he taught me polymer science, to be a good researcher, presenter, and a teacher. I would also like to thank my committee members for their participation and support. I would like to express my special thanks to Prof. Alex Green and Prof. Jeff Yarger for their helpful discussions and constant guidance. I would also like to thank Prof. Chad Borges for his helpful guidance and helping me with comprehensive exam. I would like to thank Prof. Sefaattin Tongay for his guidance and close research collaboration during the 2D polymer program. I would like to thank Lori Doemland for teaching me technical writing skills and teaching skills. I would also like to thank Albert Thompson, Fred Pena, Thomas Groy, David Lowery, and Emmanuel Soignard. The staffs at Arizona State have been a great resource. I would especially like to acknowledge Diana Convey and Manuel Roldan for their help with AFM and TEM imaging. Samrat Amin and Brian Cherry have also been very helpful with NMR spectroscopy.

I also would like to thank our collaborators in ARO project including Dr. Reza Montazami and Olivia bogle from Iowa State University, Dr. Lisa Hall and Nicholas Liesen from Ohio State University. I would like to thank collaborations with Prof. Qinghua Wang, Matt Gilliam and Yuqi Guo from Arizona State University.

I would like to thank all my group members, previous and present, for their advice, encouragement, discussions, time, and support including Jack Felmly, Dr. Yi Yang,

Bradly Grim, Mani Korah, Varun Kelkar, Srishti Gupta, Micheal Tran, Kristen Brown, Tyler Piper, Katelyn Kline, Usamma Amjad, Amodini Pathak, Ermias Dheressa, Kari Trimple, Alexis Hocken and Alexandra Schwindt.

I acknowledge the help and assistantship from my friends Dr. Duo Ma, Dr. Fan Hong, Xu Zhou, Dr. Shuoxing Jiang, Yifei Xu, Dr. Kedi Wu, Dr. Bohan Shan, Dr. Yuxia Shen, Dr. Sijie Yang and Ying Qin for their time, and support. I would like to express my special thanks to Prof. Steven Craig from Duke University, Prof. Henry Hess from Columbia University, Prof. Qiuhong Zhang from Nanjing University, Prof. Ying Yang from University of Nevada, Prof. Jiyuan(Jane) Yang from Utah Univeristy and Prof. Justin Kennemur from Florida State University, Dr.Yuqiong Dai, Dr. Qiong Wu, Dr. Guoyan Zhang and Siyang Wang for their advice, encouragement, discussions, time about my post grad school development.

Finally, I am forever grateful to my family: Xiaoxu Yang, for their continued love and support in my life endeavors. I am deeply thankful to my parents, they are always my role model, great mentors. Words cannot express my love for them. With all my heart I would like to make them proud and thank them for all their support throughout the years. I cannot ever forget my parents' sacrifices to provide me encouragement and motivation to pursue my goals. I would be nothing without them on the journey of life. Finally, I would like to thank my undergrad advisor Prof. Gaoquan Shi, he is my role model, a great mentor and a true scientist.

TABLE OF CONTENTS

CHAPTER Page

CHAPTER Page

CHAPTER Page

CHAPTER Page

Chapter 1. Introduction

1.1. Dissertation Overview

In the first half of the dissertation, the effect of the use of quantum dots (QDs) and fluorescent dye-labeled carbon nanotubes (CNTs) to modify the thermomechanical and stimuli-responsive properties of Polymer matrix composites was studied.

Following this chapter, the effect of crosslinker length and architecture on the thermomechanical properties of CNT-loaded elastomeric polymer matrix composites was reviewed. This chapter explores the thermomechanical properties of elastomeric nanocomposites prepared from bisphenol A diglycidyl ether and three amine-terminated poly(propylene oxides) (Jeffamines). The Jeffamines investigated include difunctional crosslinkers with molecular weights of 2000 and 4000 g mol^{-1} and a trifunctional crosslinker with a molecular weight of 3000 g mol^{-1}. Additionally, carbon nanotubes (CNTs) are added, up to 1.25 wt%, to each thermoset. This investigation was mainly on studying the impact of crosslinker length and architecture as well as CNT addition on the molecular weight between crosslink points in the glassy and rubbery states.

The third chapter describes the use of quantum dots (QDs) and fluorescent dye-labeled carbon nanotubes (CNTs) to modify the stimuli-responsive properties of Polymer matrix composites. In the beginning, the synthesis of fluorescence dye modified CNTs was described. The thermal set with QDs – mCNTs quenching pair was then introduced. Following the functionalization of CNTs, the fluorescent properties of thermal sets with CNTs, mCNTs, QDs and mCNTs/QDs were studied. The stimuli-

activated fluorescence property was investigated in the last. This investigation was mainly on studying the mechanism of epoxy with mCNTs/QDs quenching pair fluorescent reproducing under mechanical stimuli.

In the second half of the dissertation, the effect of the use of quantum dots (QDs) and fluorescent dye-labeled carbon nanotubes (CNTs) to modify the thermomechanical and stimuli-responsive properties of Polymer matrix composites was studied.

The fourth and fifth chapter illustrates the synthesis and characterization of segmented poly(ethylene glycol)-based ammonium ionenes functionalized with adenine and thymine nucleobases. The synthesis and structure-property relationships of poly(dimethyl siloxane)-based ionene copolymers were also discussed. This talk will discuss recent efforts to utilize the synthetic versatility of ionenes (e.g., spacer composition of PTMO or PEG) to prepare percolated ionic domains in microphase separated polymers that display a range of thermomechanical properties. Furthermore, by synthesizing two series of ionene copolymers with either PEG or PTMO spacers at various ratios with 1,12-dibromododecane will yield a range of ion contents (hard contents) and will impact nanoparticle dispersion.

The sixth chapter summarizes the dissertation's accomplishments and the seventh chapter describes potential future work.

Chapter 2. Effect of Crosslinker Length and Architecture on the Thermomechanical properties of CNT-loaded Elastomeric Polymer Matrix Composites

Meng Wang, Ermias Dheressa, Kristen A. Brown, and and Matthew D. Green*

School of Molecular Science, Arizona Stater University, Tempe, AZ 85281, USA
School for Engineering of Matter, Transport and Energy, Arizona Stater University, Tempe, AZ 85281, USA

*E-mail address: mdgreen8@asu.edu

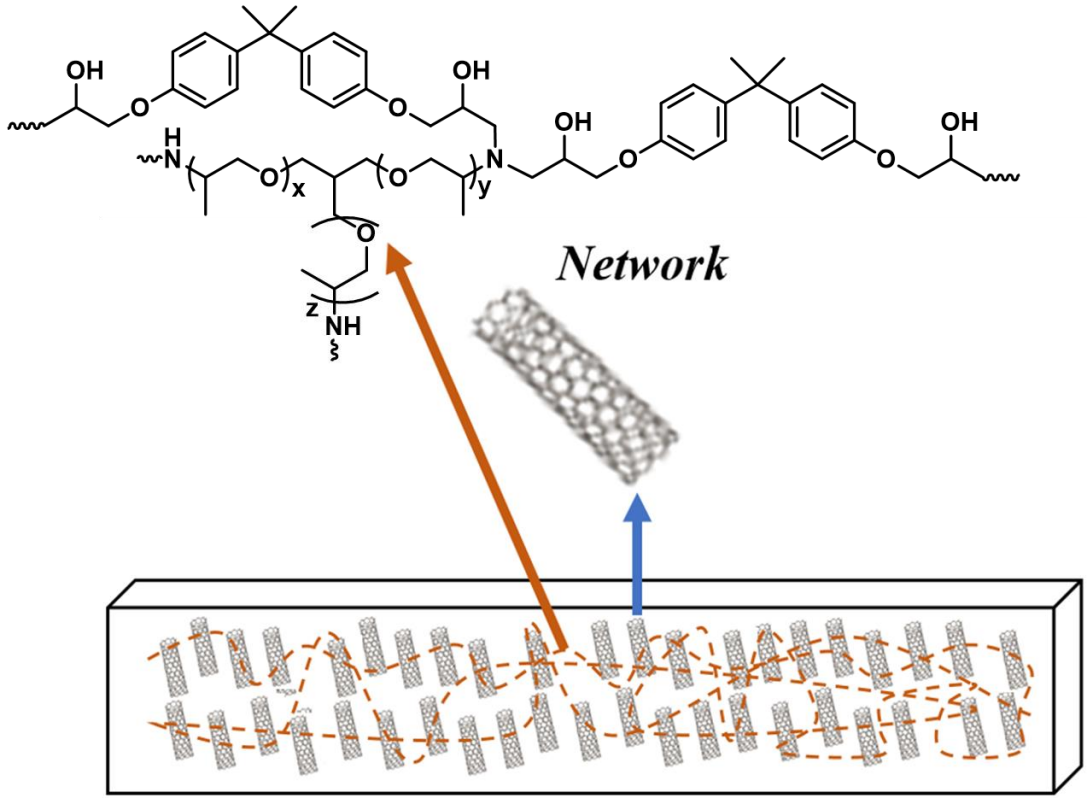

The crosslinker length and architecture as well as carbon nanotube concentration in elastomeric polymer nanocomposites direct the molecular weight between crosslinks, storage modulus, and glass transition temperature. The effect of the nanoparticle addition on the glassy and rubbery state differs; similarly, the impact as a function of crosslinker molecular weight varies.

2.1. Abstract

An evolving understanding of elastomeric polymer nanocomposites continues to expand commercial, defense, and industrial products and applications. This work explores the thermomechanical properties of elastomeric nanocomposites prepared from bisphenol A diglycidyl ether (BADGE) and three amine-terminated poly(propylene oxides) (Jeffamines). The Jeffamines investigated include difunctional crosslinkers with molecular weights of 2,000 and 4,000 g/mol and a trifunctional crosslinker with a molecular weight of 3,000 g/mol. Additionally, carbon nanotubes (CNTs) were added, up to 1.25 wt%, to each thermoset. The findings indicate that the Tg and storage modulus of the polymer nanocomposites can be controlled independently within narrow concentration windows, and that effects observed following CNT incorporation are dependent on the crosslinker molecular weight. Finally, the impact of crosslinker length and architecture as well as CNT addition on the molecular weight between crosslink points in the glassy and rubbery states are discussed.

2.2. Introduction

Polymer networks, both physical and covalent, are utilized in a multitude of consumer and industrial applications, ranging from food packaging to high-performance aerospace materials.[1, 2] Some of the more common examples include fiber-reinforced resins, such as glass fiber or carbon fiber modifiers, which are used in bicycles,

aerospace and automotive components, and building materials.[3-5] In addition to the rigid and structural resins, many of these networks include a low *Tg* soft segment at the application temperature, which imparts elastomeric behavior, including shoe soles, car tires, and many more.[6-8] The addition of nanofillers to these networks imparts secondary functionality, such as tailored thermal and/or electrical conductivity, gas permeability, and mechanical properties.[9] A significant amount of work has been performed to understand how the particles are dispersed in the polymer matrix, how the polymers and nanofillers interact at the interface, and how the nanofillers contribute toward the thermomechanical performance of the composites.[10-14] Importantly, the general class of network (physical vs. covalent) influences how the additives are introduced. For example, additives must be introduced prior to curing for covalent networks, whereas nanoparticles can be added by blending, solution casting, or other physical means in addition to in situ polymerization for physical networks.[7]

The addition of CNTs to epoxy matrices provides additional reinforcement for composite materials. The high surface area of the multi-walled CNTs allows stress applied to the epoxy resin to be transferred to a reinforcement phase within the epoxy matrix. Multi-walled CNTs are often added to improve fracture toughness and strength. There are three mechanisms associated with carbon nanotube loading. These include micromechanical interlocking, chemical bonding between the epoxy matrix and the CNTs, and the presence of van der Waals bonding between the epoxy matrix and the CNTs. For the Multi-walled CNTS used in this research, the third mechanism is most

likely responsible for the recordable changes in storage modulus values[15]. Over the years, polymer composites containing graphene-based materials, specifically carbon nanotubes (CNTs), have received significant attention.[5] This is because of the thermal stability and conductivity, mechanical reinforcement, and added electrical conductivity that CNTs provide. However, the significant inter-CNT attractive forces are difficult to overcome and often these composites suffer from aggregation at any useful nanofiller loading concentration.[16] This becomes particularly true in elastomeric composites, wherein the enthalpic interactions between the soft, flexible polymer segment are incompatible with the aromatic CNT surface. Various approaches to improve the particle-matrix compatibility have been explored, including surface functionalization reactions to match the surface chemistry of the nanoparticles to the matrix (e.g., small molecules or short polymer chains) and covalent attachment of the particle to the polymer matrix.[10, 17-19]

Several pioneers in this area, including Winey and co-workers, have demonstrated that the nanoparticles stiffen their local surroundings, impact chain entanglements and excluded volume effects, and impart unique temperature dependence to polymer mobility and diffusion.[20-24] The above strategies have experienced varying success, and all have the drawback of potentially 1) limiting the nanofiller function (e.g., the added surface groups can alter the intended function of the particle), 2) reducing the mechanical stability of the system (e.g., grafting short polymer chains can dramatically reduce the matrix glass transition temperature (Tg)), or 3) increase the system complexity beyond any practical implementation.In this work, a series of thermoset

networks were synthe-sized from bisphenol A diglycidyl ether (BADGE) and Jeffamines (polyethers terminated with amine end groups) of varying molecular weight and chain architecture. First, the thermomechanical properties of the "neat" networks were ana-lyzed, and then the properties of the composite networks with varying CNT concentrations were studied. The influence of the crosslinker length and architecture on the storage modulus, Tg, and the molecular weight between crosslinks is discussed herein. These data identify design strategies for targeting par-ticular thermomechanical performance in elastomeric polymer matrix composites.

2.3. Experimental Section

2.3.1. Materials

The materials used in this research include Bisphenol A Diglycidyl Ether (BADGE), an epoxy from Sigma-Aldrich. Jeffamines, D-2000, D-4000, and T-3000 were obtained from Huntsman and were used as the macromolecular crosslinkers to produce epoxy resins. The carbon nanotubes used were acid washed multi-walled tubes. To create the epoxy resins, the BADGE and various crosslinkers were combined using the amine hydrogen equilibrium weight, a 1:1 amine to epoxy stoichiometric ratio.

2.3.2. Resin curing procedure

To create the epoxy resins, the BADGE and jeffamines were mixed at a 1:1 amine: epoxy stoichiometric ratio. The D-2000 or T-3000 Jeffamines and BADGE were stirred for 1 hour at room temperature. The samples were then placed in the oven to cure for 4

hours at 80 °C and then for an additional 4 hours at 120 °C. The samples using Jeffamine D4000 and BADGE were stirred for 1 hour at room temperature and then cured for 12 hours at 120 °C. To create the nanocomposites, CNTs were added in quantities of 0, 0.25, 0.5, 0.75, 1 and 1.25 wt% to the different epoxy resins and stirred for 1 hour at room temperature. Then, the mixtures were cured in the oven at 80 °C for 4 hours and then for an additional 4 h at 120 °C.

2.3.3. Differential Scanning Calorimetry (DSC)

Differential Scanning Calorimetry (DSC) was performed using a TA Instruments Differential Scanning Calorimeter. DSC studies the thermal transitions found in polymers, and like DMA, identifies transitional temperatures like the Tg. DSC works by measuring the amount of energy that is either absorbed or released when a polymer is cooled or heated. DSC was used to confirm the Tg results obtained by DMA [1]. DSC was performed on each sample with a heat-cool-heat sequence. The temperature sweep started at room temperature with a ramp rate of 5°C per minute, after isothermal for 60min, the sample was cooled down to -80°C with a ramp rate of 50C per minute. Then the second heating ramp ended at 250°C with a ramp rate of 5°C per minute.

2.3.4. Dynamic Mechanical Analysis (DMA)

The research focused on measuring changes in the thermomechanical properties of different epoxy resins and nanocomposites. Dynamic Mechanical Analysis (DMA) and Differential Scanning Calorimetry (DSC) were performed to quantify the changes in Tg

and the storage moduli of the epoxy resins and nanocomposites. DMA measures the stiffness and viscoelastic behavior of different types of polymers. Dynamic Mechanical Analysis (DMA) is used primarily to characterize materials and was performed using TA Instruments Discovery Hybrid Rheometer. This analysis technique is used to identify transitional temperatures in polymers including the Tg. There is an in-phase component called a storage modulus. The storage modulus is important in measuring the effect of different curing agents as it measures the elastic response of the epoxy. When a load is applied to the polymer, the elastic response is the part of the load is stored in the material to be released following the removal of the applied stress. DMA also identifies a tan delta value which is the ratio the storage modulus and the loss modulus (the out-of-phase component) and measures energy dissipation. The higher the tan delta value, the greater the energy dissipation potential, while lower tan delta values indicate a more elastic material a greater potential to store energy rather than dissipate it [2,3,4]. DMA was performed on each sample. A temperature sweep was performed with the rheometer. The temperature sweep started at a temperature of -70C and ended at a temperature of 150C with a ramp rate of 3C per minute. The oscillation frequrency was 1 Hz.

2.3.5 Scanning Electron Microscopy

Electron Microscopy images were collected using an Amray 1910 field emission scanning electron microscopy (FE-SEM) (Amray INC., Bedford, MA). Samples were sputter-coated with gold prior to imaging.

2.4. Results and Discussion

2.4.1 Effect of Crosslinker Molecular Weight and Architecture on Thermomechanical Properties

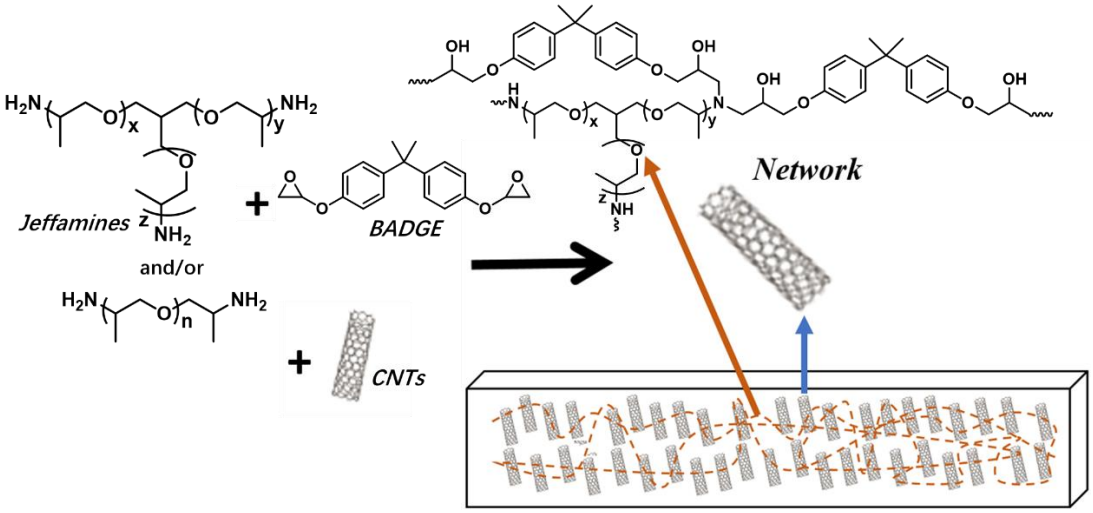

Figure 1. Synthesis of thermoset networks containing BADGE and low Tg amine-terminated polyethers (Jeffamines). Networks without CNTs and with varying concentrations of CNTs were prepared.

The spacing between anchor or crosslink points in a thermoset network dictates the material stiffness and elasticity. The crosslink density was purposely altered by using three different amine crosslinkers: D-2000, T-3000, and D-4000 polyetheramines (Jeffamines). These crosslinkers possess a poly(propylene oxide) backbone, which has a *Tg* well below room temperature. Additionally, the relatively long molecular weights, compared to common crosslinkers, for these molecules will produce an elastomeric network. The nomenclature of the crosslinkers is the following: the numerical value indicates the approximate number-average molecular weight of the crosslinker while

the “D” or “T” indicates a difunctional or trifunctional crosslinker, respectively (i.e., two vs. three primary amine end groups per molecule). Thus, in addition to changing the crosslinker length (D-2000 versus D-4000), the crosslinker architecture was also varied. These precursors were mixed, individually, with BADGE and cured as described in the experimental section (Figure 1).

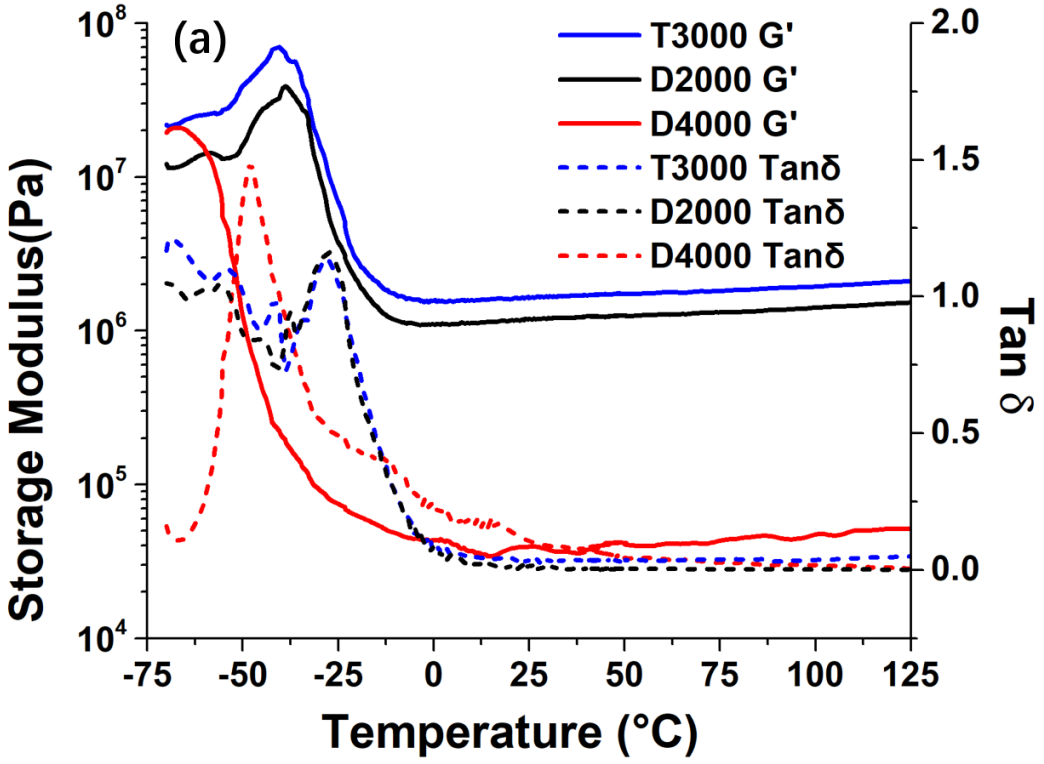

Figure 2. Thermomechanical properties of covalent networks formed between BADGE and Jeffamines of varying molecular weight and architecture without any added nanoparticles. The storage modulus (left axis) and tan delta (right axis) for the neat epoxy resins versus temperature.

The thermomechanical properties were analyzed using DMA, Figure 2, and values for *Tg* were taken from the peak of the tan delta trace. As expected, the D-4000 crosslinker

produces a significantly softer network with a lower *Tg* and lower rubbery plateau modulus. The T-3000 and D-2000 crosslinkers yielded a near-identical value for *Tg*, while the T-3000 network displayed a slightly higher glassy and rubbery plateau modulus. On a local scale the two networks experience approximately the same degree of chain mobility, but the T-3000 network behaved stiffer. Additionally, the D-4000 network displayed an enhanced dampening characteristic compared to both the D-2000 and T-3000 networks (which were very similar), observable by the increased height of the tan delta peak. This correlates to the energy absorbed by the film and was expected for the softer network. The DMA data can be used to calculate a molecular weight between crosslink (Equation 1):

$$G' = \frac{\rho RT}{Mc} \quad (1)$$

where *G'* is the storage modulus, ρ is the density of the thermoset, *R* is the universal gas constant, *T* is the absolute temperature, and *Mc* is the molecular weight between crosslinks. These data, shown in Figure 3, demonstrate how the *Tg* of two networks may be similar but the material still displays a remarkably different toughness and/or stiffness. The *Mc* values for the D-2000 and T-3000 thermosets differ by a factor of 5 despite having the same value for *Tg*.

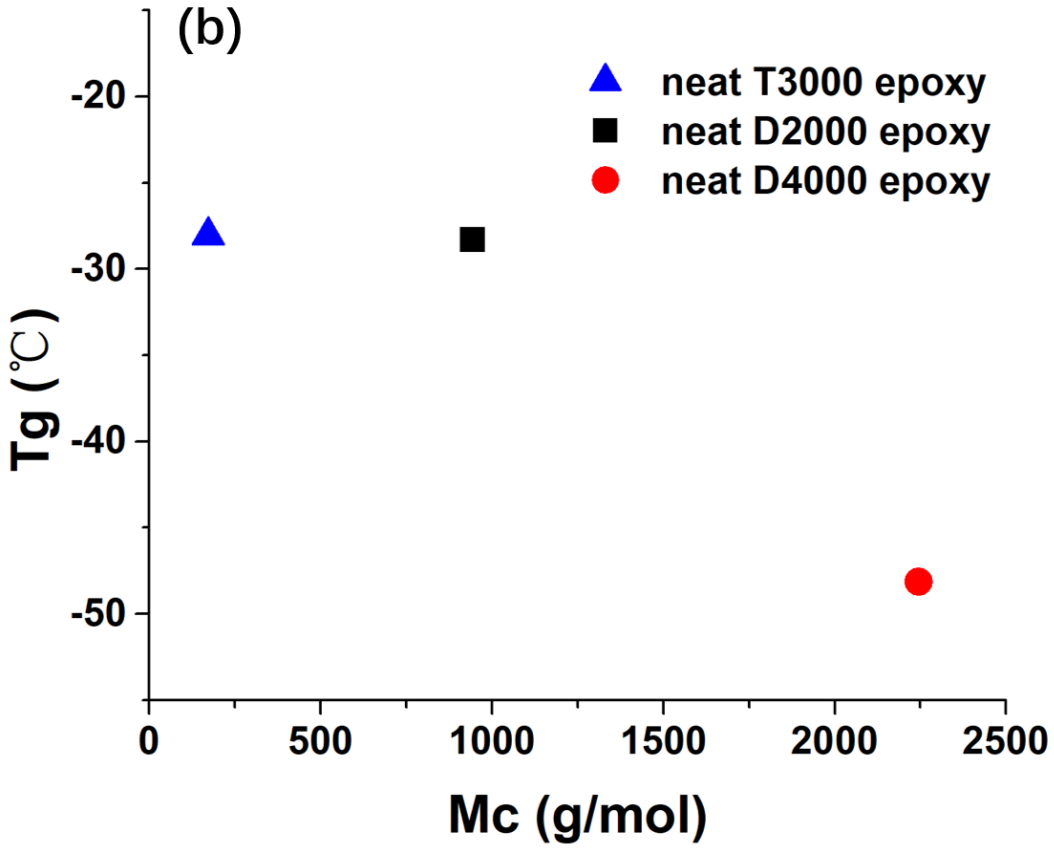

Figure 3. Thermomechanical properties of covalent networks formed between BADGE and Jeffamines of varying molecular weight and architecture without any added nanoparticles. The Tg as determined by the peak in the tan delta trace versus the molecular weight between crosslinks (Mc).

A direct comparison between the networks made from the D-2000 and the T-3000 crosslinkers suggests an equivalent molecular weight between crosslink points (i.e., the molecular weight/(# of functional groups) is equal to 1000 g/mol in both cases). However, a quick sketch of the two networks quickly reveals that the trifunctional nature of the T-3000 crosslinker increases the potential crosslink density by a factor of ~4, which is exactly reported experimentally herein.

2.4.2 Effect of CNTs at varying Concentrations on the Network Thermomechanical Properties

The influence of adding CNTs as a nanofiller on the storage modulus, *Tg*, and *Mc* was studied using DMA and DSC. First, the *Tg*, as determined by the peak in the tan delta trace, was analyzed for each crosslinker across a range of CNT concentrations (Figure 4). Consistently, the *Tg* increased at low CNT concentrations as the CNT concentration was increased. For the thermosets prepared using the T-3000 and the D-2000 crosslinker, a critical CNT concentration was reached after which the Tg began to decrease.

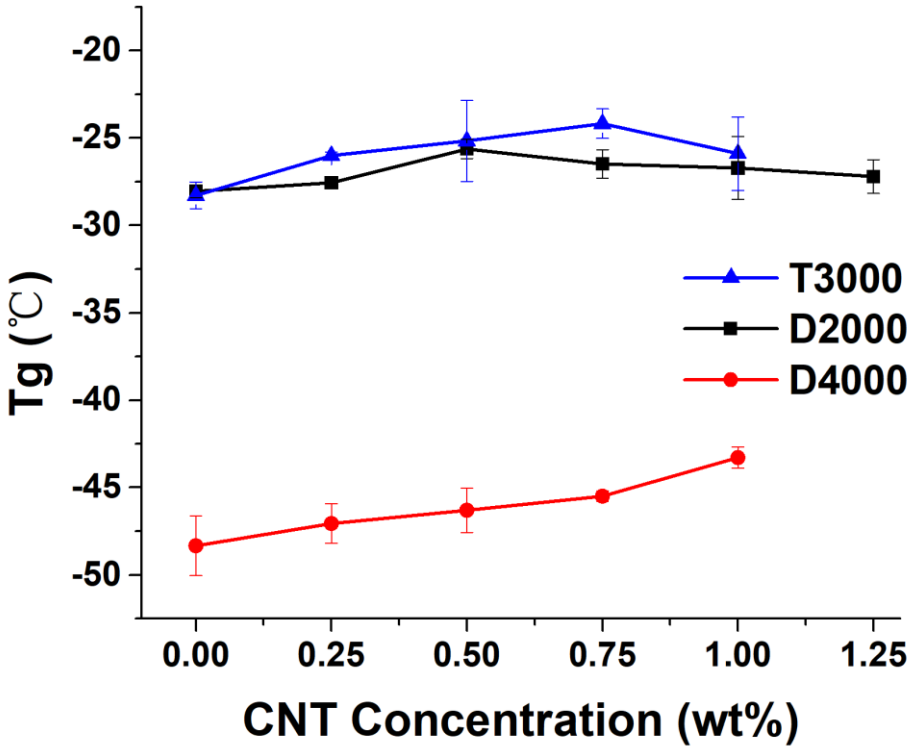

Figure 4. CNT-loaded thermosets *Tg* according to the tan delta trace for thermosets made from T-3000, D-2000, and D-4000 crosslinkers with different CNT

concentrations. The 1.25 CNT wt% sample for the T-3000 and D-4000 crosslinkers are not included because the samples were too brittle or failed to cure.

For the thermosets prepared with the D-4000 crosslinker a turnover was not observed; however, the addition of CNTs beyond 1.0 wt% prevented network formation under the standard curing conditions. Next, the rubbery storage modulus was analyzed at 23 °C (Figure 5, trends in storage modulus at other temperatures were identical). As observed in the trend for Tg as a function of CNT concentration, the storage modulus of the thermosets prepared with the T-3000 and D-2000 crosslinkers increased up to a critical CNT concentration and then decreased. The storage modulus of the thermosets prepared with the D-4000 crosslinker decreased at low CNT concentrations up to a critical concentration of 0.5 wt%; then, the storage modulus increased with further CNT addition.

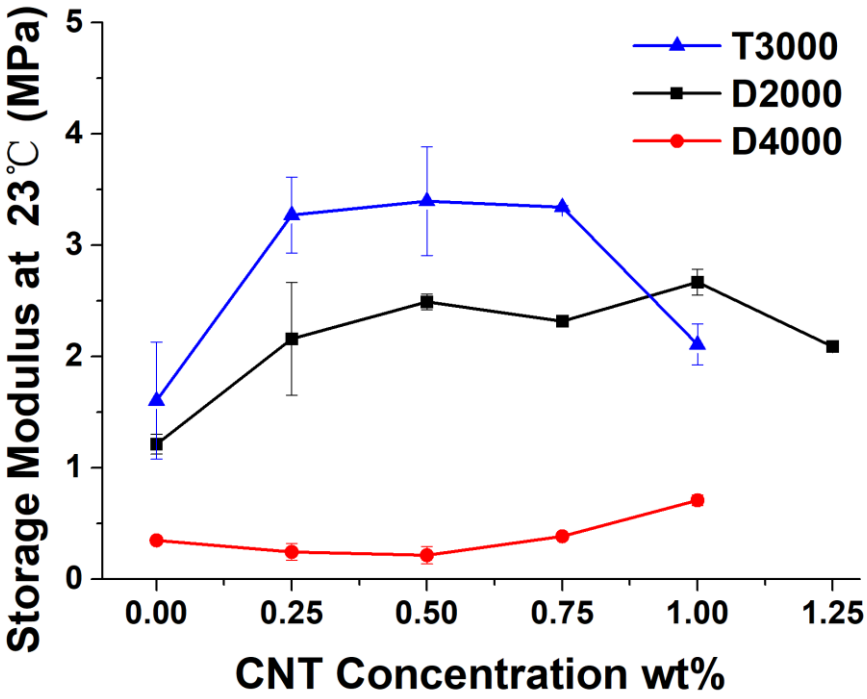

Figure 5. CNT-loaded thermosets storage modulus at 23 °C for thermosets made from T-3000, D-2000, and D-4000 crosslinkers with different CNT concentrations.

Finally, the trends observed in the Tg according to the peak in the tan delta trace were confirmed using DSC (Figure 6). As expected, the Tg determined using DMA was approximately 15 °C higher than the Tg determined using DSC.

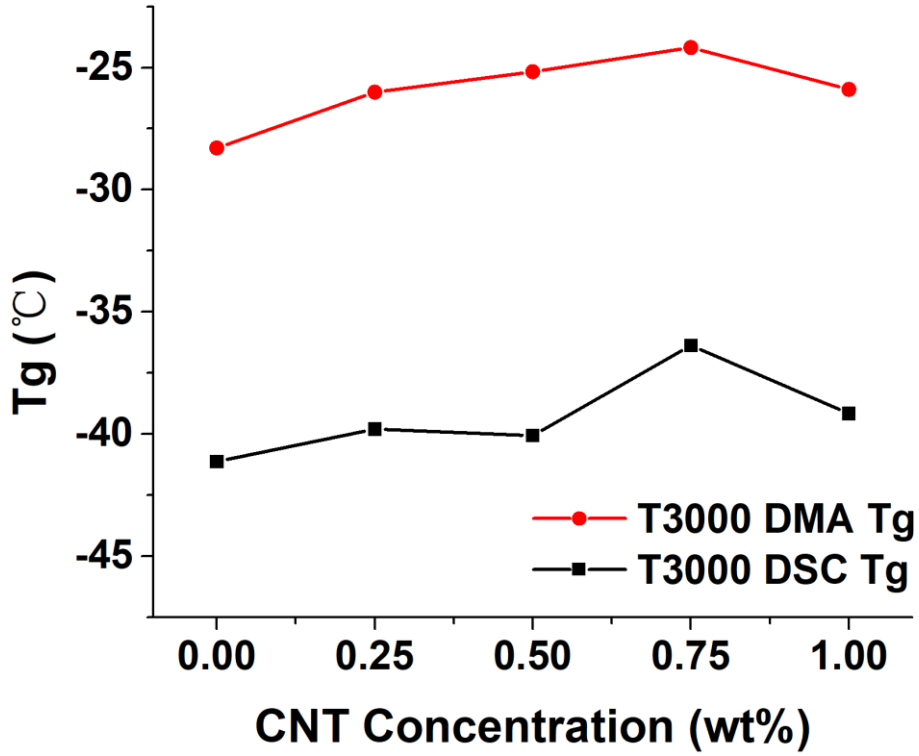

Figure 6. CNT-loaded thermosets *Tg* values determined by DMA and DSC for thermosets made with the T-3000 crosslinker containing different CNT concentrations. Error bars represent the average *Tg* or storage modulus +/- one standard deviation, determined from n>3 replicate networks.

Interestingly, the trends for the thermosets prepared with the T-3000 and the D-2000 crosslinkers show a different turnover point when comparing the tan delta *Tg* and the storage modulus plots. For example, the networks prepared with the T-3000 crosslinker show a maximum *Tg* at a CNT concentration of 0.75 wt%, but a maximum storage modulus at a CNT concentration of 0.5 wt%. Similarly, the D-2000 networks display a maximum *Tg* at 0.5 wt% CNTs but a maximum storage modulus at 1.0 wt% CNTs. This suggests that the addition of the CNTs restricts segmental chain motion to a great

extent, with additional benefits to network stiffness and toughness capable. More specifically, at lower loadings of CNTs, the entropic and excluded volume effects influence *Tg*, while at greater loadings this becomes somewhat saturated. However, further CNT addition continues to increase the interfacial area between the polymer and CNT, thus enhancing storage modulus. Recent simulation efforts from Clarke and co-workers showed a similar effect; namely, that increasing the polymer-nanoparticle interfacial area decreases the polymer diffusivity.[25-27] This finding is important for designing composites, recognizing that the storage modulus can be tailored independently of the *Tg* to some extent. The maximum in these plots is correlated to the percolation threshold, above which inter-CNT attractions overcome dispersive forces that prevent particle aggregation (i.e., continued addition no longer increases the polymer-CNT interfacial area).

The load transfer from the polymer matrix to the nanoparticle will scale with the interfacial polymer-CNT area, as noted above. Thus, in the absence of aggregation, increasing the concentration of the nanoparticle should produce a larger interfacial area and stiffen the nanocomposite. In the case of the D-4000 thermoset, the addition of the CNTs restricted local segmental motion, causing an increase in the Tg. However, at the lowest CNT loadings, the CNTs are too isolated to have an overall positive impact on the network stiffness and ultimately soften the network. At 0.5 wt%, the CNTs have a collective “positive” impact on the network, enhancing the stiffness and increasing the storage modulus.

As an aside, due to the use of acid-modified CNTs, there exists the possibility of

polymer-CNT covalent linkages. This introduces an added level of complexity, despite the fact that the amine-epoxide linkage is heavily favored in comparison to the uncatalyzed amine-carboxylic acid reaction. Evidence in support of the favored amine-epoxide linkage takes on the form of the turnover in the modulus and *Tg* plots and the failed composites above ~1 wt% for the D-4000 thermosets. Additionally, the carboxylic acid groups could produce attractive interactions with the propylene oxide-based jeffamine crosslinker; Clarke and co-workers recently showed, experimentally and computationally, that attractive interactions reduced polymer diffusion in nanocomposites.[28]

2.4.3 Molecular weight between crosslinks

The results above suggested that the effects of the CNT concentration on the *Tg* and the storage modulus were somewhat decoupled from one another. Thus, the molecular weight between crosslinks (*Mc*) was calculated for the varying crosslinker lengths and CNT concentrations (Figure 7, Figure 8). Interestingly, when the *Mc* is calculated using moduli from the glassy plateau (Figure 7) all three crosslinkers show the same, on average, monotonic decrease in *Mc* as the CNT concentration increases. The networks show the same trend in *Mc* as the "neat" thermosets, with *Mc* increasing in the order of T-3000 < D-2000 < D-4000. Since the amine-epoxide reaction is highly favored over the amine-carboxylic acid reaction (i.e., the reaction between the jeffamine and the acid-modified CNT is unlikely), the physical distance between covalent crosslinks for any given crosslinker does not change with added CNTs. Thus, the changes observed

represent an effective change in the distance between crosslinks, which is attributed to physical adhesion of the polymers to the CNTs at the polymer-CNT interface.

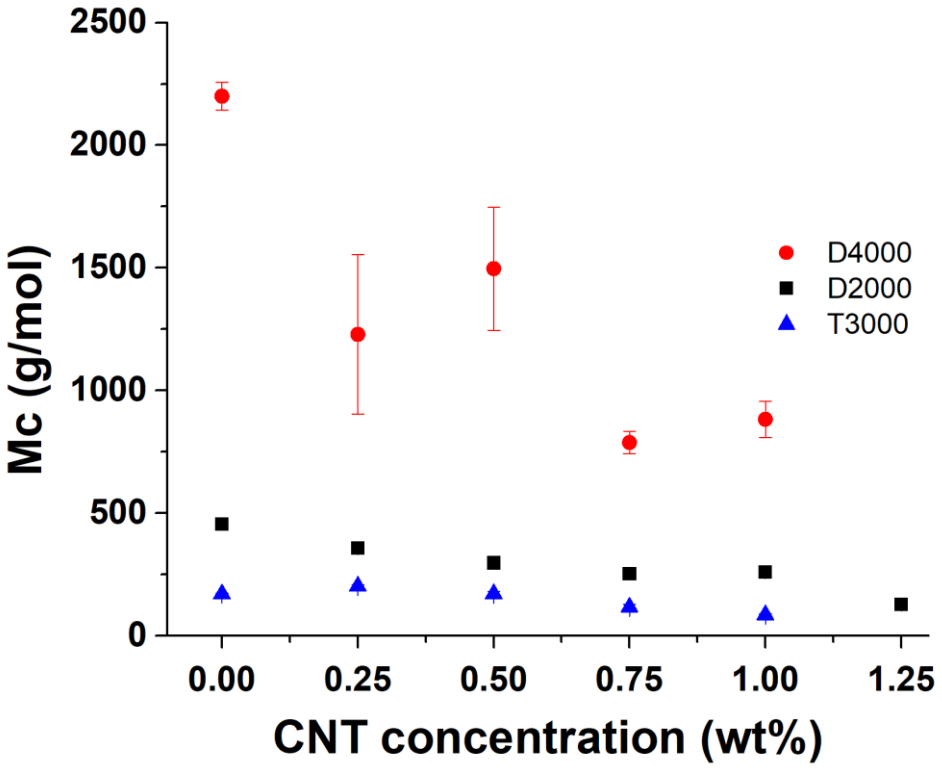

Figure 7. The molecular weight between crosslink points for networks prepared with crosslinkers of varying length and architecture with a range of CNT concentrations. *Mc* values calculated in the glassy plateau (~ -50 °C). Error bars represent the average *Mc* +/- one standard deviation, determined from n>3 replicate networks.

However, when the *Mc* is calculated using storage moduli in the rubbery plateau (Figure 8), maxima and minima are observed. This finding corroborates the trends for *Tg* and storage modulus, which have maxima or minima, and which are more relevant to the behavior of the elastomeric material in the rubbery plateau. As noted above, as the softest network, prepared with the D-4000 crosslinker, softens at low CNT loadings

the *Mc* values increase. Then, above 0.5 wt% CNT, the *Mc* decreases rapidly. For the networks formed with the T-3000 and the D-2000 crosslinkers, the opposite trend is observed: the Mc initially decreases, followed by an increase after passing the percolation threshold discussed above.

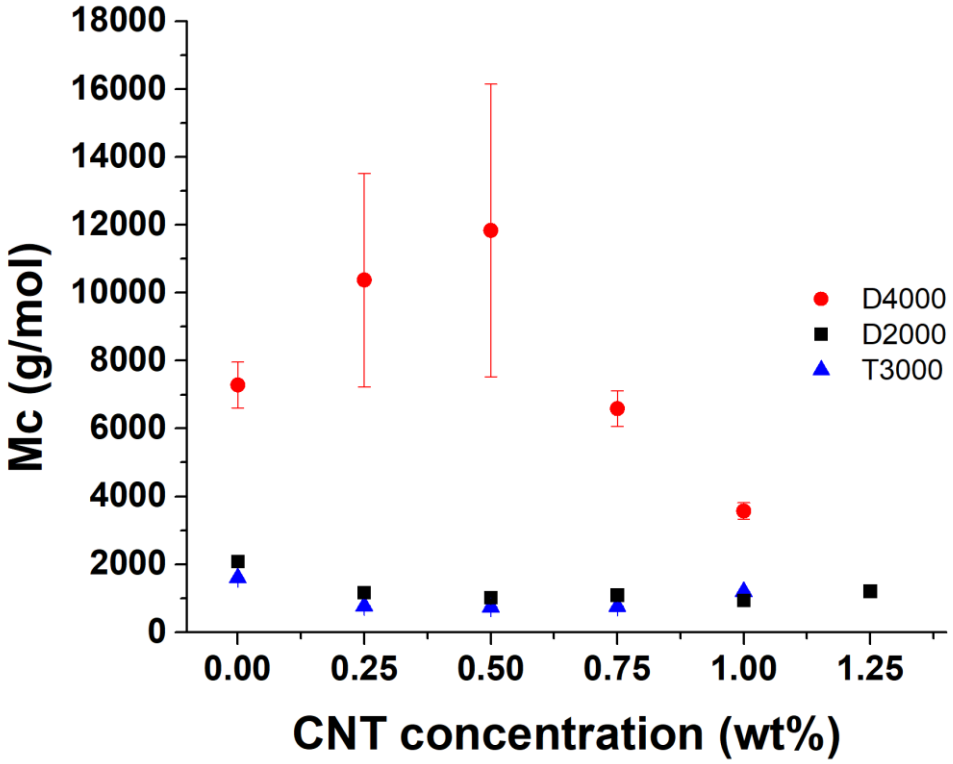

Figure 8. The molecular weight between crosslink points for networks prepared with crosslinkers of varying length and architecture with a range of CNT concentrations. *Mc* values calculated in the rubbery plateau (~23 °C). Error bars represent the average *Mc* +/- one standard deviation, determined from n>3 replicate networks.

2.5. Conclusions

The thermomechanical performance of a series of elastomeric polymer composites was analyzed. The crosslinker length and architecture can be utilized to control the

molecular weight between crosslinks, which will impact the composite stiffness, and to some extent the length of the crosslinker can be used to tune the Tg. The addition of CNTs impacts the Tg, storage modulus, and Mc, and the impact is dictated by the crosslinker length. The practical loading limit is quite low in elastomeric thermosets, ~1 wt%, as further addition interferes with the curing and network formation as well as degrades the mechanical properties above the percolation threshold. In summary, the work herein presents new findings that can be used in the design of elastomeric, multifunctional polymer composites.

Acknowledgments: This work was supported by the Army Research Office (W911NF-16-1-0271) and the Ira A. Fulton Schools of Engineering at Arizona State University.

Keywords: polymer nanocomposite, elastomeric thermoset, carbon nanotube, network

References

1. George, S. C.; Thomas, S., Transport phenomena through polymeric systems. *Prog Polym Sci* 2001, *26* (6), 985-1017.

2. Koerner, H.; Strong, R. J.; Smith, M. L.; Wang, D. H.; Tan, L.-S.; Lee, K. M.; White, T. J.; Vaia, R. A., Polymer design for high temperature shape memory: Low crosslink density polyimides. *Polymer* 2013, *54* (1), 391-402.

3. Etcheverry, M.; Barbosa, S. E., Glass Fiber Reinforced Polypropylene Mechanical Properties Enhancement by Adhesion Improvement. *Materials* 2012, *5* (6), 1084-1113.

4. Liu, W. J.; Mohanty, A. K.; Askeland, P.; Drzal, L. T.; Misra, M., Influence of fiber surface treatment on properties of Indian grass fiber reinforced soy protein based biocomposites. *Polymer* 2004, *45* (22), 7589-7596.

5. Liu, Y.; Kumar, S., Polymer/Carbon Nanotube Nano Composite Fibers-A Review. *Acs Appl Mater Inter* 2014, *6* (9), 6069-6087.

6. Montazami, R.; Spillmann, C. M.; Naciri, J.; Ratna, B. R., Enhanced thermomechanical properties of a nematic liquid crystal elastomer doped with gold nanoparticles. *Sensors and Actuators a-Physical* 2012, *178*, 175-178.

7. Pazat, A.; Barres, C.; Bruno, F.; Janin, C.; Beyou, E., Preparation and Properties of Elastomer Composites Containing "Graphene"-Based Fillers: A Review. *Polym Rev* 2018, *58* (3), 403-443.

8. van Maanen, G. J.; Seeley, S. L.; Capracotta, M. D.; White, S. A.; Bukovnik, R. R.; Hartmann, J.; Martin, J. D.; Spontak, R. J., Property and morphology development in nanocomposite thermoplastic elastomer gels. *Langmuir* 2005, *21* (7), 3106-3115.

9. Moniruzzaman, M.; Winey, K. I., Polymer nanocomposites containing carbon nanotubes. *Macromolecules* 2006, *39* (16), 5194-5205.

10. Balazs, A. C.; Emrick, T.; Russell, T. P., Nanoparticle polymer composites: Where two small worlds meet. *Science* 2006, *314* (5802), 1107-1110.

11. Crosby, A. J.; Lee, J.-Y., Polymer nanocomposites: The "nano" effect on mechanical properties. *Polym Rev* 2007, *47* (2), 217-229.

12. Hall, L. M.; Jayaraman, A.; Schweizer, K. S., Molecular theories of polymer nanocomposites. *Current Opinion in Solid State & Materials Science* 2010, *14* (2), 38-48.

13. Nair, N.; Jayaraman, A., Self-Consistent PRISM Theory-Monte Carlo Simulation Studies of Copolymer Grafted Nanoparticles in a Homopolymer Matrix. *Macromolecules* 2010, *43* (19), 8251-8263.

14. Ganesan, V.; Jayaraman, A., Theory and simulation studies of effective interactions, phase behavior and morphology in polymer nanocomposites. *Soft Matter* 2014, *10* (1), 13-38.

15. Domun, N.; Hadavinia, H.; Zhang, T.; Sainsbury, T.; Liaghat, G. H.; Vahid, S., Improving the fracture toughness and the strength of epoxy using nanomaterials - a review of the current status. *Nanoscale* 2015, *7* (23), 10294-10329.

16. Ma, P.-C.; Siddiqui, N. A.; Marom, G.; Kim, J.-K., Dispersion and functionalization of carbon nanotubes for polymer-based nanocomposites: A review. *Compos Part a-Appl S* 2010, *41* (10), 1345-1367.

17. Thompson, R. B.; Ginzburg, V. V.; Matsen, M. W.; Balazs, A. C., Block copolymer-directed assembly of nanoparticles: Forming mesoscopically ordered hybrid

materials. *Macromolecules* 2002, *35* (3), 1060-1071.

18. Lin, Y.; Boker, A.; He, J. B.; Sill, K.; Xiang, H. Q.; Abetz, C.; Li, X. F.; Wang, J.; Emrick, T.; Long, S.; Wang, Q.; Balazs, A.; Russell, T. P., Self-directed self-assembly of nanoparticle/copolymer mixtures. *Nature* 2005, *434* (7029), 55-59.

19. Rasin, B.; Chao, H.; Jiang, G.; Wang, D.; Riggleman, R. A.; Composto, R. J., Dispersion and alignment of nanorods in cylindrical block copolymer thin films. *Soft Matter* 2016, *12* (7), 2177-2185.

20. Lin, C.-C.; Cargnello, M.; Murray, C. B.; Clarke, N.; Winey, K. I.; Riggleman, R. A.; Composto, R. J., Nanorod Mobility Influences Polymer Diffusion in Polymer Nanocomposites. *Acs Macro Lett* 2017, *6* (8), 869-874.

21. Tung, W.-S.; Griffin, P. T.; Meth, J. S.; Clarke, N.; Composto, R. J.; Winey, K. I., Temperature-Dependent Suppression of Polymer Diffusion in Polymer Nanocomposites. *Acs Macro Lett* 2016, *5* (6), 735-739.

22. Meth, J. S.; Gam, S.; Choi, J.; Lin, C.-C.; Composto, R. J.; Winey, K. I., Excluded Volume Model for the Reduction of Polymer Diffusion into Nanocomposites. *J Phys Chem B* 2013, *117* (49), 15675-15683.

23. Lin, C.-C.; Gam, S.; Meth, J. S.; Clarke, N.; Winey, K. I.; Composto, R. J., Do Attractive Polymer-Nanoparticle Interactions Retard Polymer Diffusion in Nanocomposites? *Macromolecules* 2013, *46* (11), 4502-4509.

24. Karatrantos, A.; Clarke, N.; Composto, R. J.; Winey, K. I., Entanglements in polymer nanocomposites containing spherical nanoparticles. *Soft Matter* 2016, *12* (9), 2567-2574.

25. Choi, J.; Hore, M. J. A.; Meth, J. S.; Clarke, N.; Winey, K. I.; Composto, R. J., Universal Scaling of Polymer Diffusion in Nanocomposites. *Acs Macro Lett* 2013, *2* (6), 485-490.

26. Hore, M. J. A.; Composto, R. J., Functional Polymer Nanocomposites Enhanced by Nanorods. *Macromolecules* 2014, *47* (3), 875-887.

27. Karatrantos, A.; Composto, R. J.; Winey, K. I.; Clarke, N., Polymer and spherical nanoparticle diffusion in nanocomposites. *J Chem Phys* 2017, *146* (20).

28. Tung, W.-S.; Clarke, N.; Composto, R. J.; Winey, K. I., Temperature Dependence of Polymer Diffusion in MWCNT/PS Nanocomposites. *Macromolecules* 2013, *46* (6), 2317-2322.

Chapter 3. Fluorescence−Mechanoresponse Activity for Carbon nanotubes Polymer Matrix Composites

Meng Wang and Matthew D. Green*

School of Molecular Science, Arizona Stater University, Tempe, AZ 85281, USA

School for Engineering of Matter, Transport and Energy, Arizona Stater University, Tempe, AZ 85281, USA

*E-mail address: mdgreen8@asu.edu

3.1 Abstract:

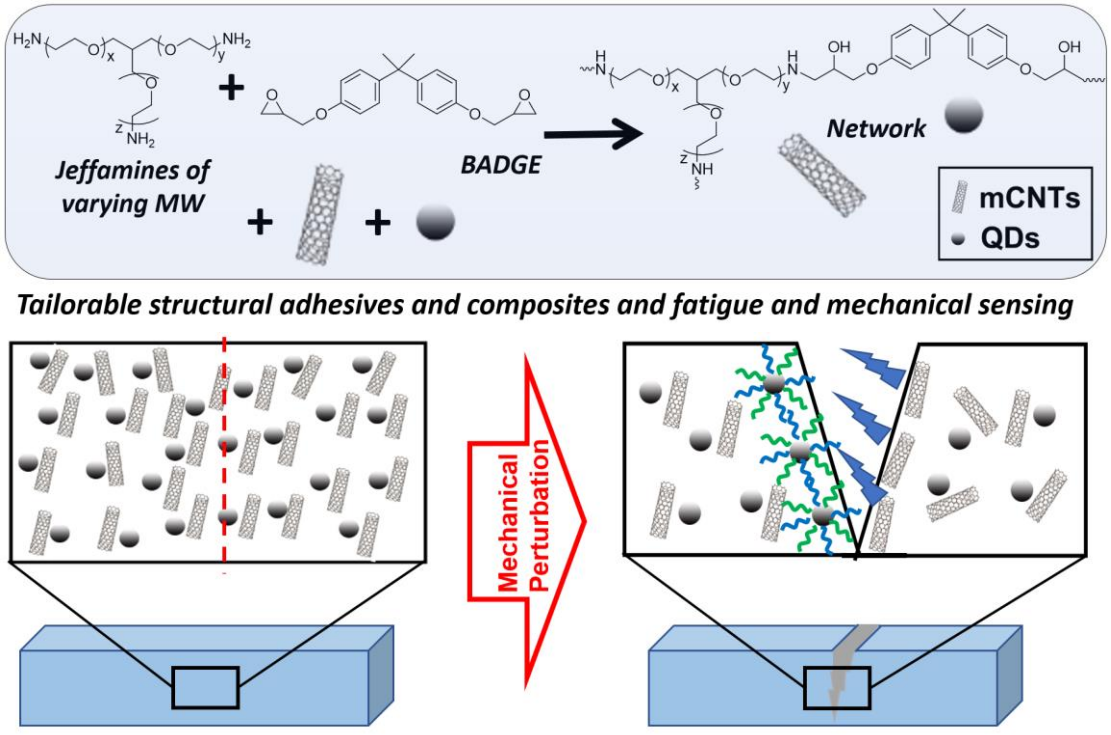

Polymer matrix composites (PMCs) offer design solutions to produce composites with tunable optical, conductive, topological, and thermomechanical properties. Because of

their ubiquitous nature, methodologies to diagnose failure or structural changes in the nanocomposites are of significant interest. Herein, we report the use of quantum dots (QDs) and fluorescent dye-labeled carbon nanotubes (CNTs) to modify the thermomechanical properties of PMCs. Pronounced changes in fluorescence emerged in the bulk following strain or at the site of physical cutting. Specifically, the transduction of mechanical force into fluorescence occurred at a strain as low as 7.5% in these elastomeric composites. This force activation of fluorescence can serve as a general strategy for the development of new PMC building blocks that impart polymeric materials with desirable functionalities ranging from damage sensing to enhancements in mechanical strength.

3.2 Introduction:

Polymer matrix composites are used in industries such as aerospace, automotive, building materials, and more. The general premise is that additives (big and small) introduce strength and functionality to the composite structure. Recent decades have explored the use of micron-scale additives (e.g., carbon fiber-reinforced composites with remarkable tensile strength), and more recently nanoscale additives. Carbon nanotubes (CNTs) were first reported by Iijima and coworkers in 1991[1] and the very first CNT polymer nanocomposite was then created by Ajayan and coworkers.[2] CNTs show a combination of various outstanding properties, and therefore could be used as substitutes or complements to the conventional nanofillers(like glassy fiber, carbon fiber and nanopartilcles) in the fabrication of multipurpose polymer nanocomposites.

In 2018, our lab reported their study of polymer composites, introduced the effect of crosslinker Length and architecture properties of CNTs containing elastomeric polymer matrix thermal mechanical properties. The crosslinker length and architecture can be utilized to control the molecular weight between crosslinks(Mc), which will impact the composite stiff-ness, and to some extent the length of the crosslinker can be used to tune the Tg. The addition of CNTs impacts the Tg, storage modulus, and Mc, and the impact is dictated by the crosslinker length. [3]. Previously, Tang and coworkers confirmed that grafting silane molecules onto the surface of CNTs significantly improved the dispersion of CNTs in an diglycidyl ether of bisphenol A/m-phenylenediamine epoxy resin, which improved the mechanical performance because the propagating cracks in the epoxy/CNT matrix bypassed the CNTs resulting in long, tortuous paths with improved CNT dispersion[4]. Kim and coworkers reported in 2013 that CNT bridges restrained crack formation, then crack propagation through the matrix resulted in CNTs breaking at the weakest points, ensuring pullout of CNTs and leaving a cavity on the other side of crack surface[5]. The pull-out mechanism is known as the most significant contribution to the mechanical properties of nano-filler enhanced epoxy matrix composites[6].

Easy and early detection of emergent (microscopic) damage in fiber-reinforced composites materials caused by the impact of objects or other mechanical loading is highly desirable: Bond and coworkers introduced the ‘bleeding’ mechanism, wherein an UV fluorescent dye leaks from fractured hollow fibers into damage sites to indicated the failure of the composite structure.[7] Burn’s lab created a model system to study the

failure mechanism of polymeric materials by placing the fluorescent protein at the interface of glass fibers and an epoxy resin. By tracking the force-induced yellow light fluorescence caused by the unfolding of the protein, researchers are able to report micron-scale damage, such as fiber fractures and fiber-matrix debonding.[8] Liu's lab investigated boron nitride additives in epoxy networks, which showed with good thermal conductivity. By tracking the thermal accumulation within the system with an infrared thermal imager, the failure of composites was located. [9] Sevostianov reported that the resistance of graphene-reinforced epoxy networks increased linearly with elongation and followed an apparent higher-order polynomial relationship with stress.[10]

Since the first phenolic resin founded in 1907, circumstances like fiber failures and composites fatigue have been studied for over one century when people facing the concept of "mechanical action of polymer". The response of polymer to mechanical stress may cause simple conformational changes to bond-bending or even bond-stretching deformations. In 1930s, the polymer pioneer Staudinger observed the mechanical degradation of polymers, later on research reported by newcomers in the following decades indicating that, by adding mechano-responding block to the polymer backbone as indicators, different strategies have been used for making sense of polymer backbone responding to mechanical stress by fluorescence change[11, 12], monitoring radical generation[13, 14], biasing reaction pathway[15],pH changing[16], color change[17], acid generation[18], small molecular generation[19] and cation generation[20].

These discoveries and efforts have created a branch of materials science and engineering called mechanoresponsive luminescent (MRL) materials. The MRL

properties are typically based on the formation of nanoscale aggregates of dyes in the polymeric matrix, in those cases stimuli caused the irreversibly or reversibly deformation of the material, and thus leading to a change of the material's optical properties.[21] This type of property could also be achieved by creating physical blends of the dye and the host polymer. Weder reported a color change upon plastic deformation within linear low-density polyethylene (LLDPE) films containing small amounts of cyano- oligo(p-phenylene vinylene)[22] It is remarkable that photophysical properties of chromophore-containing polymers could also be changed through breaking covalent bonds by mechanical force.[23] Sottos et al. first reported a mechano-active polymer in which spiropyran groups were covalently introduced to polymer chains as "mechanophore".[17] Upon tensile force, the spiro-pyran containing mechanophore undergoes a reversible ring opening reaction and, as a result, the polymer turned a reddish color. Craig's group also published work about mechano-actived fluorescence properties of polymers, in this case the spiropyran group was covalently modified to polymer backbone.[24]

Among all those strategies used above, one common point is they all required the synthesis of a novel polymer with a mechano-responsive functional group, which will increase the cost and difficulty of the polymer synthesis. Merkoci and coworkers demonstrated that CNTs could be used to quench the fluorescence of quantum dots (QDs)[25]. Doorn and co-workers introduced that SWCNTs conjugated with a redox-active dye (covalently linked to a specific bio-receptor) to cause fluorescence quenching. Furthermore, the fluorescence could be recovered via further interaction

between the bio-receptor ligand on the conjugates and target analytes: [26]. Also, Jo designed a pH sensor with CNTs quenching efficiency, by combining the CNTs with a fluorescent molecule with a synthesized pH-sensitive poly-sulfonamide linker. In this system the fluorescence of the whole system was controlled by expanded coil structure and a collapsed globule structure of poly-sulfonamide arm in the middle: at low pH condition, poly-sulfonamide arm collapsed, the fluorescence of pyrene group was brought towards CNTs with the fluorescent quenching phenomenon[27]. Aggregation-induced emission (AIE) is a photophysical phenomenon associated with chromophore aggregation coined by Prof. Tang's group in 2001.[28] In the aggregation-induced emission process, non-emissive luminogens are induced to emit by the aggregate formation.

Thus, by measuring the displacement of CNTs within the polymer matrix the mechanical stimuli of polymer matrix composite could be monitored at the macroscopic level: the fluorescence of the whole system was controlled by the distance between dye-modified CNTs (mCNTs) and QDs, the whole system stay quenched without mechanical stimuli, while the fluorescence of mCNTs and QDs could be activated by mechanical stimuli triggered abruption. In this work, a mechano-responsive epoxy-based composite material was designed based on the quenching pair of modified CNTs and quantum dots. More specifically, the fluorescent dye 7-amino-4-methyl coumarin was conjugated to the surface of CNTs, which prevented the QDs from being quenched by CNTs[29]. In general, spectral overlap between the emission of the donor and the absorbance of the acceptor is required for fluorescence quenching to occur. CdSeS/ZnS

alloyed quantum dots were then selected as the quenching pair acceptor. Dye-modified CNTs (mCNTs) and QDs should widely distribute into the thermoset with the help of ultrasonication and the molecular surface modification. The quenching pair were designed for force activation of fluorescence properties: We find that pronounced changes in fluorescence emerge following plastic deformation, indicating that in these polymeric materials the transduction of mechanical force into the fluorescence occurs in response to mechanical activation. More specifically, the mechanical stimuli such as strain-induced the aggregation of dye modified CNTs(mCNTs) within the system, which was confirmed with TEM images, this type aggregation of mCNTs resulted in the fluorescence recurrence.

3.3 Experimental Section

3.3.1 Modification of CNTs

1.0 g -COOH modified CNTs was dispersed in 20mL of N,N-Dimethylformamide (DMF) under ultrasonic for 30 min, 0.2 g 7-Amino-4-methylcoumarin and 0.5 g Dicyclohexylcarbodiimide (DCC) was then add to the solution. The reaction was performed at 80℃ with magnetic stirring for 12h. Most of the solvent was removed under vacuum filtration, wash the filter cake with DMF, toluene and isopropyl alcohol (IPA) under ultrasonic (3times each for 30min), then put the residue into vacuum oven fully removed all solvent left.

3.3.2. Preparation of mCNT composites Epoxy

12.6 g of Bisphenol A diglycidylether (BADGE) was heated under 50℃, once it all become liquid, 17 g of Jeffamine T3000 was then add to the system with magnetic stirring. Keep stirring until the liquid become homogeneous. mCNT was then added. Spin the mixture then ultrasonic for 30min. Spin the mixture again and then put the epoxy in vacuum oven under 80℃ for 4h, then raise the temperature to 120℃.

3.3.3. Preparation of QDs composites Epoxy

12.6 g of Bisphenol A diglycidylether (BADGE) was heated under 50℃, once it all become liquid, 17 g of Jeffamine T3000 was then add to the system. Keep string until the liquid become homogeneous. CdSeS/ZnS alloyed quantum dots (λem 490nm, 6nm diameter, 1mg/mL in H2O from Sigma-Aldrich) was used in this project, 0.1mL QDs solution per 10 g epoxy was added. Keep the sample under vacuum in vacuum oven 60℃ for 12h to remove the solvent. Stir the mixture until uniform then apply the ultrasonic for 30min. Stir the mixture and then put the sample in vacuum oven under 80℃ for 4h then for an additional 4 hours at 120℃.

3.3.4. Preparation of mCNT/QDs composites Epoxy

12.6 g of Bisphenol A diglycidylether (BADGE) was heated under 50℃, once it all become liquid, 17 g of Jeffamine T3000 was then add to the system. Keep string until the liquid become homogeneous. 0.25%wt mCNT was then added together with little bit DMF. CdSeS/ZnS alloyed quantum dots (λem 490nm, 6nm diameter, 1mg/mL in H2O from Sigma-Aldrich) was used in this project, 0.1mL QDs solution per 10 g epoxy

was added. Keep the sample under vacuum in vacuum oven 60℃ for 12h to remove the solvent. Spin the mixture then ultrasonic for 30min. Spin the mixture and then put the epoxy in vacuum oven under 80℃ for 4h then for an additional 4 hours at 120℃.

3.3.5. Characterization

Tensile test for epoxy was performed with Instron T3000 instrument, the limit of tension was set to be 5cm and the tensile test was performed under 0.5mm/min rate. Steady-state fluorescence emission and excitation spectra were measured on a Nanolog fluorometer (Horiba Jobin Yvon) using a quartz cuvette of 10 mm path length and corrected for the wavelength dependence of the detection system response. Diffuse reflectance Fourier transform infrared spectroscopy (DRIFT) was performed on a Nicolet iS50 FTIR spectrometer with a DTGS KBR detector, 100 scans averaged per spectra, and baseline corrections. Photoluminescence (PL) measurements for cured epoxy resin containing modified carbon nanotubes (mCNTs), QDs or both QDs and mCNTs were performed in a Renishaw InVia spectroscopy system in backscattering configuration with a 40× UV objective using a laser source of 325 nm wavelength. The laser was focused onto the sample with a spot diameter of 0.5 μm. Fluorescence microscopy was performed with Biotek Cytation 5 image reader under manual mode. Consistent parameters of LED intensity, exposure time were applied to all the samples.

3.4. Results and Discussion

3.4.1 Carbon nanotubes modification

A dye-modified CNTs was prepared to serve as a fluorescent quenching pair with the QDs. The CNTs were modified with 7-amino-4-methylcoumarin providing a blue emission wavelength of λ_{em} 460 nm. The –COOH-functionalized CdSeS/ZnS alloyed QDs possess an excitation wavelength at λ_{ex} 450 nm together with green fluorescence at λ_{em} 525 nm. First, acid-modified multi-walled CNTs were sonicated in *N,N*-dimethylformamide (DMF) for 30 min to randomly disperse the CNTs in the solution. Then, 7-amino-4-methylcoumarin and *N,N'*-dicyclohexylcarbodiimide (DCC, coupling agent) were added and the solution was heated to 80 °C for 24 h, which is an adapted protocol from the literature.[30] The dye-modified CNTs were filtered and washed with excess DMF, toluene, and isopropanol alcohol (IPA) while being ultrasonicated to remove unreacted dye and the dicyclohexylurea byproduct of the DCC-activated coupling reaction (Fig.1).

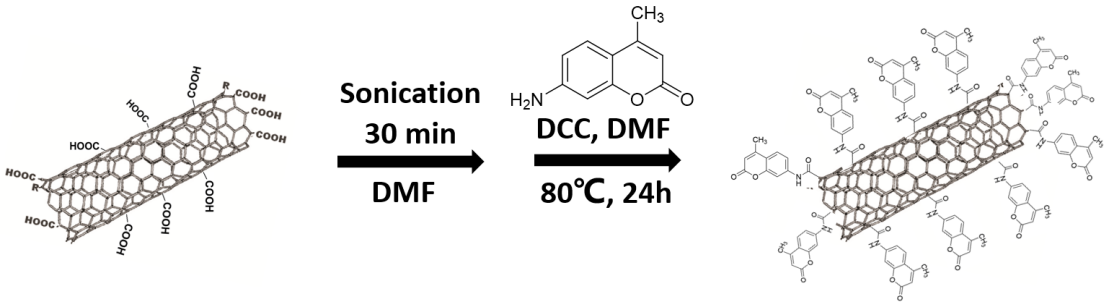

Fig. 1 Schematic detailing the procedure used to covalently attach 7-amino-4-methylcoumarin to acid-modified CNTs.

Fourier-transform infrared (FTIR) spectroscopy and fluorescence spectroscopy were used to characterize the presence of the fluorescent dye on the CNTs. Figure 2 shows the infrared transmittance spectra for the fluorescent dye, the acid-modified

CNTs, and the dye-conjugated CNTs. Distinct changes in the spectra are observed following the conjugation of the dye to the CNTs with several unique absorbance bands appearing that are attributed to the attachment of the dye onto the CNT. Specifically, the amide N-H bond appears at 1503 cm^{-1} and the R-NH-CO-R' amide bond appears at 1572 cm^{-1}, respectively. The ester bond from the coumarin ring results in an absorbance peak at 1014 cm^{-1} and 1149 cm^{-1}. Additionally, there are singlet peaks at 483 cm^{-1}, 659 cm^{-1} and 745 cm^{-1} indicating a tri-functional benzene ring (e.g., the coumarin aromatic ring). The amide bond appearance validated that coumarin dye was modified onto the surface of CNTs, as it could also be physically adsorbed to the surface of CNTs due to π-π stacking.

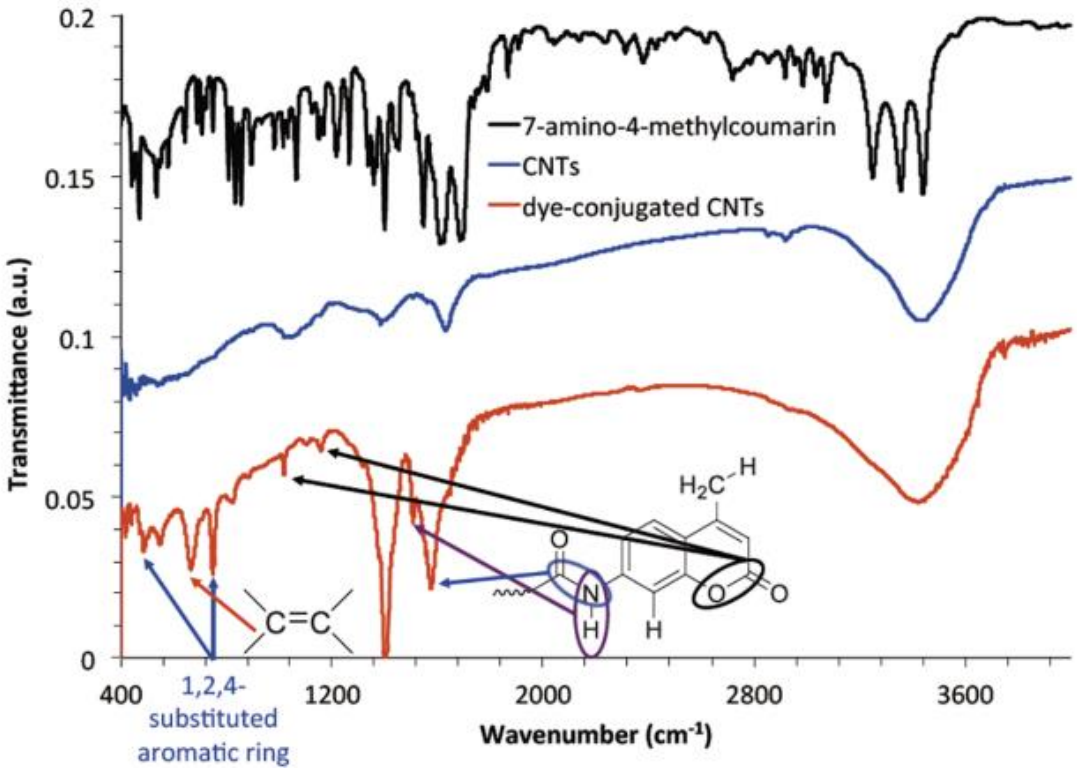

Fig. 2 FTIR spectra of (top) 7-amino-4-methylcoumarin, (middle) acid-modified multi-walled CNTs, and (bottom) dye-conjugated CNTs.

3.4.2 Fluorescence properties of mCNT and QDs

Fluorescence spectroscopy was used to measure the fluorescence properties of the CNTs, dye, and dye-modified CNTs separately as well. Excitation/emission spectra for the CNTs, the fluorescent dye, and the dye-modified CNTs, as well as an overlay plot with the emission spectrum from each of the three samples are shown in Figure 3. The fluorescence of dye-modified CNTs samples show combined fluorescence properties of the CNTs and the dye. Moreover, the fluorescence intensity increases in the order of CNTs < dye-conjugated CNTs < dye. Importantly, the dye-conjugated CNTs display an order of magnitude increase in fluorescence intensity after the dye is conjugated.

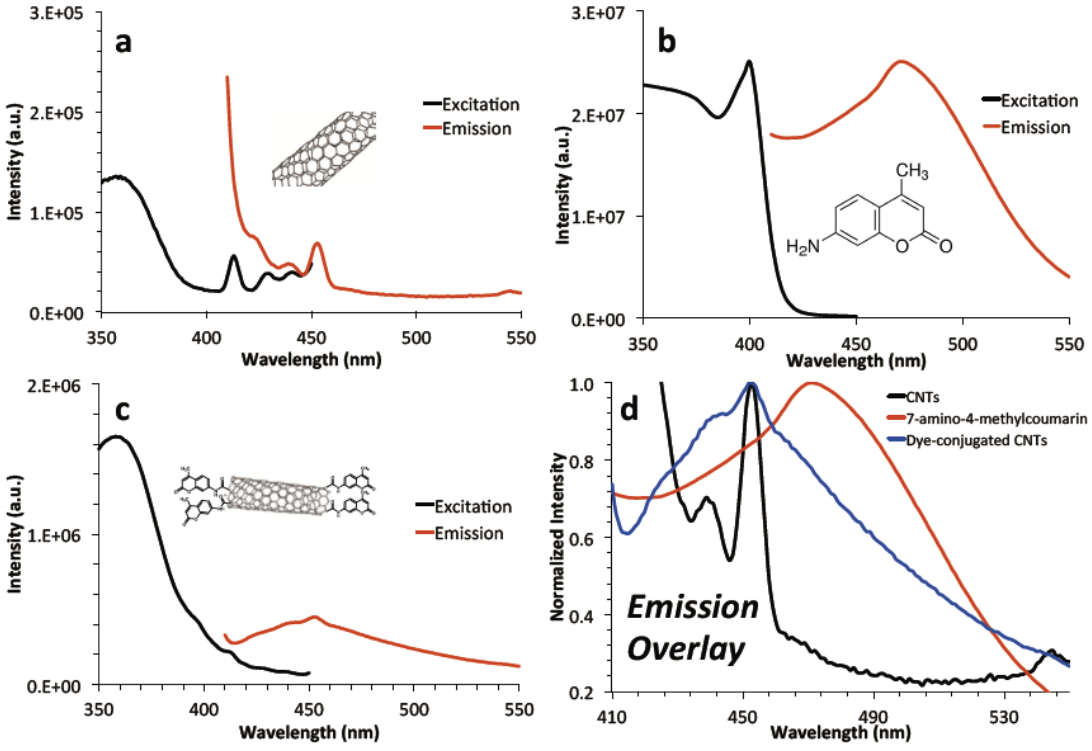

Fig. 3 Fluorescence spectroscopy data for (a) the acid-modified multi-walled CNTs, (b) the 7-amino-4-methylcoumarin fluorescent dye, (c) the dye-conjugated CNTs, and (d) an overlay of fluorescent emission for all three samples.

The fluorescence quenching phenomenon was observed via photoluminescence (PL) measurements for cured epoxy resins containing mCNTs, QDs, or both QDs and mCNTs (Fig. 4, left). As expected, the epoxy sample with mCNTs displayed a strong blue fluorescence around 425 nm, whereas the epoxy sample with QDs displayed green fluorescence at 525 nm. It is important to observe the fluorescence intensity of resin with both mCNTs and QDs dramatically decreased compared to resins with either QDs or mCNTs. Next, the coumarin dye (λ_{ex} = 450 nm) used for CNTs modification was introduced to the test of quenching pair with QDs (λ_{em} = 525 nm) (Fig. 4, right). The resin with an excess amount of dye shows a lower fluorescence intensity at 525 nm compared with the resin with an excess amount of QDs. It is important to see that even with same amount of QDs, the resin with higher dye concentration showed a weaker fluorescence at 525 nm from QDs, indicating a fluorescence quenching relationship between the QDs and the coumarin dye. Thus, in the mCNT/QDs matrix, two mechanism coexist to reduce fluorescence: (i) Förster-resonance energy transfer (FRET) between the coumarin dye and the QDs, and (ii) the quenching between CNTs and other fluorescent particles (dye and QDs) via photoinduced electron transfer (PIET)[31, 32].

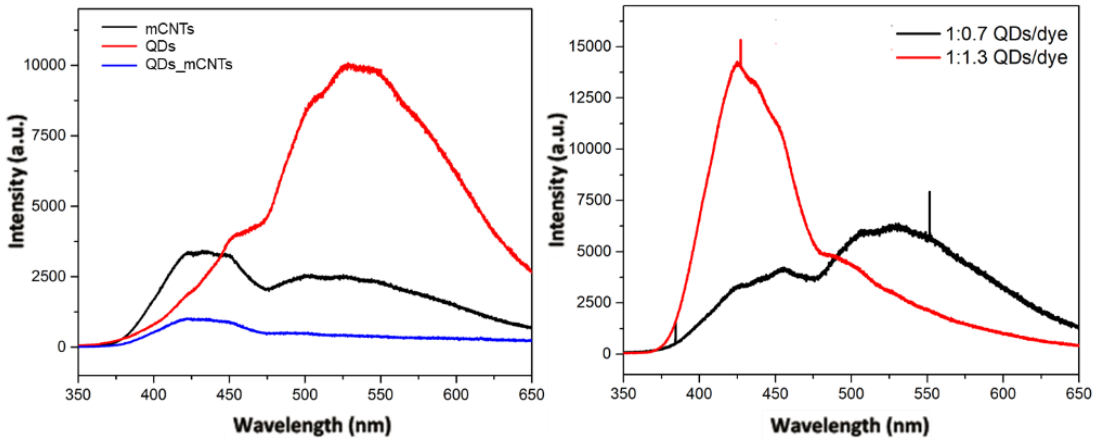

Fig. 4 Photoluminescence (PL) intensities for (left) cured resins containing 1) mCNTs, 2) QDs, or 3) both QDs and mCNTs– excitation wavelength 325 nm; and fluorescence emission intensities for (right) cured resin containing 1) dye and an excess amount of QDs, and 2) QDs and an excess amount of dye.

3.4.3. Fluorescence Microscope of Epoxy Resin with mCNTs and QDs

Next, the fluorescence characteristics of the composites were imaged using confocal microscopy. To test the ability of the QDs and the dye molecular from mCNTs to form a FRET pair in the resin, a composite containing both nanoparticles was prepared and demonstrated limited (or no) fluorescence. First, the fluorescence photos were taken for composites with mCNTs or for composites with QDs.. Specifically, the fluorescence for composites containing mCNTs and the composites with QDs were observed separately. By taking fluorescence photo at the middle of dog bone shaped sample, the resin containing mCNTs exhibit blue fluorescence with delicate green (Fig. 5a-c), which match the result from both the PL measurements and fluorescence spectroscopy above. The epoxy sample with dye modified CNTs exhibit stronger blue light fluorescence(~425 nm) while the green light fluorescence(~500nm) could be

barely observed under same exposure and gathering condition (Fig. 3c, Fig. 4 left)., for the sample with QDs, the epoxy resin brought on both green and blue fluorescence (Fig. 5d-f) while the green light fluorescence is stronger than blue light (Fig. 3c, Fig. 4 left).

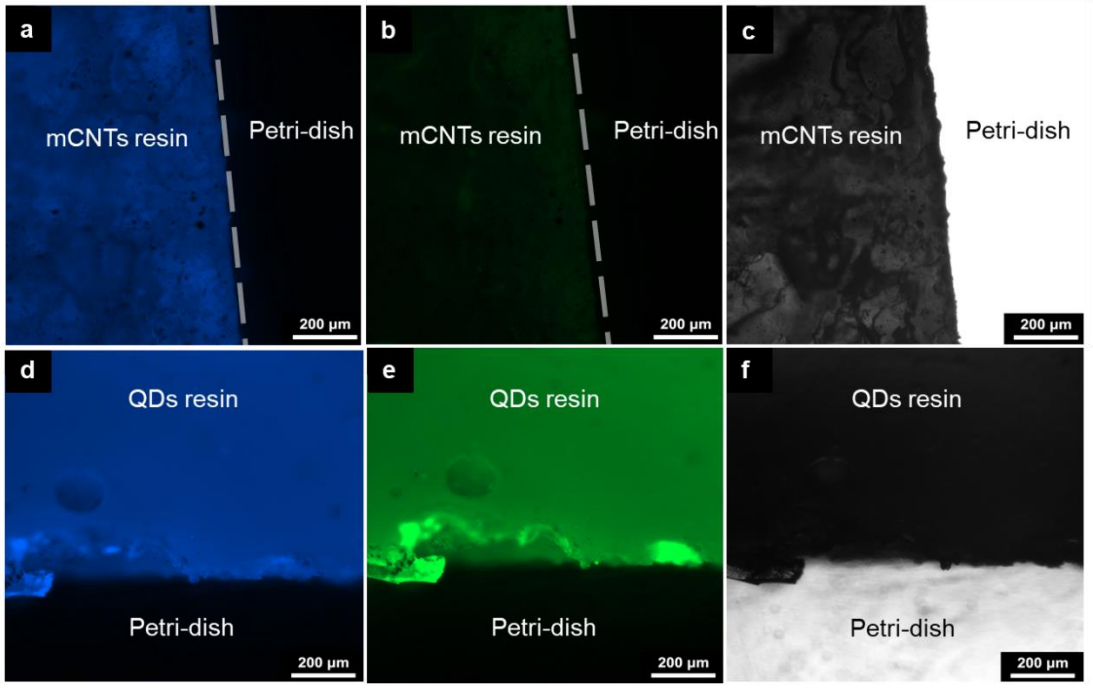

Fig. 5 Fluorescence microscopy of resins containing (top) mCNTs or (bottom) QDs. The panels show (a, d) excitation 377 nm and emission 447 nm; (b, e) excitation 469 nm and emission 525 nm; and (c, f) bright field images. QD concentration is 0.005 wt%, and mCNT concentration is 0.25 wt%.

The purpose of this work was to demonstrate mechanically-activated fluorescence in resins that quenched fluorescence in the as-prepared state. Therefore, the resins were subjected to tensile testing, which provided a static load until the sample broke. Subsequently, the resins were analyzed using fluorescent microscopy. Figure 6 shows the first test performed, wherein resins containing equal concentration of mCNTs and QDs were broken using tensile testing, and then analyzed (tested area labeled in the

schematic shown alongside Fig. 6). The fluorescence microscope photos of the pre-tensile precursors (Fig. 6 a,b left), with significantly lower fluorescence intensity than the samples on the samples after tensile testing(Fig. 6 a,b right). The mechanically triggered fluorescence follows the original intention of design: the mCNTs/QDs pair exhibit stimuli-responsive behavior while originally stay quenched. The quenching phenomenon of epoxy sample with mCNTs and QDs could because of both FRET quenching between coumarin dye and QDs, and the electron-hole energy transfer within MWCNTs and QD pairs.

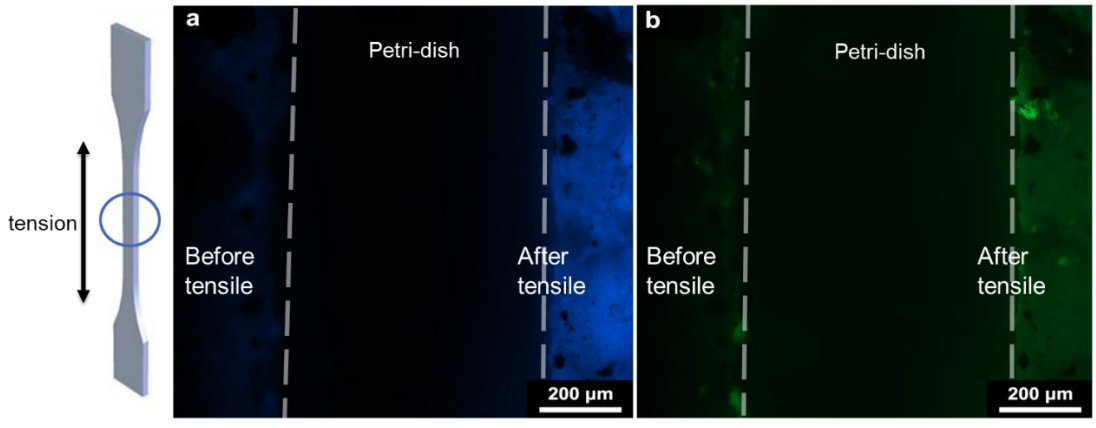

Fig. 6 Fluorescence of resin containing mCNTs and QDs before and after tension (a) excitation 377nm and emission 477 nm; (b) excitation 469 nm and emission 525 nm. QD concentration is 0.005 wt%, mCNT concentration is 0.25 wt%. Tension: 50 µm/min until break.

To find out that if the phenomenon would appear only at the area tension was applied, the resins were cut in the middle with a razor blade (cutting position and observation area labeled on the schematic in Fig. 7). In this way, a load was applied only at specific area. Again, the resins were subsequently analyzed by fluorescent

microscopy. The epoxy resin containing 0.25 wt% CNTs (i.e., not dye-modified) and 0.005 wt% QDs stayed quenched after the tensile experiment and after cutting. Indicating the quenching of QDs/CNTs is not reversible via mechanical stimuli, as the same stimuli will triggered fluorescence in the epoxy resin contains mCNTs/QDs: Metallic surfaces are known to quench the fluorescence from nearby photoexcited dipoles through resonant energy transfer, CNTs in this epoxy resin, provided the metallic surface next to the QDs, which quenched the QDs.

A similar phenomenon as epoxy resin with mCNTs/QDs after tension was observed after cutting the epoxy contains mCNTs/QDs: both samples show blue and green light fluorescence reproduced. This represent the mCNTs/QDs quenching pair in epoxy resin could be treated as damage fluorescent sensor, which fluorescence could be activated via mechanical stimuli and/or physical structure damage. Specifically, fluorescence on the cut resin cutting edge tell a different story compared with epoxy with mCNTs/QDs fluorescence photo after tensile (Fig. 7). As expected the green light fluorescence emerged in the fluorescence photo, however, the relative intensity decrease from edge area towards central part is very large, similar phenomenon also appeared in blue fluorescence photo. In our mCNTs/epoxy matrix, because of the hydrogen bonding and/or electrostatic attraction between carboxylic acid group from MWCNTs surface and epoxy curing reagents functional groups (ether group, hydroxyl group from BADGE and amino group from Jeffamine), mCNTs were well dispersed in the epoxy matrix under the pre-curing condition. The load from mechanical stimuli (via tensile or dissection progress) transmitted alone the epoxy back bone towards MWCNTs, forming

CNTs bridge between micro-crack surface and/or cavity on the fraction surface. As a result, the distance between mCNTs and QDs in the epoxy resin ‘damaged’ region increased, which weaken the quenching effect between dye-QDs, CNTs-QDs and mCNTs-QDs: as the quenching efficiency between dye-QDs decreasing, conjugated dye form mCNTs regained fluorescence property, emerging blue light fluorescence; QDs on the other hand, released from mCNTs quenching range, regained the green light fluorescence as a result. However, the matrix with CNTs/QDs matrix stayed quenched even after mechanical stimuli, this could because of conjugated dye on the MWCNTs surface weaken the electron transfer efficiency from QDs to MWCNTs of PIET quenching path way, thus the mCNTs/QDs green fluorescence recurred after mechanical stimuli.

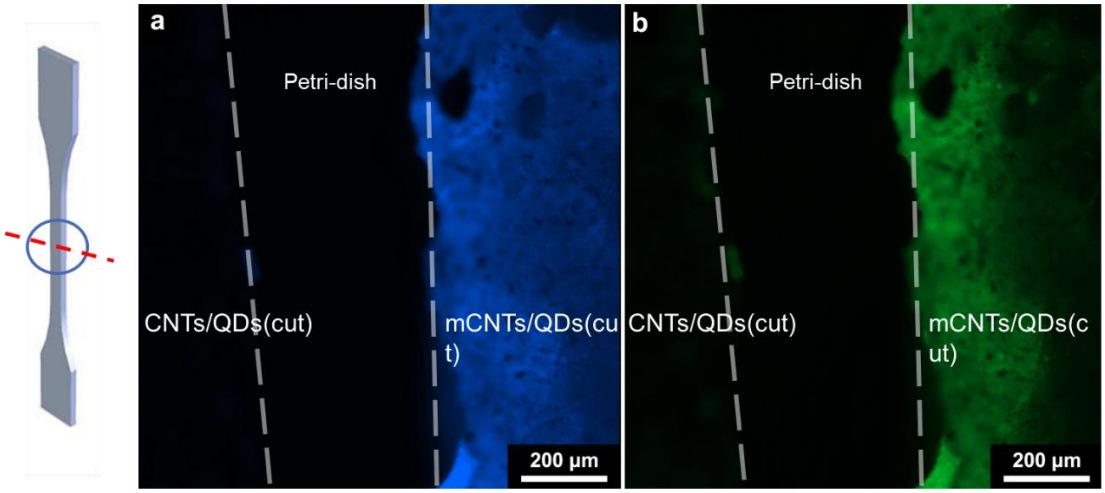

Fig. 7 Fluorescence of resin containing mCNTs and QDs before and after cut (a) excitation 377nm and emission 477 nm; (b) excitation 469nm and emission 525 nm. QDs concentration 0.005wt%, mCNTs 0.25wt%, CNTs 0.25wt%.

A potential concern was that the mechanoresponsive phenomenon of epoxy resin

containing mCNTs/QDs would be sensitive to the nanoparticle loading and the stoichiometry of QDs:mCNTs. Thus, we raised the concentration of mCNTs up to 5 wt% while the QDs concentration stay the same as 0.25 wt% sample. After the tensile test, no significant changes in fluorescence before and after tensile were observed (Fig. 8). This could be another proof that the coumarin dye on the surface of modified MWCNTs preventing the quenching of QDs on a certain degree: increasing the concentration of mCNTs in the matrix resulting in decreasing the distance between QDs and mCNTs, the matrix remained quenched after mechanical stimuli as a result. This result also confirmed the mechanism of fluorescence is not dominated by Förster resonance energy transfer (FRET). At higher mCNTs level, the chance of energy transfer to potential FRET acceptor, which is QDs in our system, should result in higher fluorescence intensity contributed by more excited QDs. However, the sample with 5 wt% mCNTs did not perform stronger blue nor green fluoresce when compared with the sample with only 0.25 wt% mCNTs.

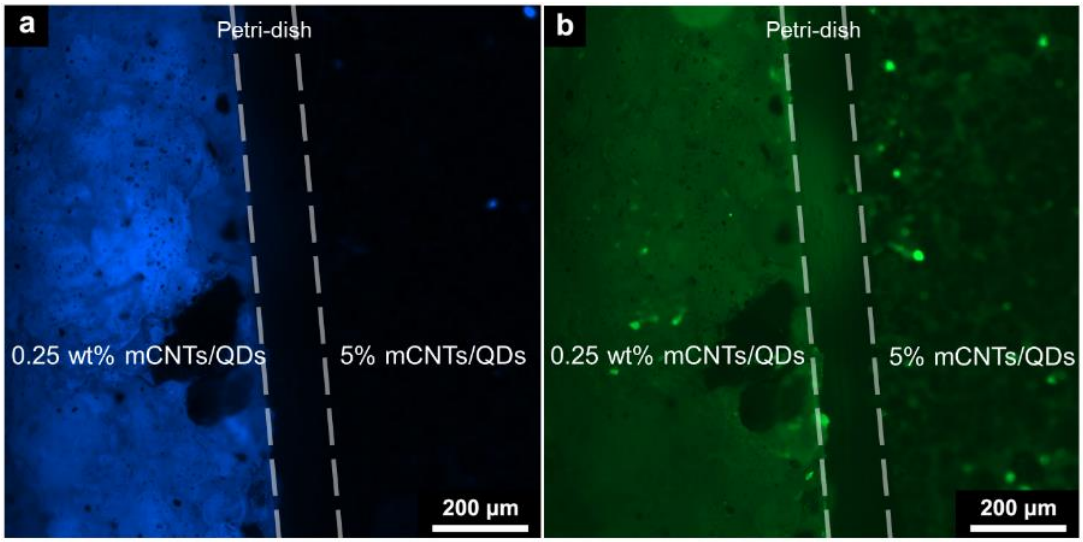

Fig. 8 Fluorescence of resins containing mCNTs and QDs after tension (a) excitation 377 nm and emission 477 nm; (b) excitation 469nm and emission 525 nm. QDs

concentration 0.005wt%, mCNTs 0.25wt%. Tension: 50μm/min till break.

Fluorescence mapping token with photoluminescence (PL) spectrum provided other details of the fluorescence intensity distribution within the epoxy matrix with mCNTs/QDs sample after tensile force. (Fig. 9) After tensile of dog bone shaped sample, fluorescence spectrums were taken at both sample center (red) and sample edge region closed to the clamp (black). As observed, the fluorescence at 450 nm and 525 nm from sample center showed almost doubled intensity strength compared with the spectrum of sample edge area, indicating the sample area experienced larger spatial displacement displayed stronger fluorescence intensity, not only that, at the sample edge the blue fluorescence (450 nm) also perform stronger than green fluorescence (525 nm).

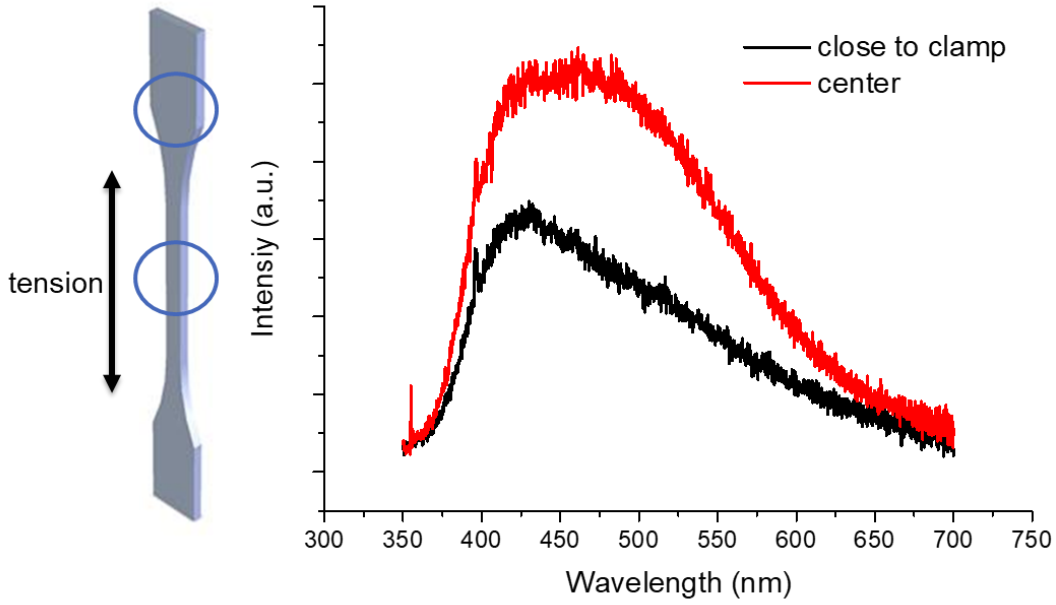

Fig. 9 Photoluminescence (PL) intensities for epoxy resins containing QDs and mCNTs– excitation wavelength 350 nm. Tension: 50 μm/min.

3.4.4. Dispersion of mCNTs and QDs in the Epoxy

For epoxy sample with 0.25 wt% mCNTs and 0.005 wt% QDs, the mCNTs and QDs dispersion within the epoxy before and after tension applied upon the sample were investigated with TEM images (Fig. 10). Before the tension applied, the mCNTs and QDs are well dispersed within the polymer matrix composite system(Fig 10a), no significant aggregation appeared while the QDs dispersed mainly in the area close to where the mCNTs appeared. This could because of the weak inter action between the mCNTs surface charging and QDs surface charging. The mCNTs revealed erect morphology within the sample before tension applied, however, the mCNTs appeared to be crooked within the epoxy sample after tension applied.

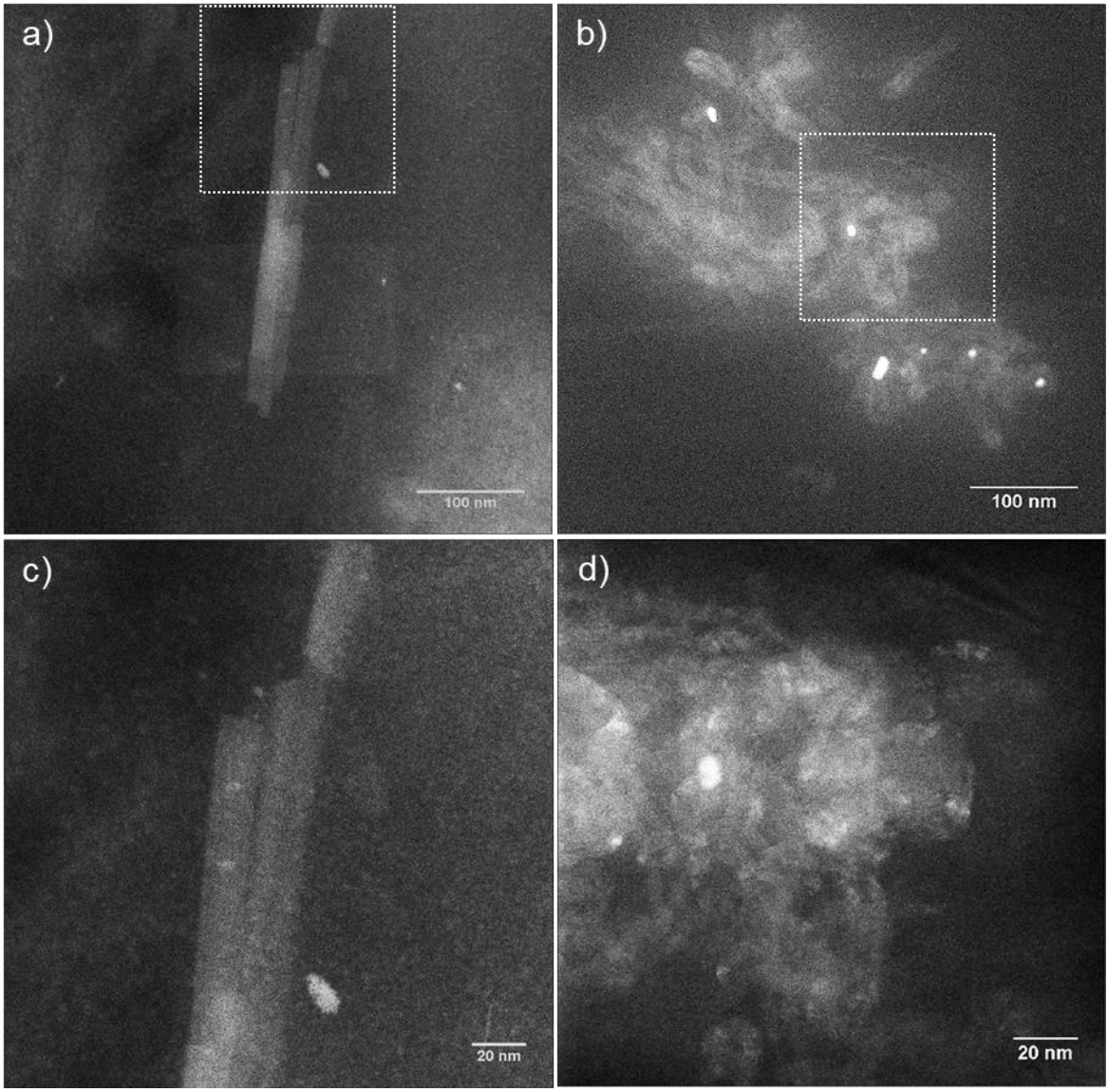

Fig. 10 TEM of resins containing mCNTs and QDs before and after tension (a) epoxy resin before tension applied; (b) epoxy resin after tension applied. (c)closer view of mCNTs within epoxy with mNCTs/QDs before tension applied. QDs observed on the surface of mCNTs as brighter dots. (d) closer view of mCNTs within epoxy with mNCTs/QDs after tension applied. QDs observed on the surface of mCNTs as brighter dots. QDs concentration 0.005wt%, mCNTs 0.25wt%. Tension: 50μm/min till break.

The TEM images also provided information about average distance between the

mCNTs and QDs within the system (Fig 5.11.). The TEM images of the epoxy resin before tension applied indicating that the QDs cluster – mCNTs distance stay in the range of 20 – 50 nm. Respectfully, after tension applied to the epoxy resin with same mCNTs and QDs concentration, the distance between QDs and mCNTs appeared to be a different story, more specifically, the QDs appeared to be separated from mCNTs and the distance between those pairs raised up to 250 nm within the system. This phenomenon indicates that the mechanical activated fluorescence undergo a distance-related mechanism. The hypothesis mechanism of fluoresces quenching and reactivating was believed to be electrons transfered from dye on the surface of mCNTs towards QDs at closing distance, the fluorescence of the epoxy sample before mechanical stimuli result in quenching. After the mechanical stimuli applied to the epoxy system, the average distance of mCNTs and QDs increased which dramatically reduced the efficiency of electron transfer between mCNTs and QDs. The excited electrons from coumarin dye on the surface of mCNTs and QDs stays in their original system, which manifested as the fluorescence renascence in the samples after mechanical stimuli applied. Previously the fluorescence of stretched epoxy sample was studied with PL test (Fig 5.9.), the dogbone shaped epoxy sample edge and sample center performed fluorescence at the same wavelength as the mCNTs and QDs. This could be the other proof that the reproduced fluorescence comes from coumarin dye on the surface of mCNTs and also the QDs itself.

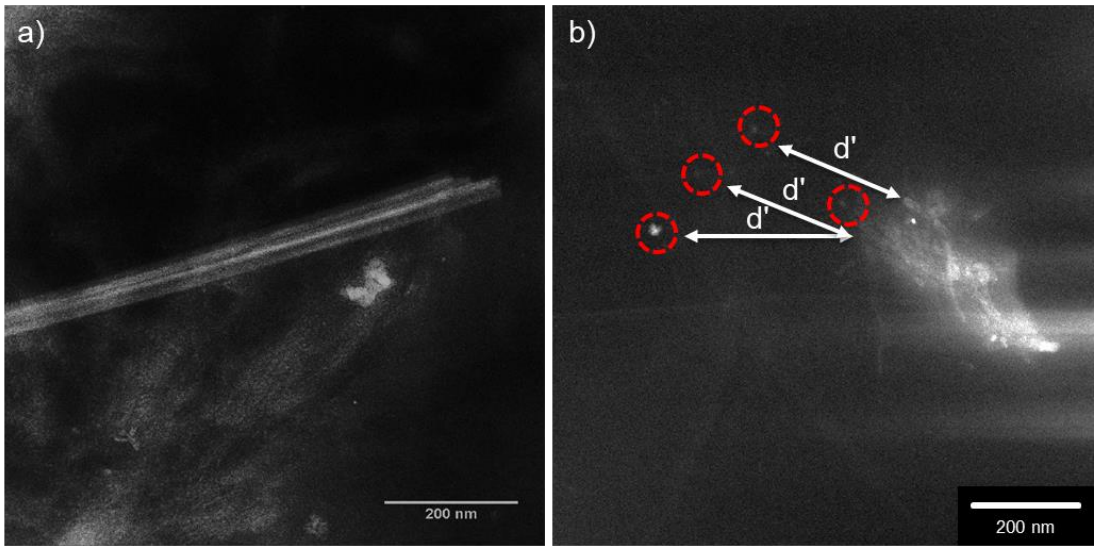

Fig 5.11. TEM images of epoxy resin with mCNTs and QDs before (left) and after (right) tension applied.

3.4.5. Limit of Strain Induced Fluorescence

Fluorescence microscopy was used in tandem with the compression tests to evaluate the fluorescent response of the self-sensing thermoset network composites, with fluorescence images taken at the strain values of 0, 2.5, 5, 7.5, 10, and 15%. The representative images for the selected strain values for the mCNTs/QDs epoxy nanocomposites can be seen in Fig. 11. These images were taken under excitation of 469 nm UV light, capturing the fluorescent emission at 525 nm. Quantification of the fluorescence via ImageJ was performed to analyze the phenomenon further,for each sample analyzed, ten fluorescence images were taken representative of the sample face and the ImageJ software calculated average fluorescence intensity values for each image. Based on the intensity/strain curve of both blue and green fluorescence of mCNTs/QDs composites, there is an overall increase in the fluorescence with an

increase of the strain applied, however, there is not a clear difference between the 0, 2.5, 5% and 7.5% strains, which would be required for damage precursor detection. There seems to be a noticeable difference between the 7.5 and 10% strain values. Respectfully, for the same sample, the blue and green strain/intensity curve exhibit similar variation tendency.

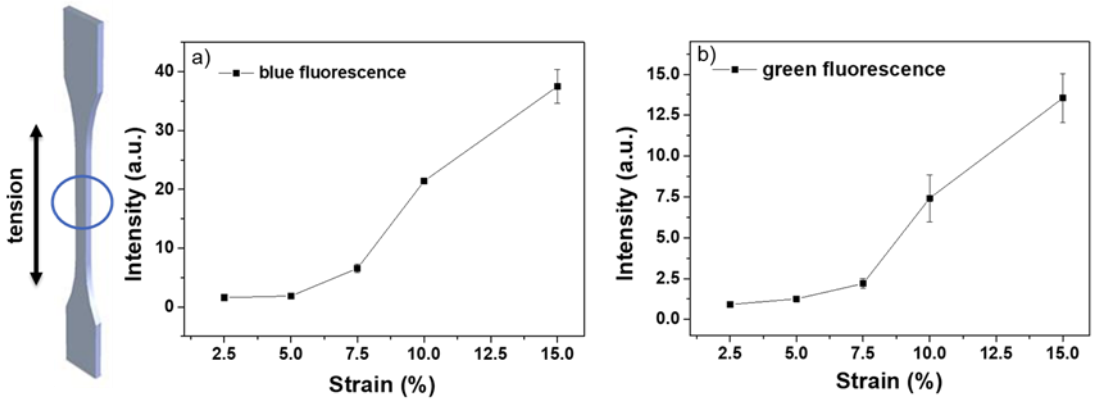

Fig. 11 The panels show different strain% mCNTs/QDs resin fluorescence intensity (via Image J) vs strain curve (a) excitation 377 nm and emission 447 nm; (b) excitation 469 nm and emission 525 nm. QDs concentration 0.005 wt%, mCNTs 0.25 wt%.

3.4.6. Mechanical Properties Influence of mCNT and QDs as Nanofillers

The tensile testing performance of the various composites is shown in Figure 12. The properties of the neat resin (without any nanoparticle added) are compared to the resins containing 1) the combination of the QDs and varies mCNTs (QDs concentration 0.005 wt%) and 2) the QDs. As the concentration of mCNTs increased, the Young's modulus enhanced together with the strain at break, the resin with 0.75 wt% mCNTs performed best mechanical properties based on Young's modulus. The 1 wt% resin appeared to be the resin with highest strain at break, however, the Young's modulus was lower than

the sample with 0.75 wt% mCNTs sample. For the epoxy resin contains 2 wt% mCNTs, the mechanical properties performed lower than the ones with lower mNCTs concentration. This could because of the mCNTs within the epoxy resin influencing the curing progress, which results in lower mechanical properties of the epoxy resin. The epoxy resin with QDs only, on the other hand, showed slightly lower mechanical properties compared with the original resin. While only a small amount of aqueous QDs solution was added to the system before curing, during the curing progress, the evaporation of water still left some vacuole within the resin. Thus the mechanical properties of resin with QDs performed lower than original epoxy resin.

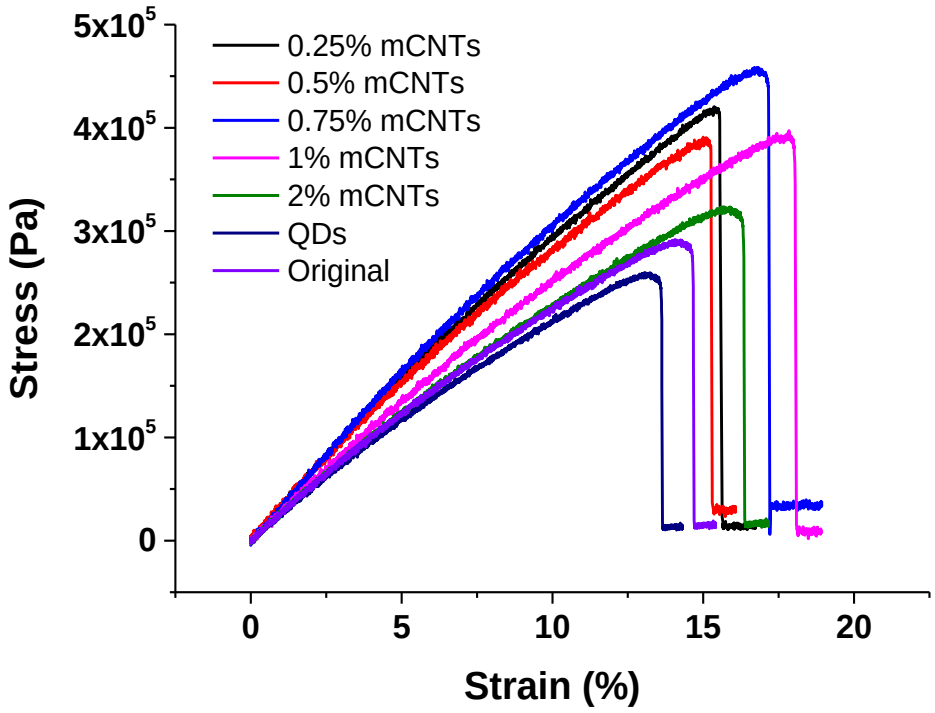

Fig. 12 Tensile analysis of resins containing 1)different concentrations of mCNTs and 0.005 wt% QDs 2) resin with 0.005 wt% QDs only 3) original resin.

3.5. Conclusions

By using a combination of nanoparticles that form a fluorescence quenching pair, we successfully enable mechanoresponsive behavior in the composite. The addition of the QDs decreases the Young's modulus and the stress at break while increasing the strain at break slightly, the addition of the mCNTs increased each of these characteristics. QDs/mCNT composites display fluorescence quenching, while fluorescence can be activated via mechanical strain and/or physical damage to the resin. Resin with QDs/CNTs appears irreversible quenching and far stronger quenching than with the dye-modified mCNTs or dye. Finally, 7.5% of mechanical strain will activate the fluorescence in the polymer matrix composites

Reference

1. Iijima, S., Helical Microtubules Of Graphitic Carbon. *Nature* 1991, *354* (6348), 56-58.

2. Ajayan, P. M.; Stephan, O.; Colliex, C.; Trauth, D., Aligned Carbon Nanotube Arrays Formed by Cutting a Polymer Resin-Nanotube Composite. *Science* 1994, *265* (5176), 1212-1214.

3. Wang, M.; Dheressa, E.; Brown, K. A.; Green, M. D., Effect of Crosslinker Length and Architecture on the Thermomechanical Properties of CNT-Loaded Elastomeric Polymer Matrix Composites. *Macromol Rapid Comm* 2018, *39* (14).

4. Ma, P. C.; Kim, J. K.; Tang, B. Z., Effects of silane functionalization on the properties of carbon nanotube/epoxy nanocomposites. *Compos. Sci. Technol.* 2007, *67* (14), 2965-2972.

5. Khan, S. U.; Pothnis, J. R.; Kim, J. K., Effects of carbon nanotube alignment on electrical and mechanical properties of epoxy nanocomposites. *Compos Part a-Appl S* 2013, *49*, 26-34.

6. Kim, J. K.; Mai, Y. W., High-Strength, High Fracture-Toughness Fiber Composites

with Interface Control - a Review. *Compos. Sci. Technol.* 1991, *41* (4), 333-378.

7. Pang, J. W. C.; Bond, I. P., A hollow fibre reinforced polymer composite encompassing self-healing and enhanced damage visibility. *Compos. Sci. Technol.* 2005, *65* (11-12), 1791-1799.

8. Makyla, K.; Muller, C.; Lorcher, S.; Winkler, T.; Nussbaumer, M. G.; Eder, M.; Bruns, N., Fluorescent Protein Senses and Reports Mechanical Damage in Glass-Fiber-Reinforced Polymer Composites. *Adv Mater* 2013, *25* (19), 2701-2706.

9. Du, B. X.; Xiao, M.; Zhang, J. W., Effect of Thermal Conductivity on Tracking Failure of Epoxy/BN Composite under Pulse Strength. *Ieee T Dielect El In* 2013, *20* (1), 296-302.

10. Wentzel, D.; Millers, S.; Sevostianov, I., Dependence of the electrical conductivity of graphene reinforced epoxy resin on the stress level. *Int J Eng Sci* 2017, *120*, 63-70.

11. Berkowski, K. L.; Potisek, S. L.; Hickenboth, C. R.; Moore, J. S., Ultrasound-induced site-specific cleavage of azo-functionalized poly(ethylene glycol). *Macromolecules* 2005, *38* (22), 8975-8978.

12. Chen, Y. L.; Spiering, A. J. H.; Karthikeyan, S.; Peters, G. W. M.; Meijer, E. W.; Sijbesma, R. P., Mechanically induced chemiluminescence from polymers incorporating a 1,2-dioxetane unit in the main chain. *Nat Chem* 2012, *4* (7), 559-562.

13. Sohma, J., Mechanochemistry of Polymers. *Prog Polym Sci* 1989, *14* (4), 451-596.

14. Lenhardt, J. M.; Ong, M. T.; Choe, R.; Evenhuis, C. R.; Martinez, T. J.; Craig, S. L., Trapping a Diradical Transition State by Mechanochemical Polymer Extension. *Science* 2010, *329* (5995), 1057-1060.

15. Hickenboth, C. R.; Moore, J. S.; White, S. R.; Sottos, N. R.; Baudry, J.; Wilson, S. R., Biasing reaction pathways with mechanical force. *Nature* 2007, *446* (7134), 423-427.

16. Du, J. Z.; Du, X. J.; Mao, C. Q.; Wang, J., Tailor-Made Dual pH-Sensitive Polymer-Doxorubicin Nanoparticles for Efficient Anticancer Drug Delivery. *J Am Chem Soc* 2011, *133* (44), 17560-17563.

17. Davis, D. A.; Hamilton, A.; Yang, J. L.; Cremar, L. D.; Van Gough, D.; Potisek, S. L.; Ong, M. T.; Braun, P. V.; Martinez, T. J.; White, S. R.; Moore, J. S.; Sottos, N. R., Force-induced activation of covalent bonds in mechanoresponsive polymeric materials. *Nature* 2009, *459* (7243), 68-72.

18. Diesendruck, C. E.; Steinberg, B. D.; Sugai, N.; Silberstein, M. N.; Sottos, N. R.; White, S. R.; Braun, P. V.; Moore, J. S., Proton-Coupled Mechanochemical Transduction: A Mechanogenerated Add. *J Am Chem Soc* 2012, *134* (30), 12446-12449.

19. Larsen, M. B.; Boydston, A. J., "Flex-Activated" Mechanophores: Using Polymer Mechanochemistry To Direct Bond Bending Activation. *J Am Chem Soc* 2013, *135* (22), 8189-8192.

20. Shiraki, T.; Diesendruck, C. E.; Moore, J. S., The mechanochemical production of phenyl cations through heterolytic bond scission. *Faraday Discuss* 2014, *170*, 385-394.

21. Pucci, A.; Bizzarri, R.; Ruggeri, G., Polymer composites with smart optical properties. *Soft Matter* 2011, *7* (8), 3689-3700.

22. Lowe, C.; Weder, C., Oligo(p-phenylene vinylene) excimers as molecular probes: Deformation-induced color changes in photoluminescent polymer blends. *Adv Mater* 2002, *14* (22), 1625-1629.

23. Weder, C., MECHANOCHEMISTRY Polymers react to stress. *Nature* 2009, *459* (7243), 45-46.

24. Gossweiler, G. R.; Hewage, G. B.; Soriano, G.; Wang, Q. M.; Welshofer, G. W.; Zhao, X. H.; Craig, S. L., Mechanochemical Activation of Covalent Bonds in Polymers with Full and Repeatable Macroscopic Shape Recovery. *Acs Macro Lett* 2014, *3* (3), 216-219.

25. Morales-Narvaez, E.; Perez-Lopez, B.; Pires, L. B.; Merkoci, A., Simple Forster resonance energy transfer evidence for the ultrahigh quantum dot quenching efficiency by graphene oxide compared to other carbon structures. *Carbon* 2012, *50* (8), 2987-2993.

26. Satishkumar, B. C.; Brown, L. O.; Gao, Y.; Wang, C. C.; Wang, H. L.; Doorn, S. K., Reversible fluorescence quenching in carbon nanotubes for biomolecular sensing. *Nat Nanotechnol* 2007, *2* (9), 560-564.

27. Cho, E. S.; Hong, S. W.; Jo, W. H., A New pH Sensor Using the Fluorescence Quenching of Carbon Nanotubes. *Macromol Rapid Comm* 2008, *29* (22), 1798-1803.

28. Luo, J. D.; Xie, Z. L.; Lam, J. W. Y.; Cheng, L.; Chen, H. Y.; Qiu, C. F.; Kwok, H. S.; Zhan, X. W.; Liu, Y. Q.; Zhu, D. B.; Tang, B. Z., Aggregation-induced emission of 1-methyl-1,2,3,4,5-pentaphenylsilole. *Chemical Communications* 2001, (18), 1740-1741.

29. Biju, V.; Itoh, T.; Baba, Y.; Ishikawa, M., Quenching of photoluminescence in conjugates of quantum dots and single-walled carbon nanotube. *J Phys Chem B* 2006, *110* (51), 26068-26074.

30. Sheehan, J. C.; Hess, G. P., A New Method of Forming Peptide Bonds. *J Am Chem Soc* 1955, *77* (4), 1067-1068.

31. Persson, B. N. J.; Lang, N. D., Electron-Hole-Pair Quenching of Excited-States near a Metal. *Phys Rev B* 1982, *26* (10), 5409-5415.

32. Barnes, W. L., Fluorescence near interfaces: the role of photonic mode density. *J Mod Optic* 1998, *45* (4), 661-699.

Chapter 4. Soft Segment Spacer Length-Properties Relation Within Liner Aliphatic Ionenes Polymers Ionenes

Meng Wang and Matthew D. Green*

School of Molecular Science, Arizona Stater University, Tempe, AZ 85281, USA
School for Engineering of Matter, Transport and Energy, Arizona Stater University, Tempe, AZ 85281, USA

*E-mail address: mdgreen8@asu.edu

4.1. Abstract

The synthesis and characterization of a series of segmented poly(ethylene glycol) (PEG)-based ammonium ionenes is described. Bromine end-capped oligomers were successfully synthesized using the reaction of 6-bromohexanoyl chloride with 1000, 2000, and 4000 g/mol PEGs. 1H NMR spectroscopy, titration studies, and matrix-assisted laser desorption ionization-time of flight (MALDI-TOF) mass spectrometry revealed the di-functionality of the oligomers. First, a series of PEG-based ammonium ionenes was synthesized from bromine end-capped PEG oligomers and N,N,N',N'-tetramethyl-1,6-hexanediamine. For this series, a single glass transition temperature (Tg) of approximately -20℃ was observed through differential scanning calorimetry (DSC). In addition, a series of PEG-based ammonium ionenes containing 1,12-dibromo-dodecane was synthesized to increase the aliphatic hard segment (HS) content(25, 50 and 75 wt %) and enhance the mechanical properties of the resulting materials. Wide-angle X-ray scattering (WAXS) profiles for these ionenes showed that

Bragg distances intensity increase linearly with the molecular weight of PEG soft segment.

4.2. Introduction

Polyionenes, specifically ammonium ionenes, are ion-containing (typically cationic) polymers that have quaternary nitrogen atoms lie directly within the macromolecular main backbone. Gibbs and coworkers[1] first synthesized low molecular weight ionenes with a polymerization of difunctional dimethylamino-N-alkyl halides In 1934. Another commonly used reaction, Menshutkin reaction, on the other hand, is also widely used for synthesizing ionene from a ditertiary amine and a dihalide. First aliphatic ionenes were reported by Rembaum and coworkers[2-4] using this reaction and explored their solution properties. The ionene polymer is generally named based on the number of methylene spacers, which correspond to the diamine (x) and dihalide (y) monomers, respectively (i.e. x,y-ionene). The properties and applications of ionenes are influenced by different parameters: chemical composition, molecular weight, charge density, counterion, solution concentration, and end-group functionality. In 2009 Prof. Long's group reported the review paper focused on structure-property relationships of well-defined cationic polymers. The design flexibility to tune charge density through ionomers selection makes ionenes ideal models for investigating structure-property relationships.[5] Ionene polymers could be separated into two general types: segmented ionenes[6-11] and nonsegmented,[1, 4] while the chemical architecture of these ionenes are either linear, cross-linked or branched. Compared with nonsegmented ionenes,

segmented ionenes performed elastomeric properties.[12-14] Nonsegmented ionenes hold shorter distances between ionic sites will result in higher charge density, water solubility will also be better but the mechanical properties were generally poorer.[5]

PEG-containing polymers have unlimited potential for biomedical material applications due to their biocompatibility and low biotoxicity.[15] Previously, Dimitrov and co-workers synthesized PEG-based ionenes in the presence of a N-methyldiethanolamine initiator with an anionic polymerization of ethylene oxide[8]. Dichloromethane was used with the presence of a strong base like CsOH or KOH to increase the PEG segment molecular weight undergoing a Williamson-type reaction. The PEG-based polymer was then quaternized to yield a PEG-based ionene. The various functionalized polymers displayed different solution behaviors. For example, when PEG-based polymer was quaternized with methyl halide, the ionene demonstrated typical polyelectrolyte behavior; however, when PEG-based polymer was quaternized with zwitterionic or perfluorinated based halide, dipole-dipole and hydrophobic interactions will result in the decreasing of hydrodynamic radius. Sukhyy and co-workers recently reported the synthesis, thermal property characterization, and ionic conductivity of novel PEG-based ionenes[9]. As they reported, changing the PEG oligomer molecular weight controlled the charge density. As expected for polyelectrolytes, the Tg increased with increasing charge content. As a result, PEG ionenes that Sukhyy and coworkers examined show a decreasing of the Tg ranged from −52 to −10 ◦C as the PEG repeat unit decreased from 21 to 2.

Our work emphasizes thermal, mechanical and morphological behavior of PEG-

based ionenes. The significance of PEG segmented ionenes compared with PTMO ionenes is the absence of SS crystallization. The disadvantage of PTMO ionenes is that crystallization occurs at ambient conditions, and thus influences modulus and ultimate mechanical behavior. WAXS analysis revealed that the longest PEG spacer facilitated polymer crystallization, while decreasing the length of the PEG spacer produced amorphous characteristics.

4.3. Experimental

4.3.1. Materials

PEG 1000, 2000 and 4000 were purchased from Sigma-Aldrich. 6-Bromohexanoyl chloride (97%) was purchased from Alfa Aesar. Triethylamine was purchased from Aldrich and distilled from calcium hydride. 1,12-Dibromododecane (98%) was purchased from Sigma-Aldrich and recrystallized from ethanol. Phenolphthalein and N,N,N0,N0-tetramethyl-1,6-hexanediamine (99%) were purchased from Acros Organics and used as received. Methanol (MeOH, HPLC grade) was purchased from Fisher and used as received.

4.3.2. Synthesis of Bromine End-Capped PEG (Br-PEG-Br)

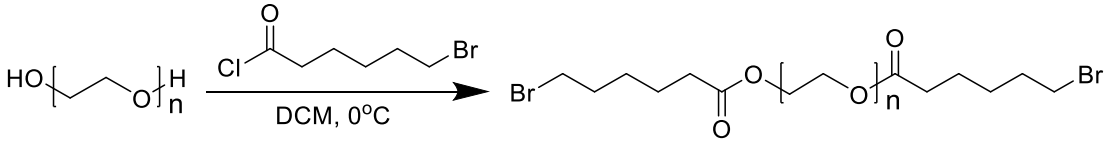

Scheme.1 Synthesis of bromine end-capped PEG using bromo-substituted acyl chlorides.

This reaction was performed according to previous literature precedent[13]. For each PEG length, the molecular weight was determined using a combination of alcohol group titration and analysis by 1H NMR spectroscopy. As an example, poly (tetramethylene oxide (PTMO,1400 g/mol, 4.98 g,3.5 mmol) and TEA (0.79 g, 7.8 mmol) were mixed in dichloromethane (23 mL) at 0 ℃, and 6-bromohexanoyl chloride (1.68 g,7.8 mmol) was added drop-wise. The mixture was slowly warmed to 23 ℃and stirred for 24 h. Following the reaction, the triethy-lammonium chloride salt was filtered, and the organic phase was washed with a saturated aqueous solution of sodium bicarbonate and water in series. The organic phase was dried over anhydrous sodium sulfate, and removed using rotary evaporation at 23℃. A clear, viscous liquid was obtained

4.3.3. PEG-based Ionene Polymer Preparation

Bromine end-capped PEG (2 g, 1 eq) and N,N,N',N'-tetramethyl-1,6-hexanediamine (1 eq) were added to a two-neck, round-bottomed flask equipped with a magnetic stirrer and nitrogen inlet. The reaction was allowed to proceed for 24 h at 80 ℃ in MeOH at 20% weight volume percent. The PEG-based ionene dissolved in MeOH was then cast into films. The slow removal of methanol was required to avoid film defects, so it was allowed to evaporate at room temperature for 3 days. Subsequently, the films were heated in TeflonTM molds at 60 ℃ for 2 days. Finally, the polymer films were dried in vacuo (0.1 mmHg) at 30 ℃ for 24 h. The yield for this reaction was 100%. Ionene films were stored in Petri dishes containing desiccant and placed in a desiccator until their

thermal, mechanical, and morphological properties were measured.

4.3.4. Synthesis of PEG-Based Ionenes having 25 wt % Hard Segment (HS)

A flame-dried, 50-mL, two-neck, round-bottomed flask was charged with bromine end-capped 1000 g/mol PEG (2.0 g, 0.5 eq) and 1,12-dibromododecane (0.48 g, 1.47 mmol, 0.5 eq). The flask was purged with nitrogen. N,N,N',N'-Tetramethyl-1,6-hexanediamine (0.64 mL, 2.90 mmol, 1 eq) was added to the flask. The polymerization was performed in the absence of solvent for 24 h at 75°C. The 2000 and 4000 g/mol PPG-ionenes containing 25 wt % HS were also synthesized under the same procedure.

4.3.5. Synthesis of PEG-Based Ionenes having 50 wt % Hard Segment (HS)

A flame-dried, 50-mL, two-neck, round-bottomed flask was charged with bromine end-capped 1000 g/mol PEG (2.0 g, 0.5 eq) and 1,12-dibromododecane (0.48 g, 1.47 mmol, 0.5 eq). The flask was purged with nitrogen. N,N,N',N'-Tetramethyl-1,6-hexanediamine (0.64 mL, 2.90 mmol, 1 eq) was added to the flask. The polymerization was performed in the absence of solvent for 24 h at 75°C. The 2000 and 4000 g/mol PPG-ionenes containing 25 wt % HS were also synthesized under the same procedure.

4.3.6. Synthesis of PEG-Based Ionenes having 75 wt % Hard Segment (HS)

A flame-dried, 50-mL, two-neck, round-bottomed flask was charged with bromine end-capped 1000 g/mol PEG (2.0 g, 0.5 eq) and 1,12-dibromododecane (0.48 g, 1.47 mmol, 0.5 eq). The flask was purged with nitrogen. N,N,N',N'-Tetramethyl-1,6-

hexanediamine (0.64 mL, 2.90 mmol, 1 eq) was added to the flask. The polymerization was performed in the absence of solvent for 24 h at 75℃. The 2000 and 4000 g/mol PPG-ionenes containing 25 wt % HS were also synthesized under the same procedure.

4.3.7. Characterization

1H NMR spectroscopic analyses were performed on Varian INOVA 400 MHz spectrometer to confirm the monomer and polymer composition at ambient temperature. Differential scanning calorimetry (DSC) was conducted on a TA Instruments Q2000 under a nitrogen flow of 50 mL/min. Samples were first heated from room temperature to 150 ℃ at a heating rate of 10 ℃/min. The cooling rate was 10 ℃/min, and the samples were cooled to -80 ℃, and subsequently were heated to 150 ℃ at the same rate. Thermogravimetric analysis (TGA) was conducted on a TA Instruments Hi-Res TGA 2950 under nitrogen at a heating rate of 10 ℃/min. Sample films were solution-cast from methanol into a TeflonTM mold and annealed at 70 ℃ in vacuo for 24 h before testing.

4.4. Results and discussion

4.4.1. Synthesis and characterization of bromine end-capped PEG

Bromine end-capped PEG was synthesized through the method mentioned previously. Respectfully, molecular structures of the bromine end-capped PEG with 1000, 2000 and 4000 g/mol molecular weight PEG segment were confirmed via ^{1}H-NMR spectroscopy (Figure 4.1, Figure 4.2, Figure 4.3). All types of the protons from the chemical structure

were found at the appropriate chemical shift position, also the integration of those two samples indication pure products were obtained from the reaction.

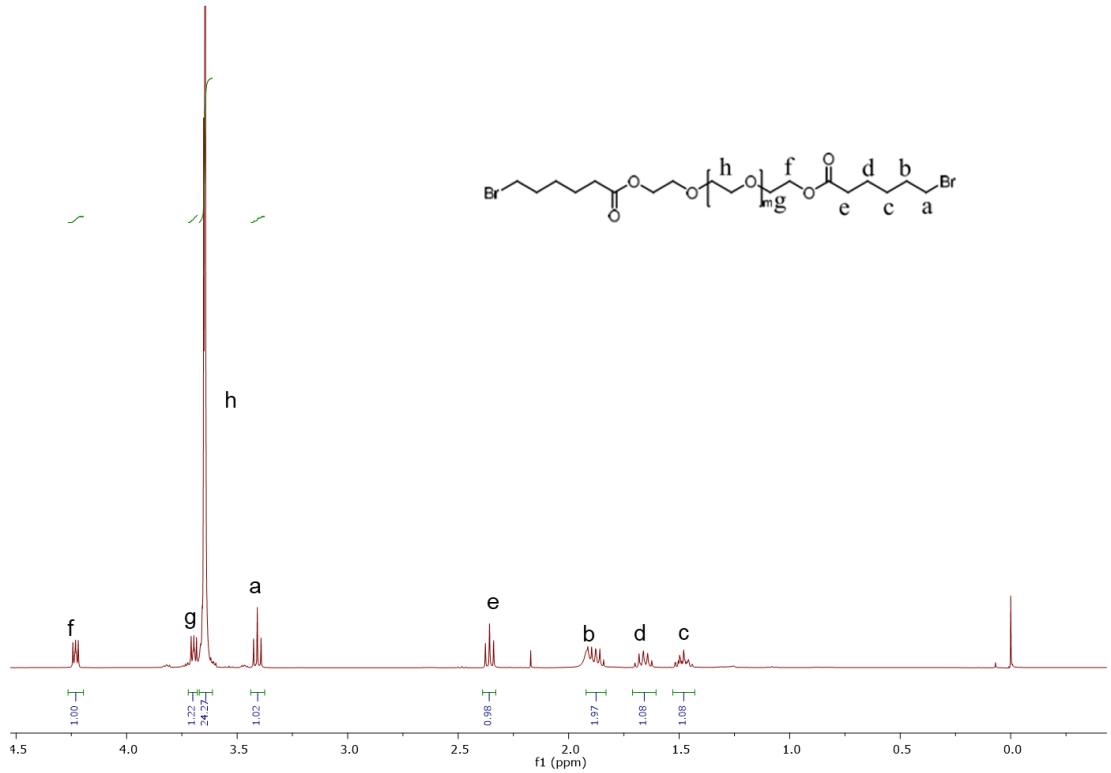

Fig 4.1. ^{1}H-NMR(CD_3Cl) of bromine end-capped PEG1000

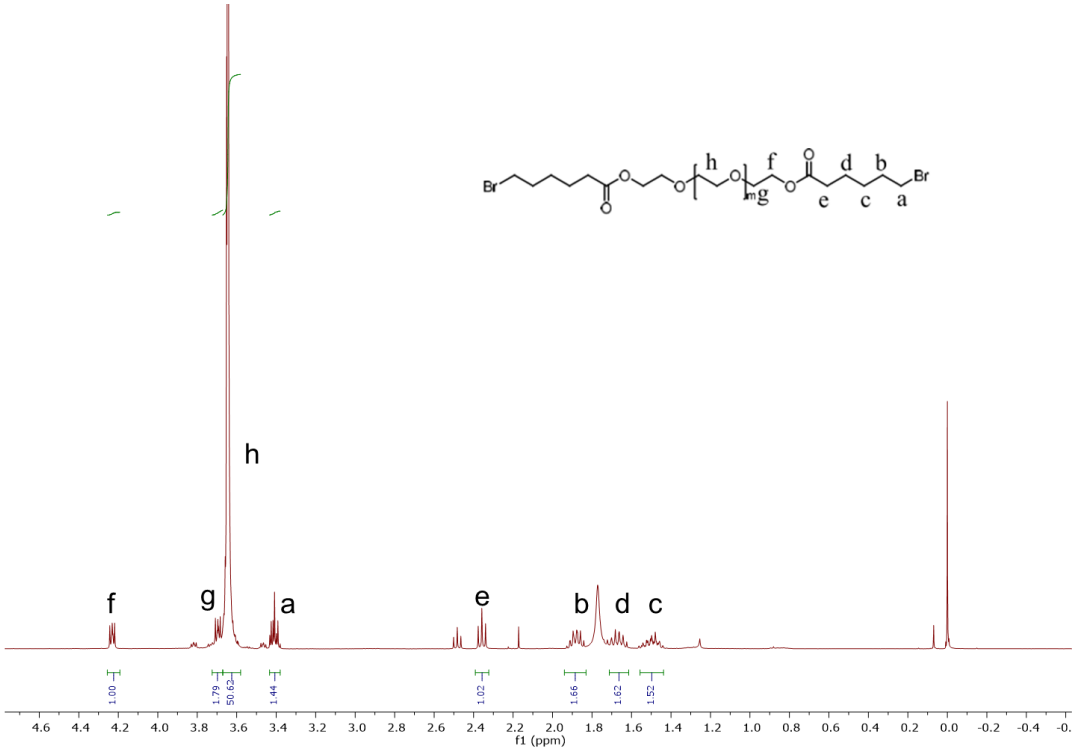

Fig 4.2. ^{1}H-NMR(CD_3Cl) of bromine end-capped PEG2000

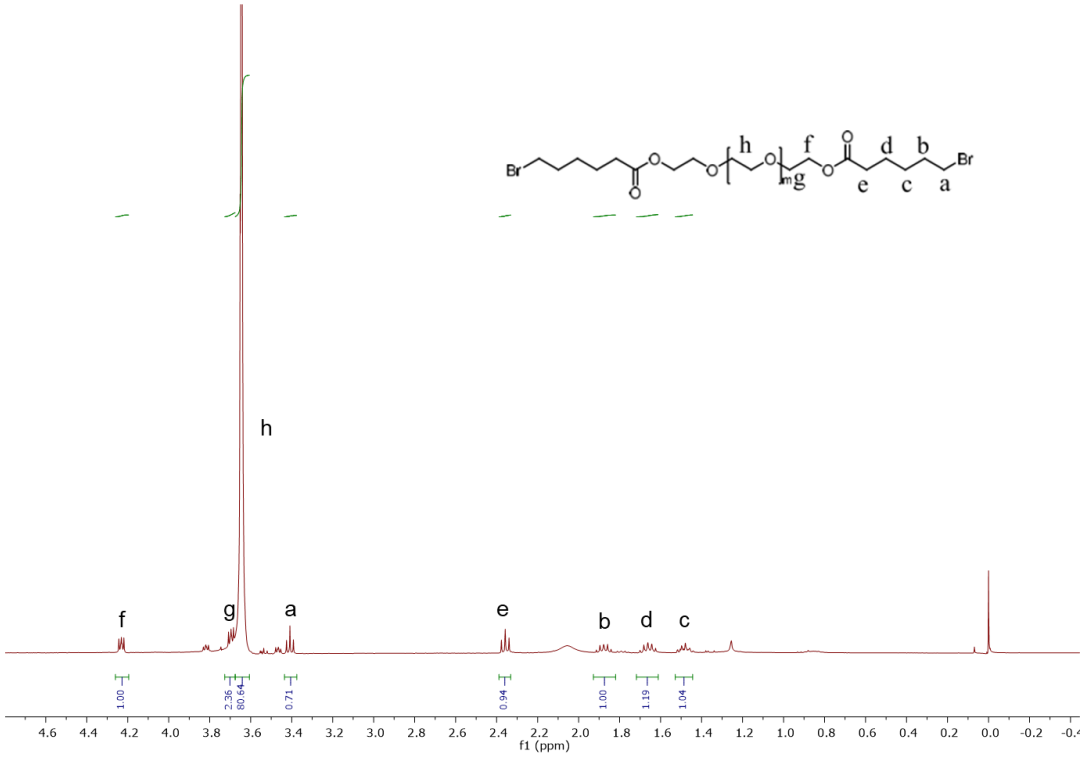

Fig 4.3. ^{1}H-NMR(CD_3Cl) of bromine end-capped PEG4000

4.4.2. Synthesis and characterization of PEG-based ammonium ionene with HS content

The chemical structure of the PEG-based ionenes was confirmed by 1H NMR spectroscopy and TGA (Figure 4.4, Figure 4.5.). The peak at 2.2 ppm, which represents the methyl protons of diamine monomers shifted to ~3.4 ppm in the polymer. This peak is due to the methyl protons connected to the quaternized nitrogens. A 1:1 stoichiometry of diamine to dihalide monomers was used to obtain high molecular weight polymers.

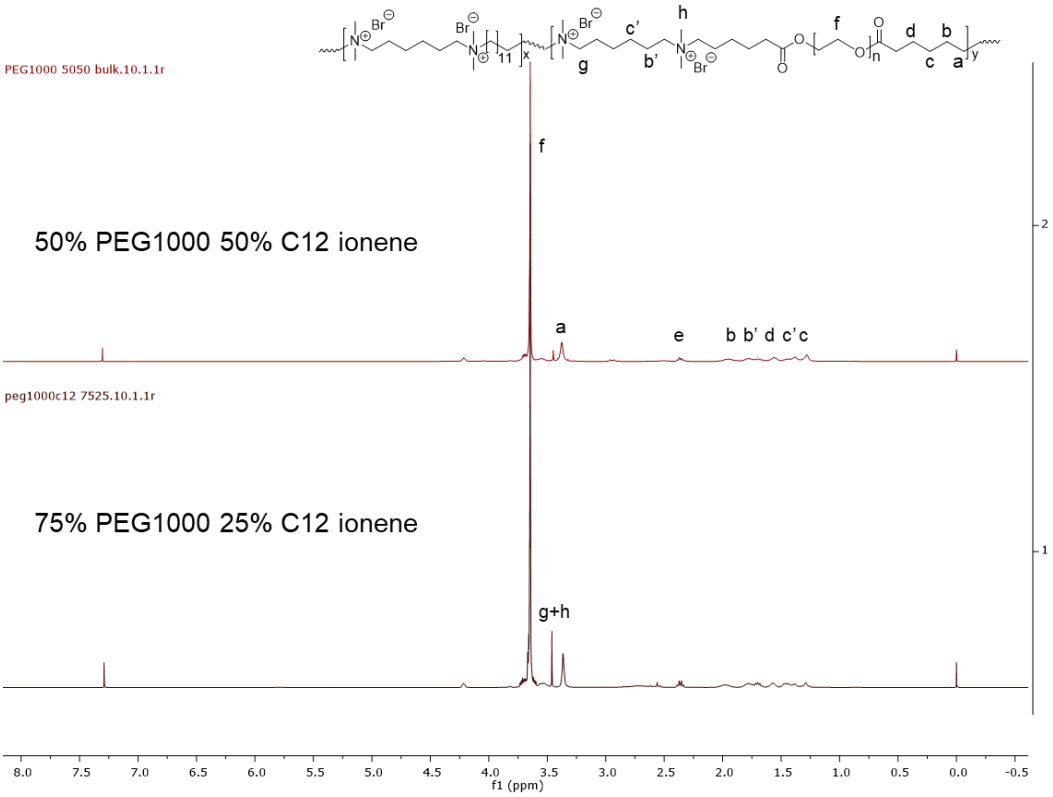

Fig 4.4. ^{1}H-NMR(CD_3Cl) of PEG1000-based ionene with 25 wt% HS and 50 wt% HS.

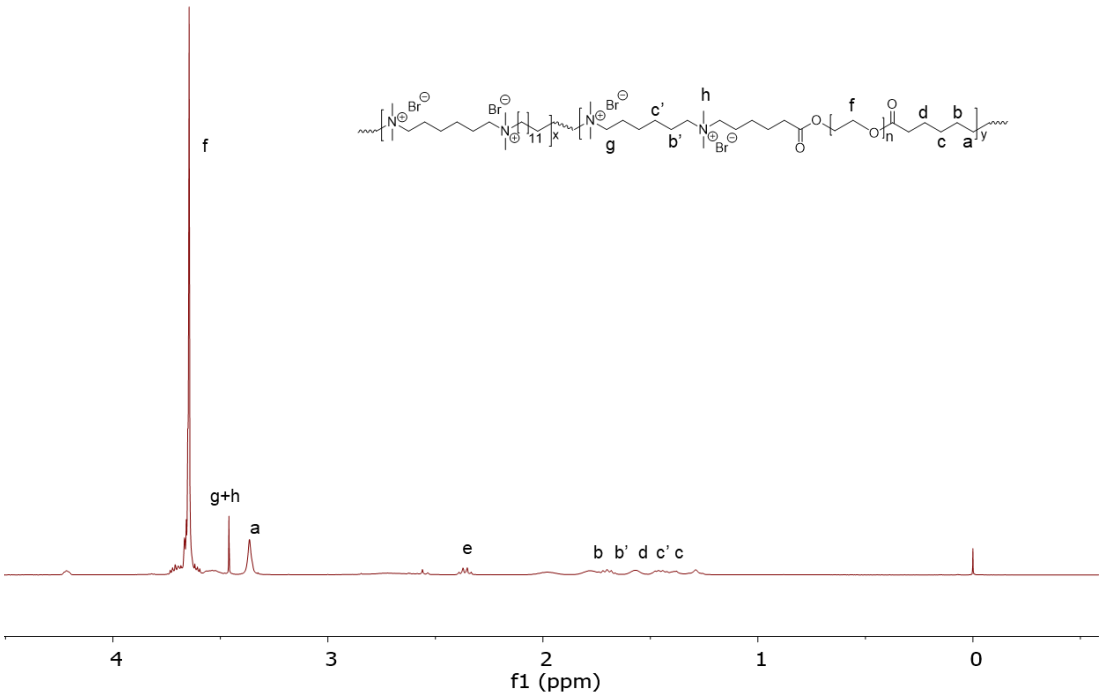

Fig 4.5. ^{1}H-NMR(CD_3Cl) of PEG2000-based ionene with 25 wt% HS.

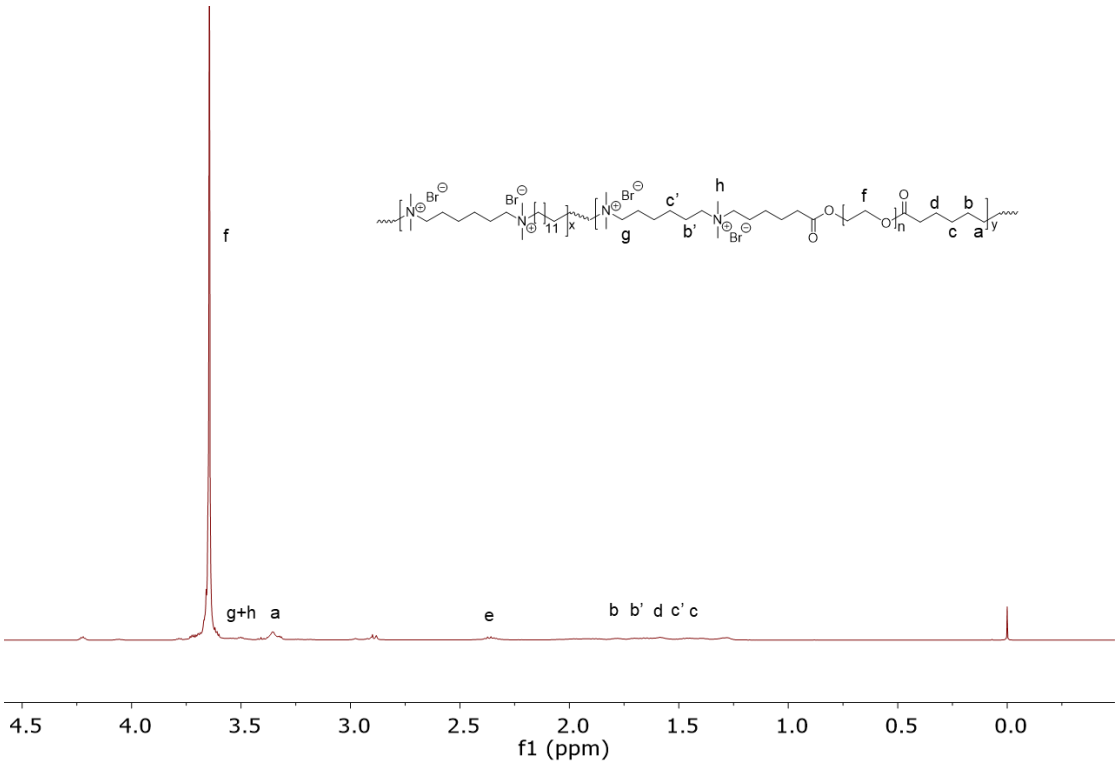

Fig 4.5. ^{1}H-NMR(CD_3Cl) of PEG4000-based ionene with 25 wt% HS.

4.4.3 Effect of hard segment content on the thermal properties of segmented PEG-based and PTMO-based ionenes.

Thermal stability was measured using TGA. 1000, 2000 and 4000 g/mol PEG ionenes containing 0, 25, 50 and 75 wt% HS exhibited weight loss at approximately 240 ºC (Figure 5.4). Thermal stability was measured using TGA, and all ionenes exhibited first weight loss at ~ 230 ℃. The actual mechanism for thermal degradation is complex; however, Chen and coworkers proposed the dequaternization of nitrogens according to the Hoffman elimination pathway. The segmented ionenes degraded in two distinct steps: the first weight loss corresponded to the weight percentage of the HS, and the second weight loss corresponded to the weight percentage of the SS.

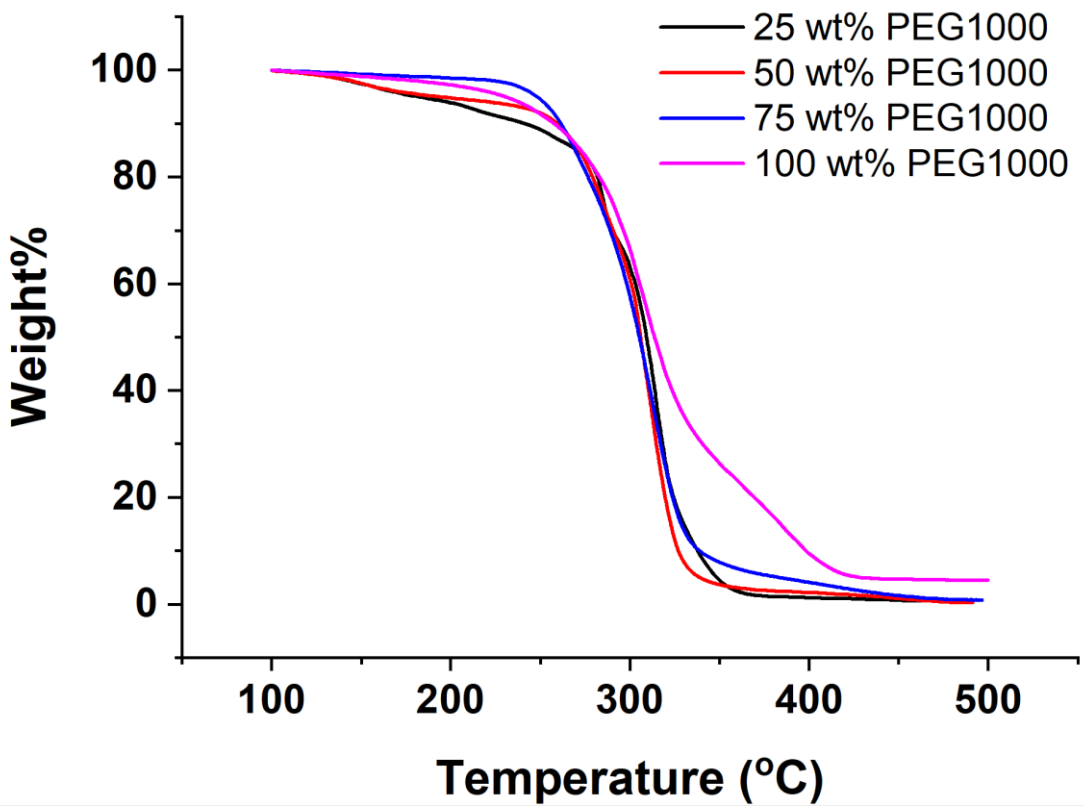

Fig 4.6. TGA overlay s of PEG1000-ionenes having 0wt%, 25 wt%, 50 wt% and 75wt% HS.

The PEG 1000 based ionene system performed two major weight lose slope. The first weight loss happened around 250℃, The actual mechanism for thermal degradation is complex; however, Chen and coworkers[16] proposed the dequaternization of nitrogens according to the Hoffman elimination pathway. The segmented ionenes degraded in two distinct steps: the first weight loss corresponded to the weight percentage of the HS, and the second weight loss corresponded to the weight percentage of the SS, which in this case is the PEG 1000 unit. The soft segment weight curve indicating the weight ratio for the ionenes, which showed an alignment with the weight ratio of the soft segment as designed. The TGA curve of PEG2000 series ionenes brought out a similar story: the first weight loss progress indicating the Hoffman elimination induced hard segment degradation, while the second weight loss curve performed uniformly distributed curves, indicating a nearly equal proportion distribution of soft segment weight ratio. This could be a proof that the ionenes are synthesized correctly.

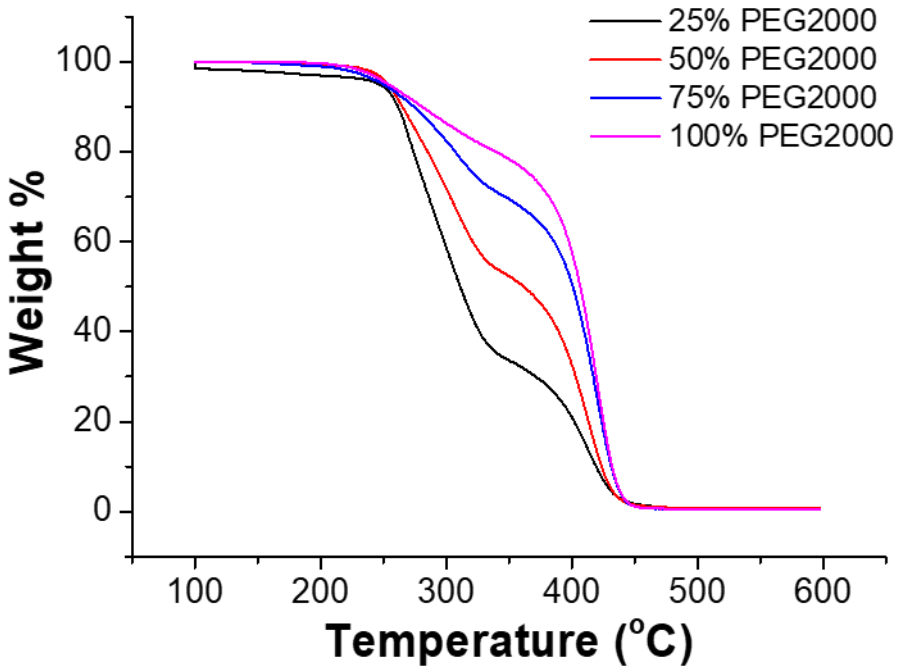

Fig 4.7. TGA overlay s of PEG2000-ionenes having 0wt%, 25 wt%, 50 wt% and 75wt% HS.

4.4.4 Effect of hard segment content on the crystallite of segmented PEG-based and PTMO-based ionenes.

As expected, the 1000 g/mol PEG ionene degraded faster than 4000 g/mol PEG ionene. The faster degradation was attributed to the higher concentrations of HS with lower SS molecular weights.

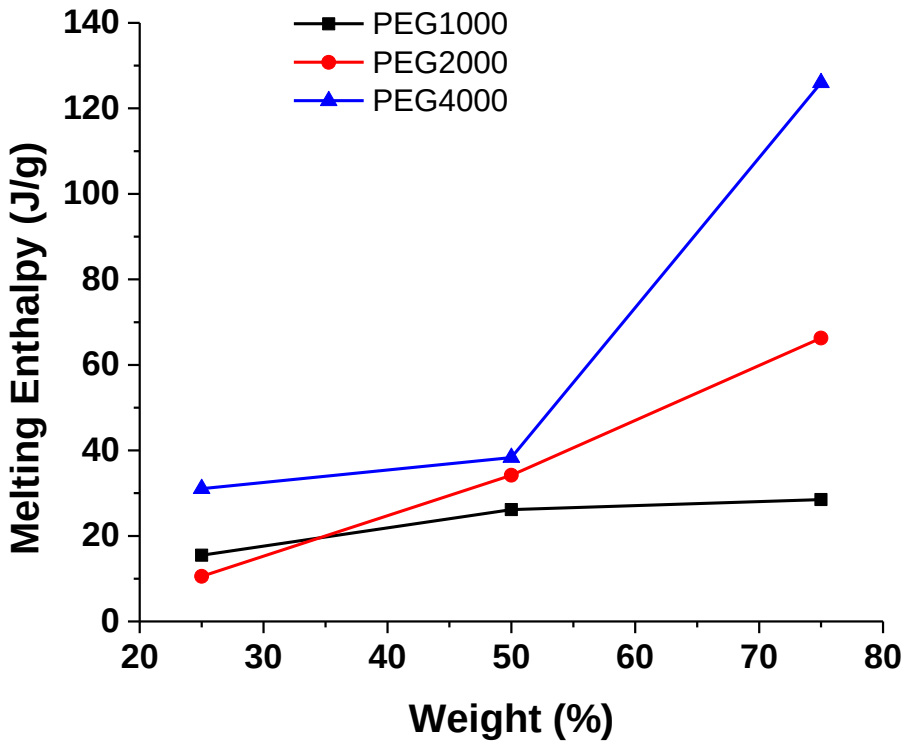

Fig 4.8. The melting enthalpy from DSC of 25 wt%, 50 wt% and 75 wt% PEG ionene.

When increasing the weight ratio of SS segment within the ionenes system, the melting enthalpy from DSC was observed increasing. This should because of the increasing of the SS ratio, more soft segment packing took place within the ionene. This phenomenon also leading to an increase of melting temperature of soft segment crystallite.

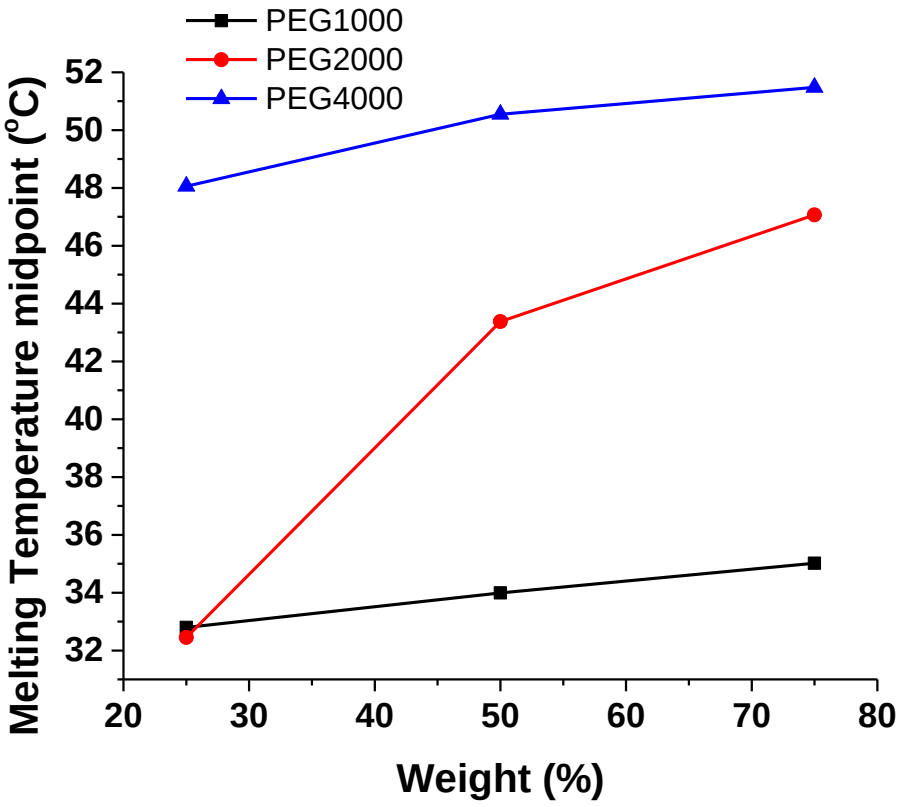

Fig 4.9. The melting temperature midpoint from DSC of 25 wt%, 50 wt% and 75 wt% PEG ionene.

The crystalline properties of the prepared samples were investigated by DSC and X-ray Diffraction (XRD). The summarized DSC data (Fig 4.9) generalized the result of melting enthalpy, which is a representation of crystallite within the system due to the linear relationship between the melting enthalpy and crystallization of the SS in the ionene. A liner relation between the SS weight ratio and PEG ionene ionenes melting enthalpy was observed.

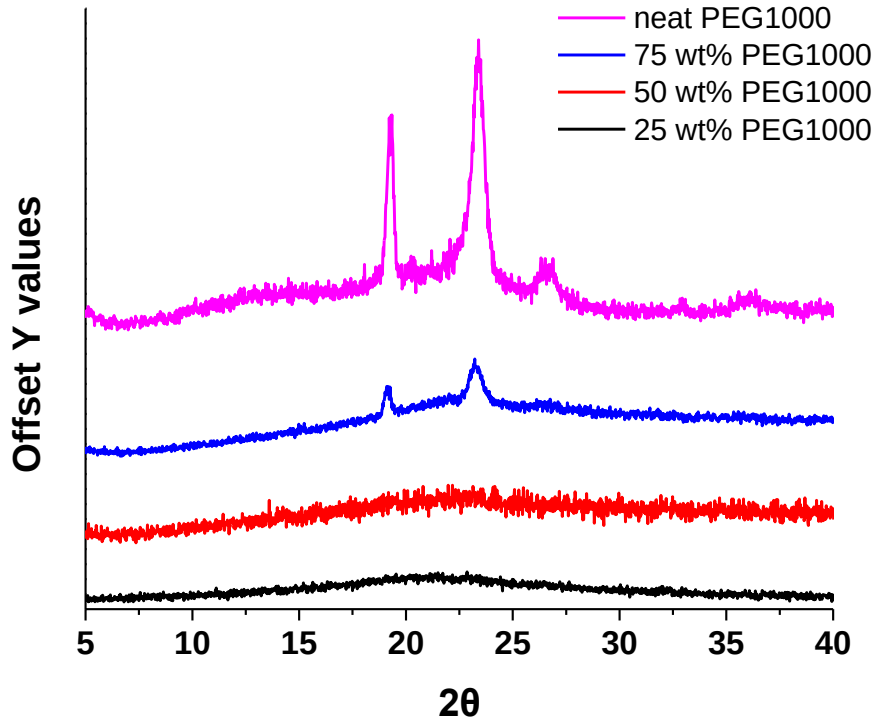

Fig 4.10. The XRD result of PEG1000 ionenes with different HS ratio.

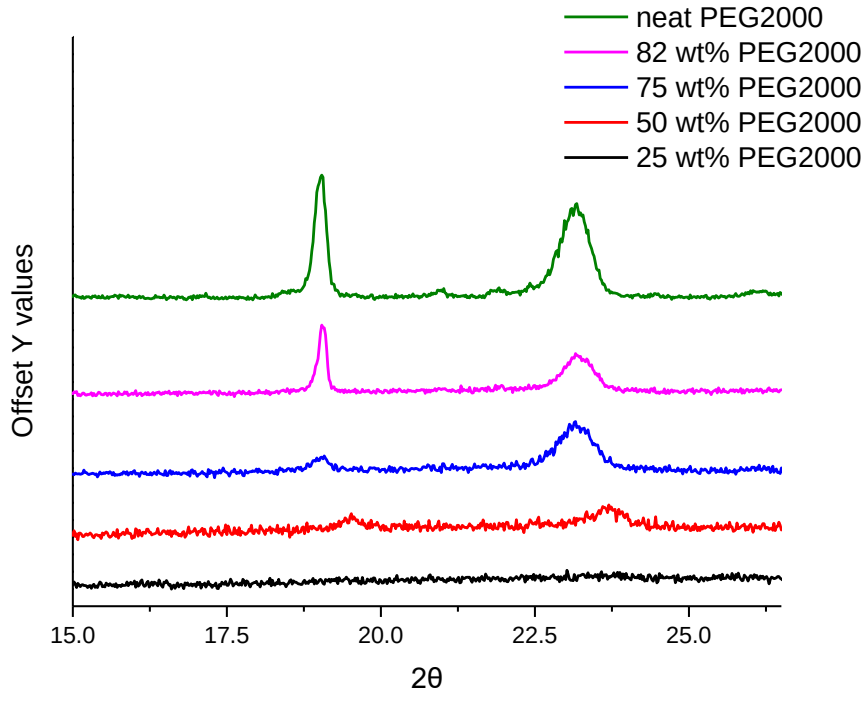

Fig 4.11. The XRD result of PEG2000 ionenes with different HS ratio.

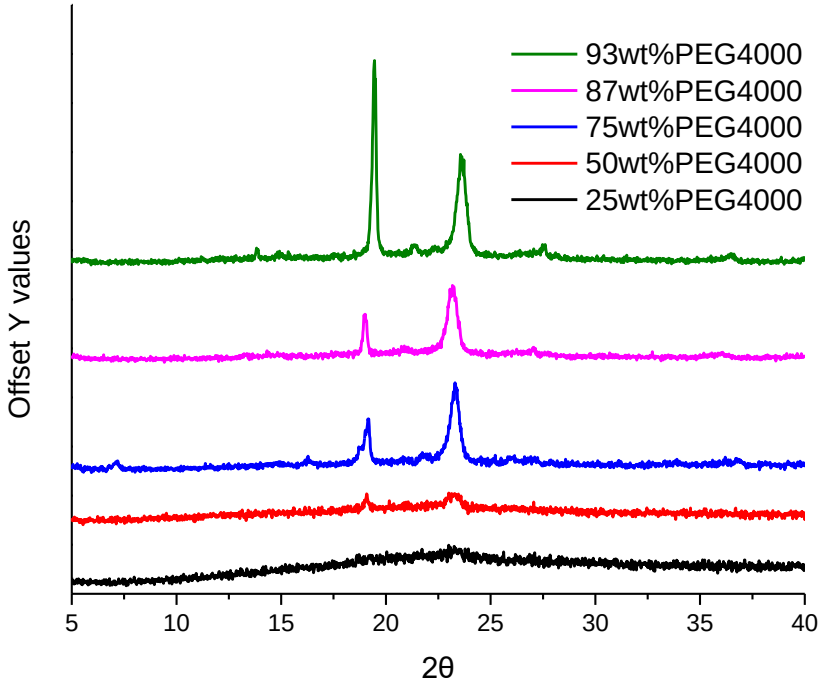

Fig 4.12. The XRD result of PEG4000 ionenes with different HS ratio.

The crystalline properties of the prepared samples were investigated by X-ray Diffraction (XRD). The result of the typical XRD pattern was shown in Figure 4.10., 4.11 and 4.12. The two prominent peaks of PEG (at 2θ = 19.2 and 23.4°) were presented in this pattern, indicating the presence of PEG polymer block. Within the PEG 1000 ionenes samples XRD results, the PEG prominent peaks were observed when the PEG segment weight ratio reached 50%, indicating the aggregation of PEG segment start over 75wt% sample while in 50wt% sample no obvious peak observed, indicating the PEG segment randomly distributed within the system under this weight ratio. Within the PEG 2000 ionenes samples XRD results, the PEG prominent peaks were observed when the PEG segment weight ratio reached 50%, indicating the aggregation of PEG segment start over 50wt% sample while in 25wt% sample no obvious peak observed,

indicating the PEG segment randomly distributed within the system under this weight ratio. The peak intensity at 19.2^{o} show an evidently increasing when the PEG segment weight ratio raised over 80%. The XRD results of PEG 4000 ionenes, however, presented a different version of story that the two prominent peaks from PEG segment were observed within ionene sample with the PEG domain weight ratio as low as 25wt%. The first visibly increasing of peak intensity of both peaks at 19.2 and 23.4 were observed at 75wt% PEG segment sample. Also, the peak intensity of peak at 19.2 displayed a distinct enhancement when the weight ration of PEG segment reaches 93wt%.

4.5. Conclusion

A series of water-soluble random copolymer ionenes were synthesized from 1,12-dibromododecane, N,N,N′,N′-tetramethyl-1,6-hexanediamine, and 1,12-bis(N,Ndimethylamino)dodecane via the Menshutkin reaction. ^{1}H NMR spectroscopy confirmed the ionene structures. PEG-based ionenes showed a single glass transition temperature. For both PEG-based ionene, at lower soft segment(SS) weight ratio range, the microphase separation phenomenon was observed with DSC. The ionenes thermally degraded in one step. The onset degradation temperature was observed at around 248 ºC. The x-ray scattering indicated then increasing of crystallite within the system when the soft segment weight ratio enhanced.

Reference

1. Gibbs, C. F.; Marvel, C. S., Quaternary ammonium salts from bromopropyldialkylammes IV Formation of four-membered rings. *J Am Chem Soc* 1934, *56*, 725-727.

2. Hadek, V.; Noguchi, H.; Rembaum, A., Electrical Properties of 7,7',8,8'-Tetracyanoquinodimethane Salts of Ionene Polymers and Their Model Compounds. *Macromolecules* 1971, *4* (4), 494-&.

3. Noguchi, H.; Rembaum, A., Reactions of N,N,N',N'-Tetramethyl-Alpha,W-Diaminoalkanes with Alpha,W-Dihaloalkanes .1. 1-Y Reactions. *Macromolecules* 1972, *5* (3), 253-&.

4. Rembaum, A.; Baumgart.W; Eisenber.A, Aliphatic Ionenes. *J Polym Sci Pol Lett* 1968, *6* (3pb), 159-&.

5. Williams, S. R.; Long, T. E., Recent advances in the synthesis and structure-property relationships of ammonium ionenes. *Prog Polym Sci* 2009, *34* (8), 762-782.

6. Kohjiya, S.; Ohtsuki, T.; Yamashita, S., Poly-Electrolyte Behavior of an Ionene Containing Poly(Oxytetramethylene) Units. *Makromol Chem-Rapid* 1981, *2* (6-7), 417-420.

7. Kohjiya, S.; Yamashita, S., Synthesis and Physical-Properties of Elastomeric Poly(Oxytetramethylene) Ionene. *Kaut Gummi Kunstst* 1991, *44* (12), 1128-1132.

8. Dimitrov, I. V.; Berlinova, R. V., Synthesis of poly(ethylene oxide)s bearing functional groups along the chain. *Macromol Rapid Comm* 2003, *24* (9), 551-555.

9. Burmistr, M. V.; Sukhyy, K. M.; Shilov, V. V.; Pissis, P.; Polizos, G.; Spanoudaki, A.; Gomza, Y. P., Structure, thermal properties and ionic conductivity of polymeric quaternary ammonium salts (polyionenes) containing ethylene oxide and aliphatic chain fragments. *Solid State Ionics* 2005, *176* (19-22), 1787-1792.

10. Somoano, R.; Yen, S. P. S.; Rembaum, A., .6. Electronic Conductivity of Elastomeric Ionenes. *J Polym Sci Pol Lett* 1970, *8* (7), 467-&.

11. Williams, S. R.; Salas-de la Cruz, D.; Winey, K. I.; Long, T. E., Ionene segmented block copolymers containing imidazolium cations: Structure-property relationships as a function of hard segment content. *Polymer* 2010, *51* (6), 1252-1257.

12. Rutkowska, M., Polyester Polyurethane Ionomers. *J Appl Polym Sci* 1986, *31* (5), 1469-1482.

13. Tamami, M.; Williams, S. R.; Park, J. K.; Moore, R. B.; Long, T. E.,

Poly(Propylene Glycol)-Based Ammonium Ionenes as Segmented Ion-Containing Block Copolymers. *J Polym Sci Pol Chem* 2010, *48* (19), 4159-4167.

14. Schreiner, C.; Bridge, A. T.; Hunley, M. T.; Long, T. E.; Green, M. D., Segmented imidazolium ionenes: Solution rheology, thermomechanical properties, and electrospinning. *Polymer* 2017, *114*, 257-265.

15. Petersen, H.; Fechner, P. M.; Martin, A. L.; Kunath, K.; Stolnik, S.; Roberts, C. J.; Fischer, D.; Davies, M. C.; Kissel, T., Polyethylenimine-graft-poly(ethylene glycol) copolymers: Influence of copolymer block structure on DNA complexation and biological activities as gene delivery system. *Bioconjugate Chem* 2002, *13* (4), 845-854.

16. Ruckenstein, E.; Chen, X. N., Covalent cross-linking of polymers through ionene formation and their thermal de-cross-linking. *Macromolecules* 2000, *33* (24), 8992-9001.

Chapter 5. Spacer Structure-Properties Relation Within Liner Aliphatic Ionenes Polymers

Meng Wang and Matthew D. Green*

School of Molecular Science, Arizona Stater University, Tempe, AZ 85281, USA
School for Engineering of Matter, Transport and Energy, Arizona Stater University, Tempe, AZ 85281, USA

*E-mail address: mdgreen8@asu.edu

5.1. Abstract

Water-soluble random copolymer ammonium ionenes with different charge densities were synthesized using the Menshutkin reaction from bromine end-capped PTMO, bromine end-capped PEG, 1,12-dibromododecane and N,N,N′,N′-tetramethyl1,6-hexanediamine. The macromolecular structures of PEG-based ionene and PTMO-based ionenes were confirmed by ^{1}H NMR spectroscopy and TGA. All PEG-based ionenes showed a single glass transition temperature (Tg) using differential scanning calorimetry (DSC) while the PTMO-based ionenes did not performed glass transition temperature within the test range(-80 ◦C to 150 ◦C). For both PEG-based and PTMO-based ionene, at lower soft segment(SS) weitght ratio range, the microphase separation phenomenoen were observed with DSC. Thermogravimetric analysis (TGA) aslso showed a two step degradation. The first degradation temperature(ionene charging domain degradataion) was observed around 248 ºC. The x-ray scattering indicated then increasing of crystallite within the system when the soft segment weight ratio enhanced.

5.2. Introduction

Previously, based on the reaction of a x-bis(dimethylamino) PTMO oligomers with 1,4-dibromo-p-xylene, Leir and co-workers[1] reported the synthesizing of poly (tetramethylene oxide) (PTMO) ionenes. In 1989, Feng and coworkers[2, 3] investigated the structure-property relationships of polymer ionenes with PTMO as the soft segments (SSs). Those poly ionenes performed elastomeric status, the strain-induced crystallization of the PTMO segment enhanced tensile strengths. Small-angle X-ray scattering (SAXS) analysis confirmed the microphase separation between the dihalide components compared with the PTMO segment. Also, when compared with the higher molecular weight PTMO segments, the ionene having a lower molecular weight PTMO segments are performing better mechanical properties. This unique phenomenon could be contributed to a higher density of ionic associations and stronger physical cross-links. Ikeda et al.[4] reported the effect of counterion type on the morphology of PTMO-containing ionenes. By comparing poly ionenes with different types of counterions (Cl^- and Br^-), Ikeda and coworkers proved that different counterions will influence the size of the ionic domains and distance between the domains. Specifically, Ionenes with bromide counterions showed smaller ionic domains compared with ionenes compared with chloride counterions.

Within the system, the combination of neutral organic and ionic regions in the polymer chains results in biphasic materials containing relatively strong organic crystallites and ionic aggregates. Those two types of aggregation also contribute to the mechanical performance of the polymer ionenes. It is known that the stress-strain behavior is mainly dominated by the soft segment structure and properties, Robbins's

investigation noted that using bromide as counter anion for the ionenes, the mechanical performance of those ionenes were better when compared with the ones contains chloride instead.[5] Prof. Bara and cow-workers observed a self-healing character and shape memory in the ionene-polyamides. The self-healing properties of this type of material are attributed to the inter- and/or intra-molecular forces such as ionic interaction and H-bonding between amide groups. As expected, these features are thermally dependent, as the physical behavior will be altered as the Tg is approached.[6] The film will return to its original state after the application of heat.

Similar self-healing properties were also reported on polyurethanes. [7-11] The hydrogen-bonding of urethane linkages enhanced the phase separation by way of increasing the polarity difference between hard and soft segments in polyurethane elastomers. Both thermal and mechanical properties could be dramatically influenced by the extent of phase separation. Also, the polyurethane polymers performing performed potential for shape memory and self-healing properties with the help of hydrogen-bonding rich environment. By the same token, phase separation could be possibly increased by the incorporation of ionic bonding to the polyurethane backbone due to the highly polar characteristics of ionic bonds. Previously, people developed that polymer with ethylene and methacrylic acid, where some of the methacrylic acid groups exist as their respective sodium salts presented shape memory properties.[12]

Segmented ionenes possessing oligomeric spacers between charge sites were first synthesized in order to obtain ionene polymers with excellent mechanical properties. As shown in this section, many of these segmented ionenes behave mechanically

similarly to polyurethanes. However, polyurethanes are prepared using hazardous isocyanates that produce amines upon hydrolysis. Conversely, ionene synthesis is proposed as more environmentally friendly and inherently less toxic. Furthermore, well-defined polyurethanes are typically prepared in a two-step process; however, ionenes are synthesized in a single step, suggesting a manufacturing advantage over polyurethanes.

Prof. Long and co-worker's study of PTMO-based ionenes focused on the effect of polymer architecture and molecular weight using linear and highly branched PTMO ionenes. They determined that branching structure of soft segment within the system negatively influenced ionic aggregation, regardless of PTMO segment molecular weight. In addition, polymer architecture did not influence Tg. In highly branched PTMO ionenes, DMA results confirmed that the ionic aggregates did not persist since soft segment had melted. However, PTMO ionenes with linear structure performed a linear rubbery plateau region that persisted until ~175 ◦C. They also proved that under certain conditions, the linear structural PTMO ionenes possessed excellent mechanical properties which is similar to the thermoplastic polyurethanes (35 MPa tensile strength and elongations >1000%). Respectfully, the highly branched ionenes revealed lower tensile strengths and elongations. This result suggested that the presence of branching disrupted ionic aggregate formation. Similar result was reported by Loveday et al. who asserted that ionic groups placed regularly along the backbone in a linear fashion were important for favorable mechanical performance.[13]

Previously, Jakeways et al. reported the structure-mechanical properties relation of

varies of polymer contains terephthalate units within the main chain. By comparing the mechanical properties they proved that when comparing poly(ethylene terephthalate) (2GT), poly(trimethylene terephthalate) (3GT), and poly(tetramethylene terephthalate) (4GT), the aliphatic unit length within the mainchain will influence the mechanical property of the polymer. More specifically, those polymer exhibited a ranking of both the recovery and shrinkage behavior of these materials is in the order 3GT > 4GT > 2GT.[14, 15] This results indicating that the spacer between the phenyl ring within the polymer backbone will result in varies mechanical properties of polymer. This phenomenon could because of spacer influencing the π-π stacking between different polymer chains.

Polyethylene glycol contains 2 less carbon within the repeat unit when comparing with PTMO. PEG-containing polymers have unlimited potential for biomedical material applications due to their biocompatibility and low biotoxicity.[16] Previously, Dimitrov and co-workers synthesized PEG-based ionenes in the presence of a N-methyldiethanolamine initiator with an anionic polymerization of ethylene oxide[17]. Dichloromethane was used with the presence of strong base like CsOH or KOH to increase the PEG segment molecular weight undergoing a Williamson-type reaction. The PEG-based polymer was then quaternized to yield a PEG-based ionene. The various functionalized polymers displayed different solution behaviors. For example, when PEG-based polymer was quaternized with methyl halide, the ionene demonstrated typical polyelectrolyte behavior; however, when PEG-based polymer was quaternized with zwitterionic or perfluorinated based halide, dipole-dipole and hydrophobic

interactions will result in the decreasing of hydrodynamic radius. Sukhyy and co-workers recently reported the synthesis, thermal property characterization, and ionic conductivity of novel PEG-based ionenes[18]. As they reported, changing the PEG oligomer molecular weight controlled the charge density. As expected for polyelectrolytes, the Tg increased with increasing charge content. As a result, PEG ionenes that Sukhyy and coworkers examined show a decreasing of the Tg ranged from −52 to −10 ◦C as the PEG repeat unit decreased from 21 to 2.

Our work emphasizes thermal, mechanical and morphological behavior of PEG2000-based ionenes and PTMO2000-based ionenes. The significance of PEG segmented ionenes compared with PTMO ionenes is the absence of SS crystallization. The disadvantage of PTMO ionenes is that crystallization occurs at ambient conditions, and thus influences modulus and ultimate mechanical behavior. With respect to mechanical performance, it is known that stress-strain behavior is predominantly influenced by the soft segment structure, this study confirmed that the choice of aliphatic repeat unit rigidity will influence the soft segment aggregation and the crystallization property within the individual ionene system. Also, the thermal stability between the two systems has been studied.

5.3. Experimental

5.3.1. Materials

PEG 2000 and PTMO 2000 was purchased from Sigma-Aldrich. 6-Bromohexanoyl chloride (97%) was purchased from Alfa Aesar. Triethylamine was purchased from Aldrich and distilled from calcium hydride. 1,12-Dibromododecane (98%) was purchased from Sigma-Aldrich and recrystallized from ethanol. Phenolphthalein and

N,N,N',N'-tetramethyl-1,6-hexanediamine (99%) were purchased from Acros Organics and used as received. Methanol (MeOH, HPLC grade) was purchased from Fisher and used as received.

5.3.2. Synthesis of Bromine End-Capped PEG (Br-PEG-Br)

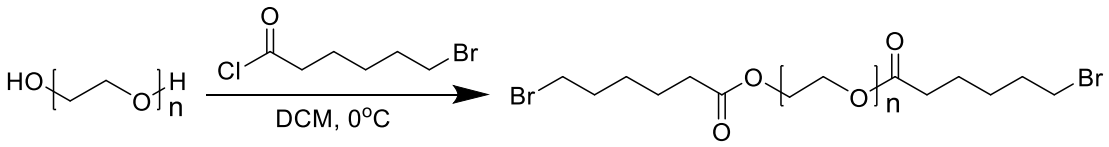

Scheme.1 Synthesis of bromine end-capped PEG using bromo-substituted acyl chlorides.

This reaction was performed according to previous literature precedent[19]. For each PEG length, the molecular weight was determined using a combination of alcohol group titration and analysis by 1H NMR spectroscopy. As an example, poly (tetramethylene oxide (PTMO, 2000 g/mol, 7.00 g,3.5 mmol) and TEA (0.79 g, 7.8 mmol) were mixed in dichloromethane (23 mL) at 0 ℃, and 6-bromohexanoyl chloride (1.68 g,7.8 mmol) was added drop-wise. The mixture was slowly warmed to 23 ℃and stirred for 24 h. Following the reaction, the triethy-lammonium chloride salt was filtered, and the organic phase was washed with a saturated aqueous solution of sodium bicarbonate and water in series. The organic phase was dried over anhydrous sodium sulfate, and removed using rotary evaporation at 23℃. A clear, viscous liquid was obtained

5.3.3. PEG-based polymer ionene preparation

Bromine end-capped PEG (2.48 g, 1 eq) and N,N,N',N'-tetramethyl-1,6-hexanediamine (1 eq) were added to a two-neck, round-bottomed flask equipped with a magnetic stirrer and nitrogen inlet. The reaction was allowed to proceed for 24 h at 80 ℃ in MeOH at 20% weight volume percent. The PEG-based ionene dissolved in MeOH was then cast into films. The slow removal of methanol was required to avoid film defects, so it was allowed to evaporate at room temperature for 3 days. Subsequently, the films were heated in TeflonTM molds at 60 ℃ for 2 days. Finally, the polymer films were dried in vacuo (0.1 mmHg) at 30 ℃ for 24 h. The yield for this reaction was 100%. Ionene films were stored in petri dishes containing desiccant and placed in a desiccator until their thermal, mechanical, and morphological properties were measured.

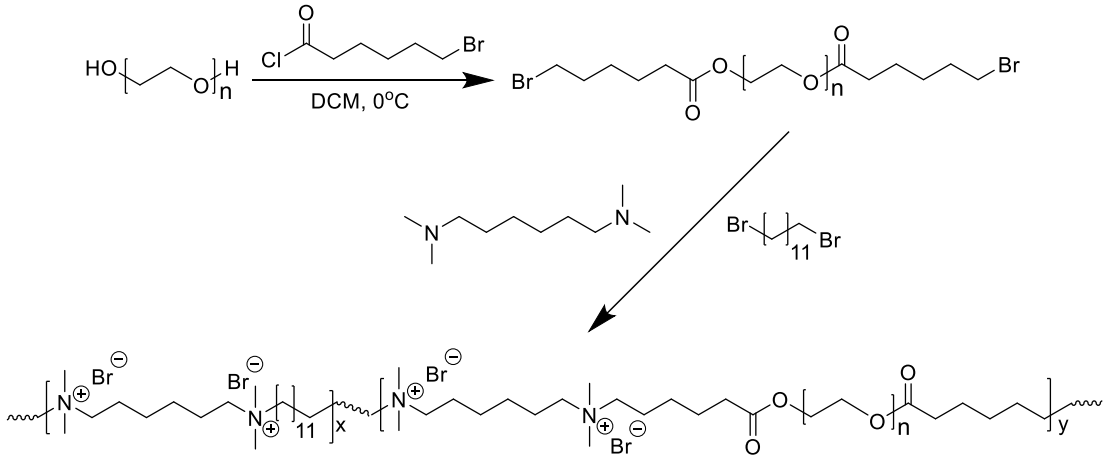

Scheme.2 Synthesis of ionene with bromine end-capped PTMO and 1,12-dibromododecane.

5.3.4. Synthesis of PEG-Based Ionenes having 25 wt % Hard Segment (HS)

A flame-dried, 50-mL, two-neck, round-bottomed flask was charged with bromine end-capped 2000 g/mol PEG (1.44 g, 0.58 mmol) and 1,12-dibromododecane (0.48 g, 1.47 mmol). The flask was purged with nitrogen. N,N,N',N'-Tetramethyl-1,6-hexanediamine (0.35 g, 2.05 mmol, 0.79 eq) was added to the flask. The polymerization was performed in the methanol as a solvent for 24 h at 75°C.

5.3.5. Synthesis of PEG-Based Ionenes having 50 wt % Hard Segment (HS)

A flame-dried, 50-mL, two-neck, round-bottomed flask was charged with bromine end-capped 2000 g/mol PEG (0.96 g, 0.40 mmol) and 1,12-dibromododecane (0.96 g, 2.94 mmol). The flask was purged with nitrogen. N,N,N',N'-Tetramethyl-1,6-hexanediamine (0.57 g, 3.33 mmol) was added to the flask. The polymerization was performed in the methanol as a solvent for 24 h at 75°C.

5.3.6. Synthesis of PEG-Based Ionenes having 75 wt % Hard Segment (HS)

A flame-dried, 50-mL, two-neck, round-bottomed flask was charged with bromine end-capped 2000 g/mol PEG (0.48 g, 0.19 eq) and 1,12-dibromododecane (1.44 g, 4.41 mmol). The flask was purged with nitrogen. N,N,N',N'-Tetramethyl-1,6-hexanediamine (0.79 g, 4.60 mmol) was added to the flask. The polymerization was performed in the methanol as a solvent for 24 h at 75°C.

5.3.7. Synthesis of Bromine End-Capped PTMO (Br-PTMO-Br)

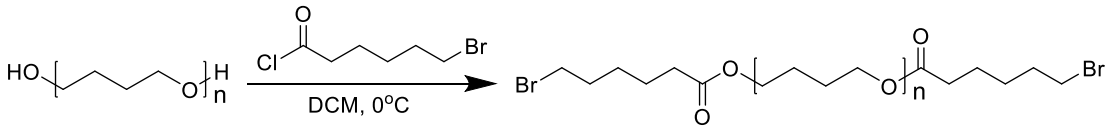

Scheme.3 Synthesis of bromine end-capped PTMO using bromo-substituted acyl chlorides.

This reaction was performed according to previous literature precedent[19]. The molecular weight was determined using a combination of alcohol group titration and analysis by 1H NMR spectroscopy. As an example, poly (tetramethylene oxide (PTMO, 2000 g/mol, 7.00 g, 3.5 mmol) and TEA (0.79 g, 7.8 mmol) were mixed in dichloromethane (23 mL) at 0 ℃, and 6-bromohexanoyl chloride (1.68 g,7.8 mmol) was added drop-wise. The mixture was slowly warmed to 23 ℃and stirred for 24 h. Following the reaction, the triethy-lammonium chloride salt was filtered, and the organic phase was washed with a saturated aqueous solution of sodium bicarbonate and water in series. The organic phase was dried over anhydrous sodium sulfate, and removed using rotary evaporation at 23℃. A clear, viscous liquid was obtained.

5.3.8. Synthesis of PTMO-Based Ionenes having 25 wt % Hard Segment (HS)

A flame-dried, 50-mL, two-neck, round-bottomed flask was charged with bromine end-capped 2000 g/mol PTMO (1.44 g, 0.58 mmol) and 1,12-dibromododecane (0.48 g, 1.47 mmol). The flask was purged with nitrogen. N,N,N’,N’-Tetramethyl-1,6-hexanediamine (0.35 g, 2.05 mmol, 0.79 eq) was added to the flask. The polymerization was performed in the methanol as a solvent for 24 h at 75℃.

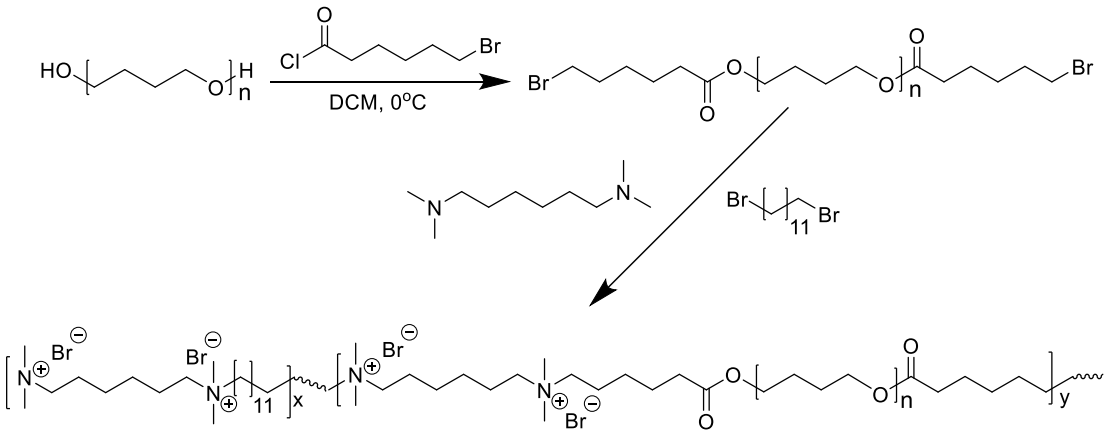

Scheme.4 Synthesis of ionene with bromine end-capped PTMO and 1,12-dibromododecane.

5.3.9. Synthesis of PTMO-Based Ionenes having 50 wt % Hard Segment (HS)

A flame-dried, 50-mL, two-neck, round-bottomed flask was charged with bromine end-capped 2000 g/mol PTMO (0.96 g, 0.40 mmol) and 1,12-dibromododecane (0.96 g, 2.94 mmol). The flask was purged with nitrogen. N,N,N',N'-Tetramethyl-1,6-hexanediamine (0.57 g, 3.33 mmol) was added to the flask. The polymerization was performed in the methanol as a solvent for 24 h at 75°C.

5.3.10. Synthesis of PTMO-Based Ionenes having 75 wt % Hard Segment (HS)

A flame-dried, 50-mL, two-neck, round-bottomed flask was charged with bromine end-capped 2000 g/mol PTMO (0.48 g, 0.19 eq) and 1,12-dibromododecane (1.44 g, 4.41 mmol). The flask was purged with nitrogen. N,N,N',N'-Tetramethyl-1,6-hexanediamine (0.79 g, 4.60 mmol) was added to the flask. The polymerization was performed in the methanol as a solvent for 24 h at 75°C.

5.3.11. Characterization

1H NMR spectroscopic analyses were performed on Varian INOVA 400 MHz spectrometer to confirm the monomer and polymer composition at ambient temperature. Differential scanning calorimetry (DSC) was conducted on a TA Instruments Q2000 under a nitrogen flow of 50 mL/min. Samples were first heated from room temperature to 150 ℃ at a heating rate of 10 ℃/min. The cooling rate was 10 ℃/min, and the samples were cooled to -80 ℃, and subsequently were heated to 150 ℃ at the same rate. Thermogravimetric analysis (TGA) was conducted on a TA Instruments Hi-Res TGA 2950 under nitrogen at a heating rate of 10 ℃/min.

5.4. Results and Discussion

5.4.1. Synthesis and characterization of bromine end-capped PEG and bromine end-capped PTMO2000

H-NMR result of bromine end-capped PEG and bromine end-capped PTMO

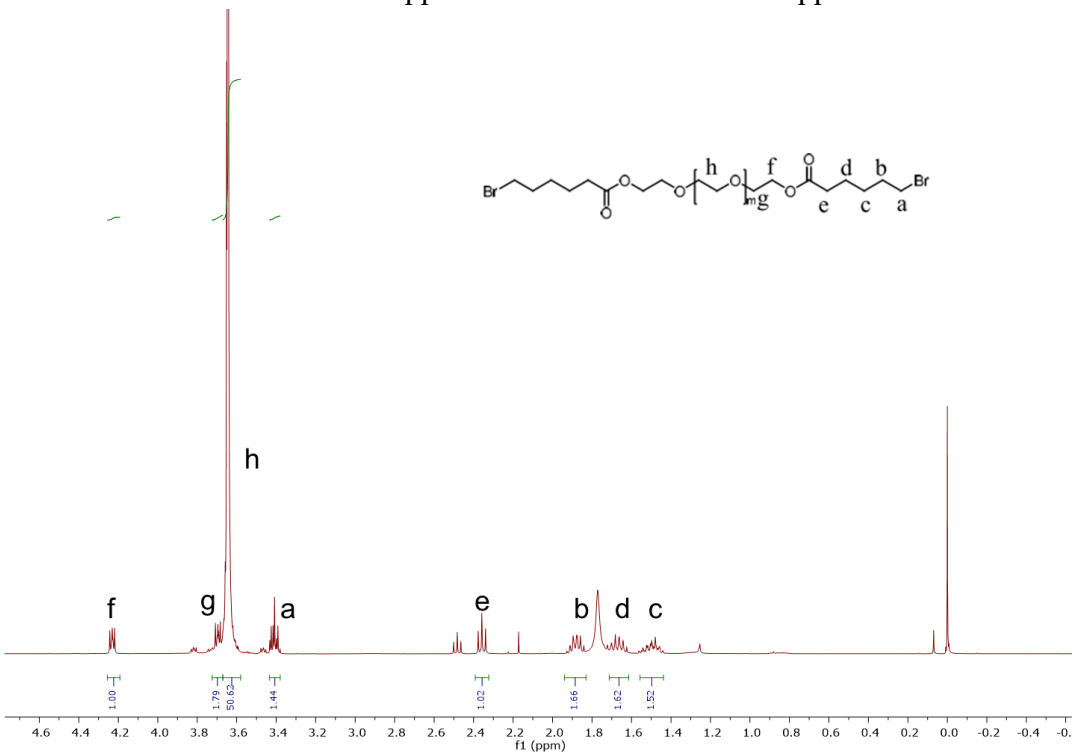

Fig 5.1. ^{1}H-NMR(CD_3Cl) of bromine end-capped PEG

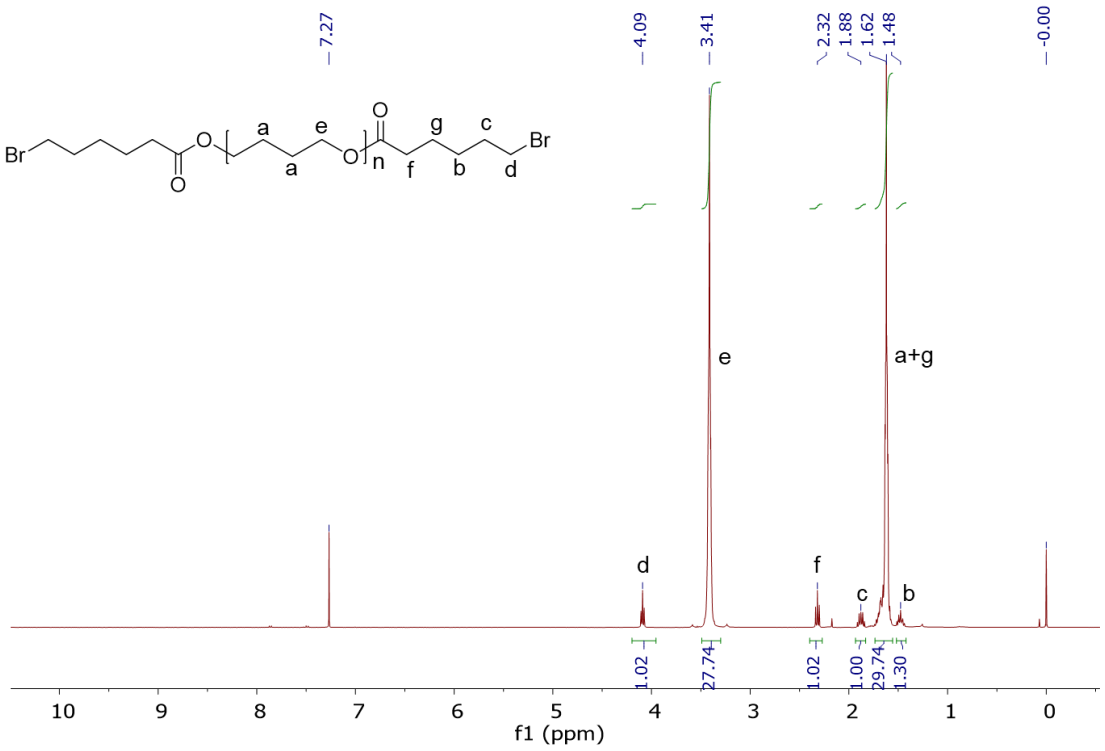

Fig 5.2. ^{1}H-NMR(CD_3Cl) of bromine end-capped PTMO2000

The chemical structure of the bromine end-capped PEG and bromine end-capped PTMO2000 were confirmed by 1H NMR spectroscopy (Figure 5.1, Figure 5.2). More specifically, all types of the protons from the chemical structure were found at the appropriate chemical shift position, also the intergration of those two samples indication pure products were obtained from the reaction.

5.4.2. Synthesis and characterization of PEG2000-based ammonium ionene with HS content

The chemical structure of the PEG-based ionenes were confirmed by 1H NMR spectroscopy and TGA (Figure 5.3, Figure 5.4). The peak at 2.2 ppm, which represents the methyl protons of diamine monomers shifted to ~3.4 ppm in the polymer. This peak is due to the methyl protons connected to the quaternized nitrogens. A 1:1 stoichiometery of diamine to dihalide monomers was used to obtain high molecular

weight polymers.

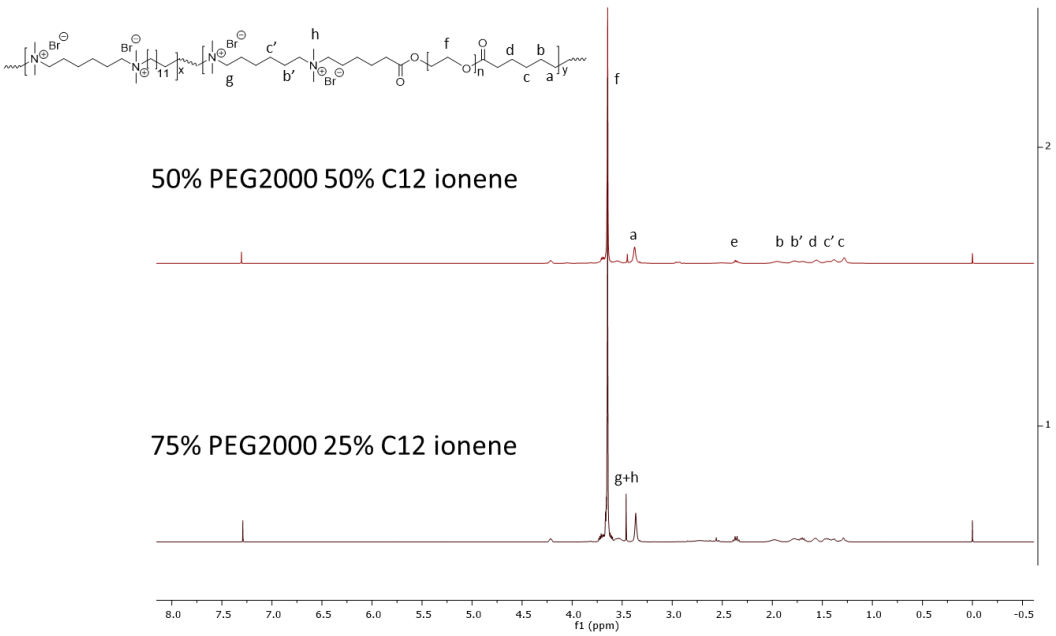

Fig 5.3. ^{1}H-NMR(CD_3Cl) of bromine end-capped PEG2000 ionenes

Thermal stability was measured using TGA. 2000 g/mol PEG ionenes containing 0, 25, 50 and 75 wt% HS exhibited weight loss at approximately 240 ºC (Figure 5.4). Thermal stability was measured using TGA, and all ionenes exhibited first weight loss at ~ 230 ℃. The actual mechanism for thermal degradation is complex; however, Chen and coworkers proposed the dequaternization of nitrogens according to the Hoffman elimination pathway. The segmented ionenes degraded in two distinct steps: the first weight loss corresponded to the weight percentage of the HS, and the second weight loss corresponded to the weight percentage of the SS. As expected, the PEG ionene degraded slower than PTMO ionene, which is due to the higher decomposition temperature.

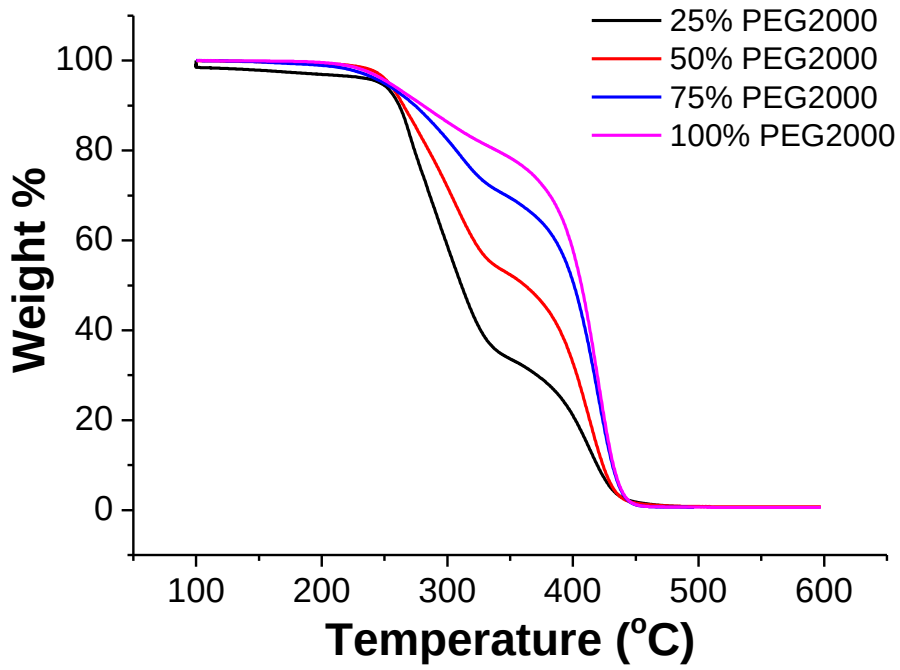

Fig 5.4. TGA overlay s of PEG2000-ionenes having 0wt%, 25 wt%, 50 wt% and 75wt% HS.

5.4.3. Synthesis and characterization of PTMO2000-based ammonium ionene with HS content

The chemical structure of the PEG-based ionenes were confirmed by 1H NMR spectroscopy and TGA (Figure 5.5). The peak at 2.2 ppm, which represents the methyl protons of diamine monomers shifted to ~3.4 ppm in the polymer. This peak is due to the methyl protons connected to the quaternized nitrogens. A 1:1 stoichiometery of diamine to dihalide monomers was used to obtain high molecular weight polymers. Also, peaks at ~ 1.5 ppm become smooth swell indicating the forming of polymer.

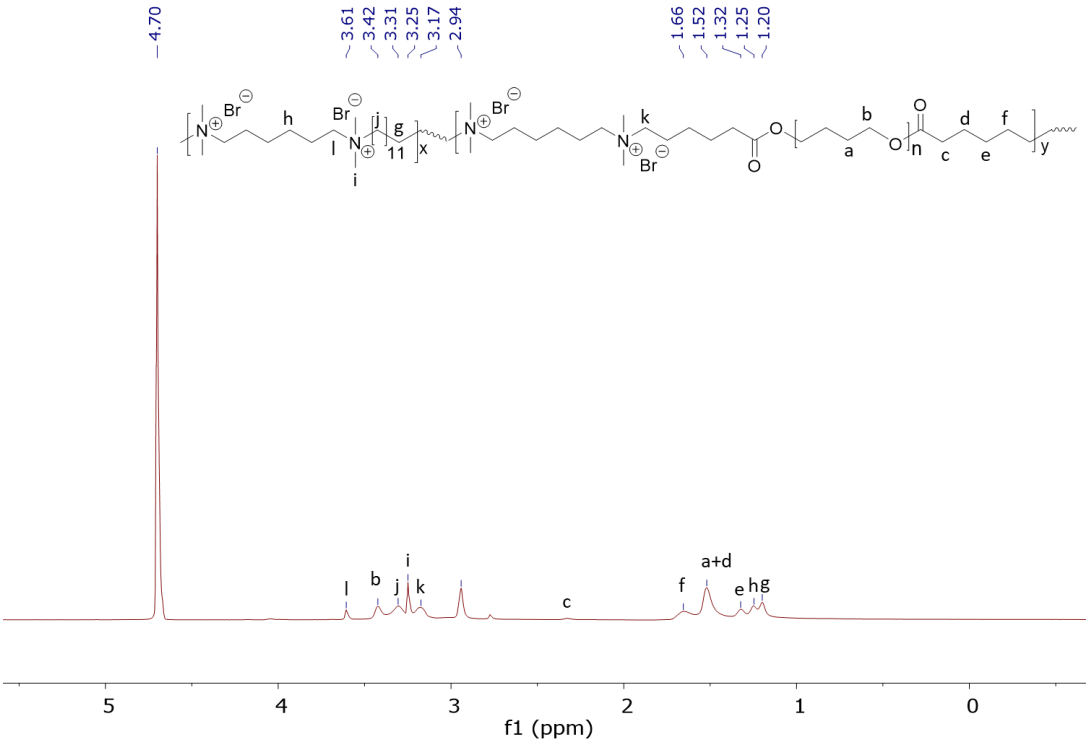

Fig.5.5. ^{1}H-NMR(D_2O) of bromine end-capped PTMO2000 ionenes with 50 wt% HS.

Thermal stability was measured using TGA. 2000 g/mol PEG ionenes containing 0, 25, 50 and 75 wt% HS exhibited weight loss at approximately 240 ºC (Figure 5.4). Thermal stability was measured using TGA, and all ionenes exhibited first weight loss at ~ 230 ℃. The actual mechanism for thermal degradation is complex; however, Chen and coworkers proposed the dequaternization of nitrogens according to the Hoffman elimination pathway. The segmented ionenes degraded in two distinct steps: the first weight loss corresponded to the weight percentage of the HS, and the second weight loss corresponded to the weight percentage of the SS. As expected, the PEG ionene degraded slower than PTMO ionene, which is due to the higher decomposition temperature. It's worth noting that the second weight loss of PTMO ionenes with and/or without start at less than 300 ºC, which is due to the decomposing of PTMO segment.

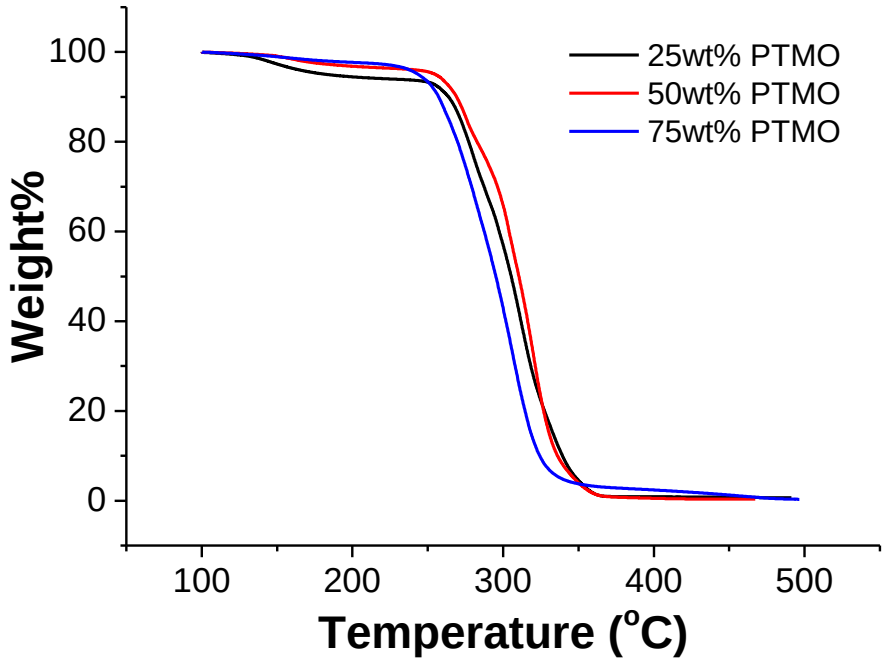

Fig 5.6. TGA overlay s of PEG2000-ionenes having 0wt%, 25 wt%, 50 wt% and 75wt% HS.

5.4.4. Effect of hard segment content on the thermal and mechanical properties of segmented PEG-based and PTMO-based ionenes.

The DSC revealed a single Tg for all ionenes. For the PEG-based ionene sample, DSC analysis revealed a single Tg for all ionenes at approximately -20 ℃, which corresponded to the Tg of the PEG phase (2000 g/mol). For 25 wt% PEG ionenen, one special Tg was observed around 62 ℃. This behavior was due to the microphase separation of PEG SS from the ionic HS. The molar ratio of N,N,N′,N′-tetramethyl-1,6-hexanediamine is increasing when increasing the HS weight ratio. Increasing the shorter segment bearing the quaternized nitrogens, will lead to a higher charge density within the polymer backbone. In general, the increase in charge density leads to an increase in Tg.[20] By comparing the Tg of PEG domain, the Tg decreased from -13 ℃

in 25 wt% PEG ionenes to -28 °C within the 50 wt% PEG ionenes(Fig 5.7. and Fig 5.8.). Herein, we need to consider that as the ratio of PEG segment is increasing and the ratio of HS is decreasing accordingly, the chain lengths and hence the molecular weight of these ionenes would increase. Thus, this fact can slightly affect the Tg values.

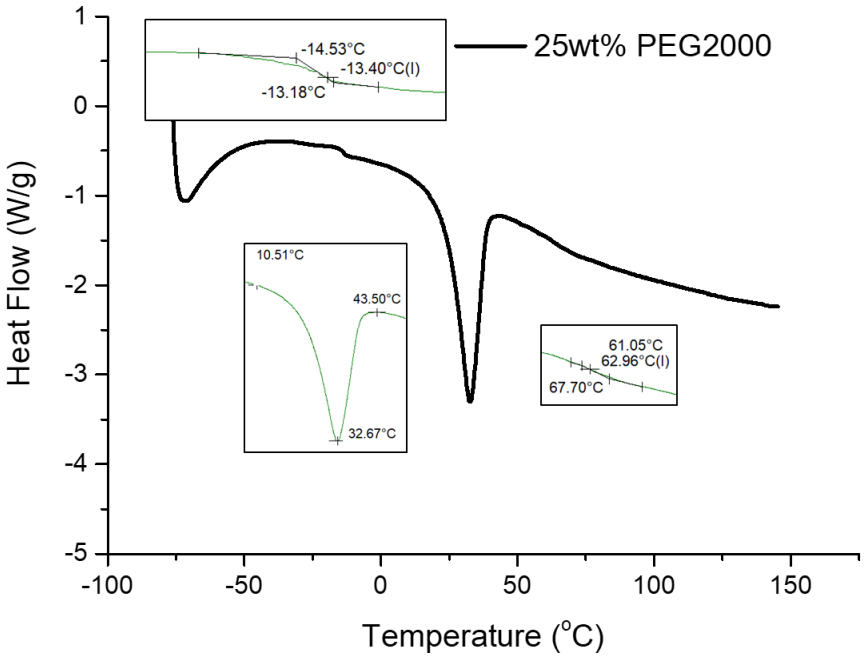

Fig 5.7. DSC result of 25 wt% PEG2000 ionene.

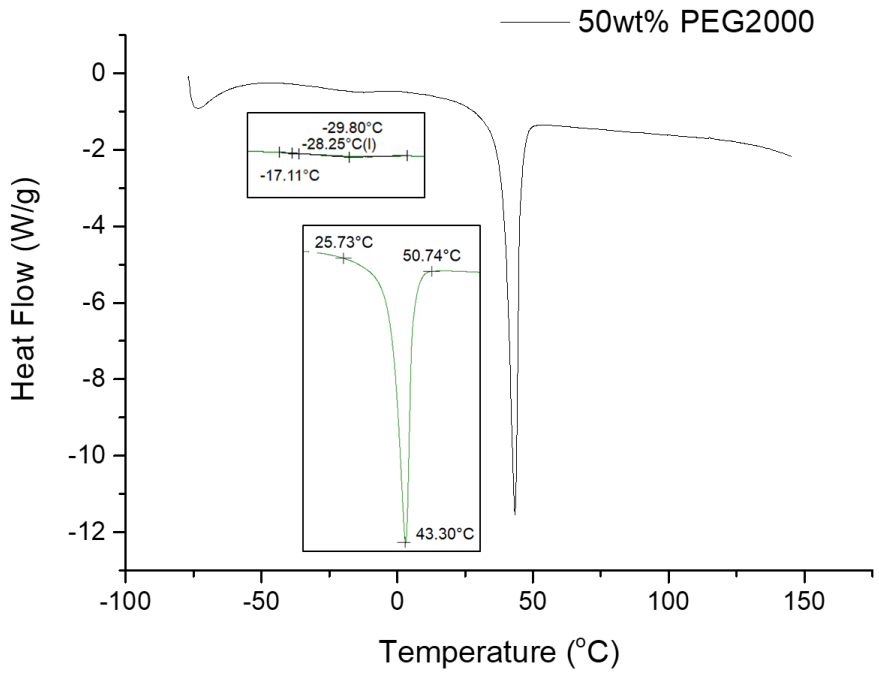

Fig. 5.8. DSC result of 50 wt% PEG2000 ionene.

For 25 wt% PTMO ionene, one special Tg was observed around 120 ℃. This behavior was due to the microphase separation of PEG SS from the ionic HS. When increasing the weight ratio of PTMO segment within the system to 50 wt%, similar phenomenoen appears around 60 ℃. This behavior was due to the microphase separation of PEG SS from the ionic HS.

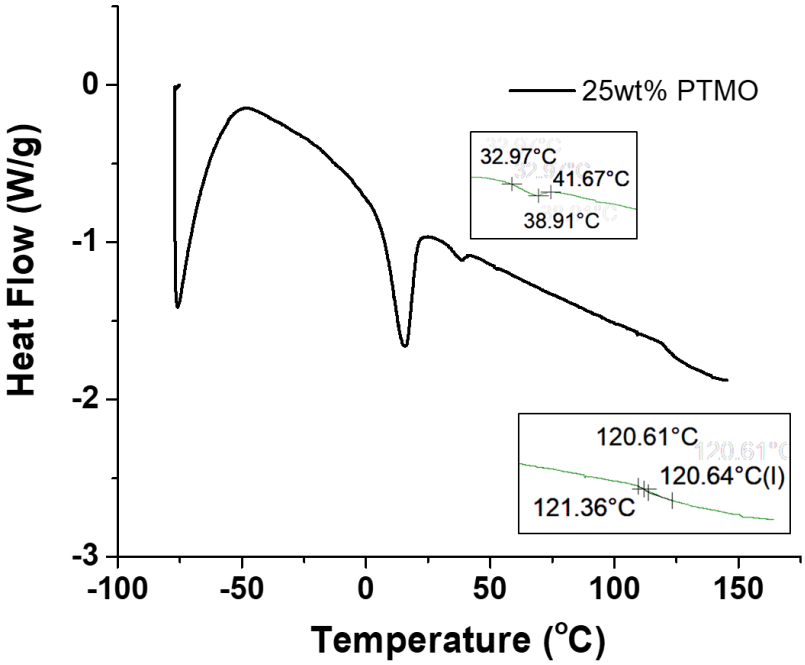

Fig. 5.9. DSC result of 25 wt% PEG2000 ionene.

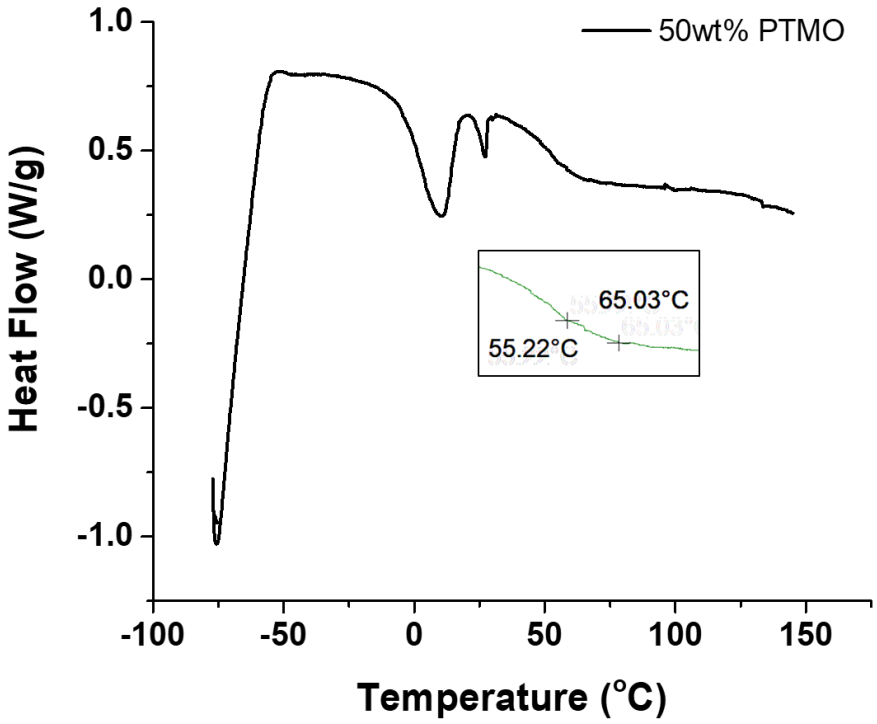

Fig. 5.10. DSC result of 50 wt% PEG2000 ionene.

When increasing the weight ratio of SS segment within the ionenes system, the melting enthalphy from DSC was orbsered increasing. This should because of the in creasing of the SS ratio, more soft segment packing took place within the ionene. This phenomenon also leading to an increasing of melting temperature of soft segment crystallite.

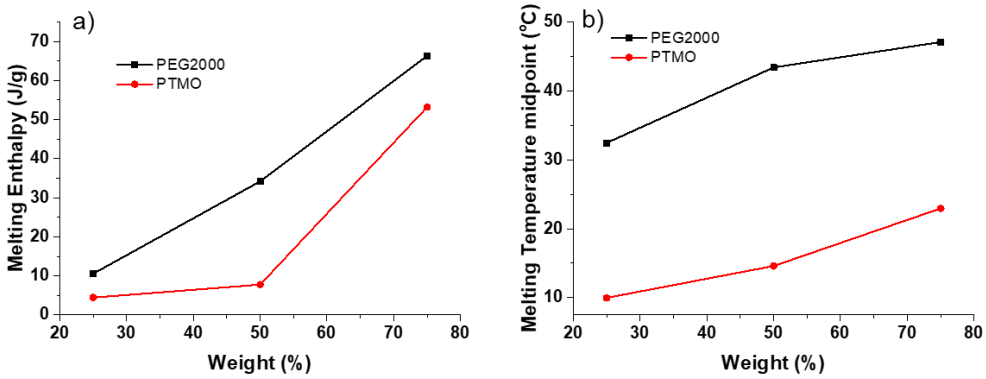

Fig. 5.11. DSC result of 25 wt%, 50 wt% and 75 wt% PEG2000 ionene. Fig. 11a, the melting enthalpy of PEG-based ionenes and PTMO-based ionenes. Fig. 11b, the melting temperature midpoint of PEG-based ionenes and PTMO-based ionenes.

5.4.5 Effect of Hard Segment Content on the Crystallite of Segmented PEG-based and PTMO-based Ionenes

The crystalline properties of the prepared samples were investigated by DSC and X-ray Diffraction (XRD). The summarized DSC data (Fig 5.11. a) generalized the result of melting enthalpy, which is a represent of crystallite within the system due to the liner relationship between the melting enthalpy and crystallization of the SS in the ionene. An liner realation between the SS weight ratio and PEG 2000 ionene ionenes melting enthalpy was observed. The PTMO ionenes brought a similar story, when the weight ratio of SS increased, melting enthalpy showed a non-liner upward trend. This could because of the melting temperature of PTMO 50 wt% ????? The melting temperature

of 50 wt% PTMO ionene confirmed the result out of that. Also, the melting temperature of PTMO saries ionenes indicating that XRD test result under room temperature might be influenced because of the PTMO ionenes melting/melt while runging the test or beforehead.

The result of typical XRD pattern was shown in Figure 5.12. and Fig 5.13. The two prominent peaks of PEG (at 2θ = 19.2 and 23.4°) were presented in this pattern, indicating the presence of PEG polymer block. Within the PEG 2000 ionenes samples XRD results, the PEG prominent peaks were observed when the PEG segment weight ratio reached 50%, indicating the aggregation of PEG segment start over 50wt% sample while in 25wt% sample no obvious peak observed, indicating the PEG segment randomly distributed within the system under this weight ratio. The PEG crystallinity of peak at 23.4^{o} reaches XXX at 75wt% ration of PEG segment. The peak intensity at 19.2^{o} show an evidently increasing when the PEG segment weight ratio raised over 80%. The PTMO XRD diffraction peaks at 19.5^{o} and 24.0^{o} were observed within PTMO ionene samples with PTMO segment over 75wt%, indicating weaker soft segment assembling presented within PTMO sample compared with PEG sample. This could due to the weaker inter molecular force between PTMO compared to PEG segment. Which also could be the reason why PTMO based ionene polymer performed lower melting temperature compared with PEG based ionene polymers.

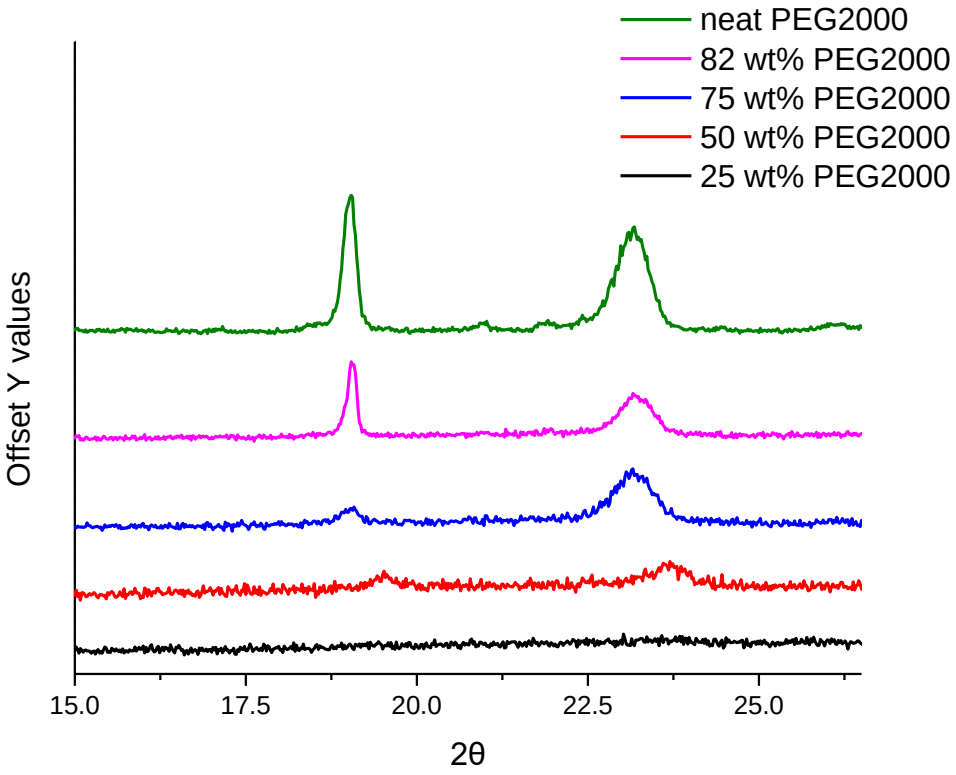

Fig. 5.12. Overlayed XRD result of PEG2000 ionene with different HS weight ratio.

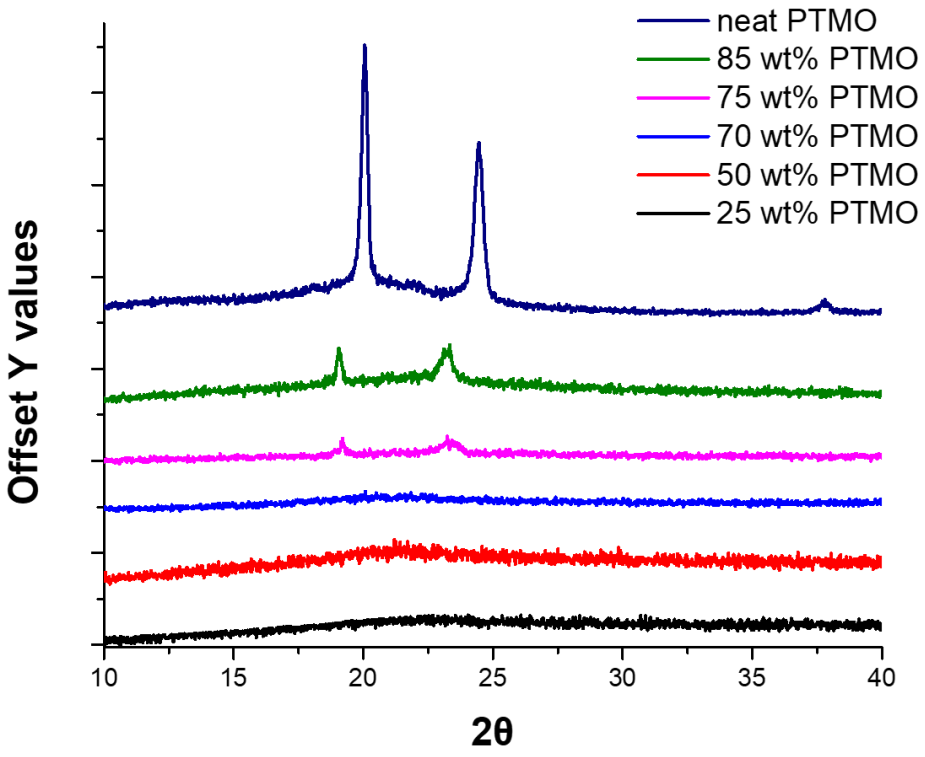

Fig. 5.13. Overlayed XRD result of PTMO2000 ionene with different HS weight ratio.

5.5. Conclusion

A series of water-soluble random copolymer ionenes were synthesized from 1,12-dibromododecane, N,N,N′,N′-tetramethyl-1,6-hexanediamine, and 1,12-bis(N,Ndimethylamino)dodecane via the Menshutkin reaction. 1H NMR spectroscopy confirmed the ionene structures. PEG-based ionenes showed a single glass transition temperature. Their glass transition temperature increased from -30 ºC to -13 ºC as the charge density of ionenes increased. While the PTMO-based ionene did not performed glass transition temperature within the -80 ºC to 150 ºC range. For both PEG-based and PTMO-based ionene, at lower soft segment(SS) weitght ratio range, the microphase separation phenomenoen were observed with DSC. The ionenes thermally degraded in one step. The onset degradation temperature was observed at around 248 ºC. The x-ray scattering indicated then increasing of crystallite within the system when the soft segment weight ratio enhanced.

Reference

1. Leir, C. M.; Stark, J. E., Ionene Elastomers from Polytetramethylene Oxide Diamines and Reactive Dihalides .1. Effect of Dihalide Structure on Polymerization and Thermal Reversibility. *J Appl Polym Sci* 1989, *38* (8), 1535-1547.

2. Feng, D.; Venkateshwaran, L. N.; Wilkes, G. L.; Leir, C. M.; Stark, J. E., Structure-Property Behavior of Elastomeric Segmented Ptmo Ionene Polymers .2. *J Appl Polym Sci* 1989, *38* (8), 1549-1565.

3. Feng, D.; Wilkes, G. L.; Leir, C. M.; Stark, J. E., Morphological Investigation of Polytetra-Methyleneoxide-Dibromoxylene Segmented Ionene Polymers by Transmission Electron-Microscopy and Small-Angle X-Ray-Scattering. *J Macromol Sci Chem* 1989, *A26* (8), 1151-1181.

4. Ikeda, Y.; Yamato, J.; Murakami, T.; Kajiwara, K., Aliphatic poly(oxytetramethylene) ionenes: effect of counter-anion on the properties and morphology. *Polymer* 2004, *45* (25), 8367-8375.

5. Klun, T. P.; Wendling, L. A.; Vanbogart, J. W. C.; Robbins, A. F., Structure Property Relationships of Ionene Polymers. *J Polym Sci Pol Chem* 1987, *25* (1), 87-109.

6. Kammakakam, I.; O'Harra, K. E.; Dennis, G. P.; Jackson, E. M.; Bara, J. E., Self-healing imidazolium-based ionene-polyamide membranes: an experimental study on physical and gas transport properties. *Polym Int* 2019, *68* (6), 1123-1129.

7. Yang, Y.; Urban, M. W., Self-Repairable Polyurethane Networks by Atmospheric Carbon Dioxide and Water. *Angew Chem Int Edit* 2014, *53* (45), 12142-12147.

8. Urban, M. W.; Davydovich, D.; Yang, Y.; Demir, T.; Zhang, Y. Z.; Casabianca, L., Key-and-lock commodity self-healing copolymers. *Science* 2018, *362* (6411), 220-+.

9. Yang, Y.; Urban, M. W., Self-Healing of Polymers via Supramolecular Chemistry. *Adv Mater Interfaces* 2018, *5* (17).

10. Leng, J. S.; Lan, X.; Liu, Y. J.; Du, S. Y., Shape-memory polymers and their composites: Stimulus methods and applications. *Prog. Mater. Sci.* 2011, *56* (7), 1077-1135.

11. Huang, L.; Yi, N.; Wu, Y.; Zhang, Y.; Zhang, Q.; Huang, Y.; Ma, Y.; Chen, Y., Multichannel and Repeatable Self-Healing of Mechanical Enhanced Graphene-Thermoplastic Polyurethane Composites. *Adv Mater* 2013, *25* (15), 2224-2228.

12. Williams, K. A.; Dreyer, D. R.; Bielawski, C. W., The underlying chemistry of self-healing materials. *Mrs Bull* 2008, *33* (8), 759-765.

13. Loveday, D.; Wilkes, G. L.; Bheda, M. C.; Shen, Y. X.; Gibson, H. W., STRUCTURE-PROPERTY RELATIONSHIPS IN SEGMENTED POLYVIOLOGEN IONENE ROTAXANES. *Journal of Macromolecular Science-Pure and Applied Chemistry* 1995, *A32* (1), 1-27.

14. Ward, I. M.; Wilding, M. A.; Brody, H., MECHANICAL-PROPERTIES AND STRUCTURE OF POLY(META-METHYLENE TEREPHTHALATE) FIBERS. *J Polym Sci Pol Phys* 1976, *14* (2), 263-274.

15. Jakeways, R.; Ward, I. M.; Wilding, M. A.; Hall, I. H.; Desborough, I. J.;

Pass, M. G., CRYSTAL DEFORMATION IN AROMATIC POLYESTERS. *J Polym Sci Pol Phys* 1975, *13* (4), 799-813.

16. Petersen, H.; Fechner, P. M.; Martin, A. L.; Kunath, K.; Stolnik, S.; Roberts, C. J.; Fischer, D.; Davies, M. C.; Kissel, T., Polyethylenimine-graft-poly(ethylene glycol) copolymers: Influence of copolymer block structure on DNA complexation and biological activities as gene delivery system. *Bioconjugate Chem* 2002, *13* (4), 845-854.

17. Dimitrov, I. V.; Berlinova, R. V., Synthesis of poly(ethylene oxide)s bearing functional groups along the chain. *Macromol Rapid Comm* 2003, *24* (9), 551-555.

18. Burmistr, M. V.; Sukhyy, K. M.; Shilov, V. V.; Pissis, P.; Polizos, G.; Spanoudaki, A.; Gomza, Y. P., Structure, thermal properties and ionic conductivity of polymeric quaternary ammonium salts (polyionenes) containing ethylene oxide and aliphatic chain fragments. *Solid State Ionics* 2005, *176* (19-22), 1787-1792.

19. Tamami, M.; Williams, S. R.; Park, J. K.; Moore, R. B.; Long, T. E., Poly(Propylene Glycol)-Based Ammonium Ionenes as Segmented Ion-Containing Block Copolymers. *J Polym Sci Pol Chem* 2010, *48* (19), 4159-4167.

20. Tsutsui, T.; Tanaka, R.; Tanaka, T., MECHANICAL RELAXATIONS IN SOME IONENE POLYMERS .1. EFFECT OF ION CONCENTRATION. *Journal of Polymer Science Part B-Polymer Physics* 1976, *14* (12), 2259-2271.

Chapter 6. Stimuli triggered crystallite in PTMO/PEG Ionenes

Meng Wang and Matthew D. Green*

School of Molecular Science, Arizona Stater University, Tempe, AZ 85281, USA
School for Engineering of Matter, Transport and Energy, Arizona Stater University, Tempe, AZ 85281, USA

*E-mail address: mdgreen8@asu.edu

6.1 Abstract

Stimuli (Strain) induced crystallization is a phenomenon in which an initially amorphous solid material undergoes a phase transformation due to the application of strain. Strain crystallization occurs in natural rubber, as well as other elastomers and polymers. Segmented ionenes are a class of thermoplastic elastomers that contain a permanent charged group within the polymer backbone and a spacer segment with a low glass transition temperature (Tg) to provide flexibility. Ionenes are of interest because of their synthetic versatility, unique morphologies, and ionic nature. Using phase changing ionene-based nanocomposites could be extended to create reversible mechanically, electrically, optically, and/or thermally responsive materials depending on constituent nanoparticles and polymers. This talk will discuss recent efforts to utilize the synthetic versatility of ionenes (e.g., spacer composition of PTMO or PEG) to prepare percolated ionic domains in microphase separated polymers that display a range of thermomechanical properties. Furthermore, by synthesizing two series of ionene copolymers with either PEG or PTMO spacers at various ratios with 1,12-

dibromododecane will yield a range of ion contents (hard contents) and will impact nanoparticle dispersion. More specifically, the nanoparticle dispersion within the polymer-rich polymer matrix composites could be assembled simultaneously into three scales by control the crystallization of polymers: well-dispersed, engulfed by the crystallization polymer; assembled into sheets between lamellar blocks of polymer crystallite; or, aggregate into nanoparticles clusters.

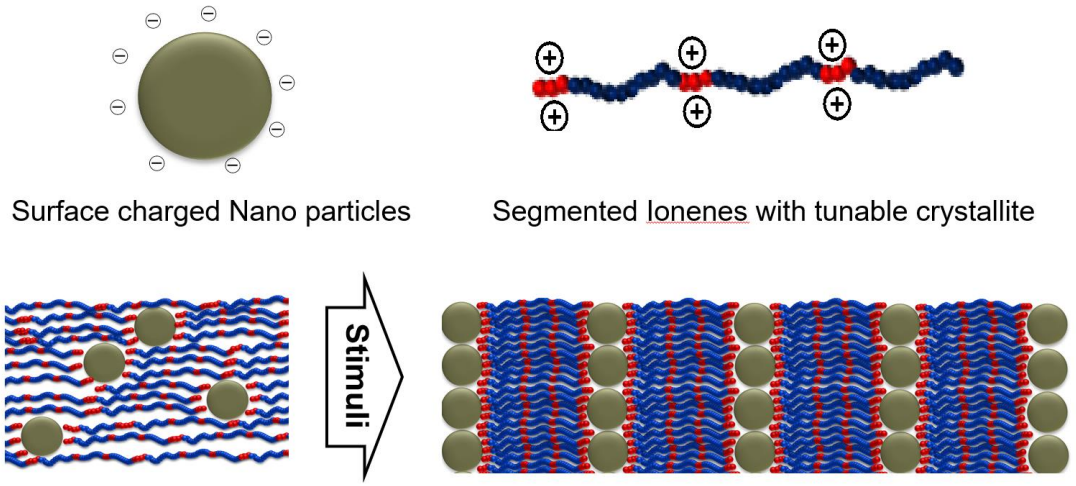

6.2 Introduction

Stimuli (Strain) induced crystallization is a phenomenon in which an initially amorphous solid material undergoes a phase transformation due to the application of strain. Strain crystallization occurs in natural rubber, as well as other elastomers and polymers.

Polymers at elevated temperatures, above the melting temperature, are modeled as viscoelastic liquids. On cooling, depending on the molecular structure and the cooling rate, the solid that is formed can be either amorphous or semi-crystalline. Polymers with regular structures form semi-crystalline solids while those with irregular structures are

unable to crystallize because the chains are too irregular to permit regular packing. The crystallization rate for polymers that do crystallize is usually observed to be zero at the melting temperature and at the glass transition temperature with a maximum at a temperature in between these two temperatures. The glass transition temperature is the temperature below which the polymer molecules lose their mobility and are ``frozen'' or vitri®ed. Polymers such as polyethylene in solid form are always semi-crystalline as their crystallization rates at temperatures below the melting point is very high, and it is not possible to cool the polymer rapidly enough to a temperature below the glass transition temperature without substantial crystallization taking place. For polymers such as polyethylene terephthalate (PET) which crystallize slowly, the melt has to be cooled slowly for substantial crystallization to take place. If these polymers are quenched to a temperature below their glass transition temperature, they remain in an amorphous state. When amorphous PET is subsequently deformed at temperatures just above the glass transition temperature, crystallization induced by the deformation takes place.[1]

Natural rubber (NR), cis-1,4-polyisoprene, is a widely used material in elastomeric parts because it combines very large elastic strain with a high tensile strength and a remarkable crack growth resistance.[2]These outstanding properties are partly attributed to the strain-induced crystallization (SIC) phenomenon that occurs in NR. In particular, the induced crystallites are supposed to slow down, deviate, and even stop crack growth, either for static or cyclic loading conditions. This ability to crystallize under strain is often explained by the high regularity of 1 the macromolecular structure, i.e., its

percentage of chains being in cis-configuration, which is very close to 100% in NR. Synthetic isoprene rubber (IR) exhibits a lower crystallinity than NR because of the lower regularity of the macromolecular structure, even though it can contain more than 98% of chains in cis-configuration. Some authors also argue that the non-rubber components in NR (6 wt. % of proteins and lipids) play a major role in its excellent mechanical properties, because they enhance its capacity to crystallize.[3]SIC was discovered in 1925 by Katz,[4] who was the first to show the x-ray diffraction pattern of a uniaxially stretched NR.

Poly(ethylene terephthalate) (PET) is one of the most commercially important polyesters. For polymers such as polyethylene terephthalate (PET) which crystallize slowly, the melt has to be cooled slowly for substantial crystallization to take place. If these polymers are quenched to a temperature below their glass transition temperature, they remain in an amorphous state. When amorphous PET is subsequently deformed at temperatures just above the glass transition temperature, crystallization induced by the deformation takes place. Most PET articles are manufactured by deforming at these temperatures as the amount and orientation of the crystalline phase (and hence the mechanical properties of the ®nal solid) can be controlled by imparting the right amount of deformation.[1] A two-dimensional analytical method was used to deconvolute the diffraction pattern into isotropic and anisotropic contributions. The isotropic and anisotropic fractions remained almost constant after stretching was stopped and during crystallization, suggesting that the strain-induced crystallization occurs mainly in the mesophase, supporting the hypothesis that the intermediate mesophase acts as a

precursor for crystallization in oriented PET.[5]

Poly(trimethylene terephthalate) (PTT) is an oddnumbered aromatic polyester. Compared to the two familiar "even-numbered" poly(ethylene terephthalate) (PET) and poly(butylene terephthalate) (PBT) with two and four methylene units, respectively, there are very few studies on PTT because the polymer was not readily available until recently.1 PTT has some unusual mechanical properties. Ward et al.[6] were among the first to systematically study PTT fiber properties and deformation. They found PTT to have very good tensile elastic recovery. It was ranked in the unexpected descending order of PTT > PBT > PET. In a follow-up study, PTT fiber was deformed in situ in a wide-angle X-ray diffractometer, and changes in the fiber period d-spacing along the c-axis were measured as a function of strain. [7]

In-situ synchrotron small-angle X-ray scattering (SAXS) was used to follow orientationinduced crystallization of isotactic polypropylene (i-PP) in the subcooled melt at 140 °C after step shear under isothermal conditions. The melt was subjected to a shear strain of 1428% at three different shear rates (10, 57, and 102 s-1) using a modified Linkam shear stage. The SAXS patterns showed strong meridional reflections due to the rapid development of oriented polymer crystallites within the melt. On the basis of the SAXS data, a schematic representation of nucleation and growth in orientation-induced crystallization of i-PP is proposed. During flow, orientation causes alignment of chain segments of polymer molecules and results in the formation of primary nuclei in the flow direction. These nuclei facilitate the growth of oriented crystal lamellae that align perpendicular to the flow direction.[8]

Poly(lactic acid) or polylactide (PLA) is a kind of biosourced polymer with promising capabilities for structural applications in substitution of oil-based plastics. However, as most of the presently known biopolymers, PLA cannot actually challenge the so-called commodity plastics in the domain of mechanical performances, noticeably regarding strength and resilience.[9]

Kohjiya et al. reported the first segmented ionene based on PTMO in 1981. The tensile behavior of the PTMO ionenes was consistent with typical microphase separated elastomers. Ionenes with amorphous PTMO segments demonstrated elastomeric properties due to the formation of ionic domains that served as physical cross-links. Conversely, semi-crystalline ionenes displayed a higher modulus and yield point with increased toughness relative to the amorphous ionenes. At 300% elongation, all the polymers exhibited some extent of stress-induced crystallization. Interestingly, the polymers possessed what is known as shape-memory properties. In other words, after stretching the ionene polymer film using a tensile test apparatus, the polymer possessed some form of permanent set. However, the film returned to its original state upon application of heat. With respect to mechanical performance, while it is known that stress–strain behavior is predominantly influenced by the soft segment structure, this study also confirmed that the choice of anion can influence mechanical performance. The investigators noted that when the anion was bromide, tensile strengths were higher in comparison to ionenes with chloride anions[10]. This was consistent with the work of Ikeda et al.[11] It is also important to note that ionene polymers are very hygroscopic in nature due to their ionic domains. This is critical for mechanical testing because the

presence of water weakens ionic domain interactions. In other words, if ionic clusters are disrupted, lower tensile strengths will result. DMA results demonstrated that the PTMO ionenes did not behave like polyurethane elastomers, since the rubbery plateau was very flat. This is similar to the DMA results obtained by Ikeda et al[11]. Under ambient conditions, the linear PTMO ionenes possessed excellent mechanical properties similar to thermoplastic polyurethanes (35 MPa tensile strength and elongations >1000%), while the highly branched ionenes possessed lower tensile strengths and elongations. This data suggested that the presence of branching disrupted ionic aggregate formation, which was consistent with the work of Loveday et al. who asserted that ionic groups placed regularly along the backbone in a linear fashion were important for favorable mechanical performance[12].

It is well-known that varying nanoparticle (NP) dispersion in polymer, metal, or ceramic matrices can dramatically improve material properties.[13] While uniform NP spatial distribution is usually the focus,[14] many situations benefit from spatially nonuniform, anisotropic NP organization. Nature teaches us that hierarchical NP ordering, as achieved in the case of nacre (a hybrid composed of 95% inorganic aragonite and 5% crystalline polymer, e.g., chitin), strongly improves mechanical properties relative to the building blocks. Specifically, a nanoscale ∼10 nm thick crystalline biopolymer layer mediates parallel layers of aragonite, forming “bricks”, which subsequently assemble into “brick-and-mortar” superstructures at the micrometer scale and larger.[15]

By leveraging the hierarchical structure of the lamellar semicrystalline polymer

morphology, more specifically, by tuning the crystal growing rate, the NPs were partitioning into the three zones: NPs that are engulfed by the crystallization front and remain spatially well-dispersed; (ii) NPs assembled into sheets at the 10−100 nm scale, and (iii) NP aggregates at the 1−10 μm scale.

Using phase changing ionene-based nanocomposites could be extended to create reversible mechanically, electrically, optically, and/or thermally responsive materials depending on constituent nanoparticles and polymers. This talk will discuss recent efforts to utilize the synthetic versatility of ionenes (e.g., spacer composition of PTMO or PEG) to prepare percolated ionic domains in microphase separated polymers that display a range of thermomechanical properties. Furthermore, by synthesizing two series of ionene copolymers with either PEG or PTMO spacers at various ratios with 1,12-dibromododecane will yield a range of ion contents (hard contents) and will impact nanoparticle dispersion.

The general idea of synthesis ionene based elastomer is placing roughly 75 weight percent soft segment and together with around 25 hard segment with higher glass transition temperature within the system. Previously, within the PEG or PTMO system, the polymers with elastomer properties are not achieved until the soft segment weight ratio reached around 50 weight percent level. This could because of the hard segment 1,12-Dibromododecane within the system did not provide advisable glass transition temperature for the system. Moreover, the 1,12-Dibromododecane segment is not providing other types of interchain force except for the ionic interaction. Recently, Prof. Bara and co-workers reported imidazole based self-healing ionene elastomers with

decent mechanical properties.[16] Within the imidazole based ionene system, the functional elements incorporated into these ionene-polyamides contribute to the organization of the polymer chains and the overall structuring of the material. The ionic interactions, π-π stacking interaction between different chains and H-bonding draw the polymer chains close together, creating figurative 'pinch points' between the chains which can be considered as a non-covalently crosslinked network. The interactions result in dense but flexible materialswith tightly packed or intertwined chains. The synthesis of the imidazole based ionene was listed in scheme 6.1.

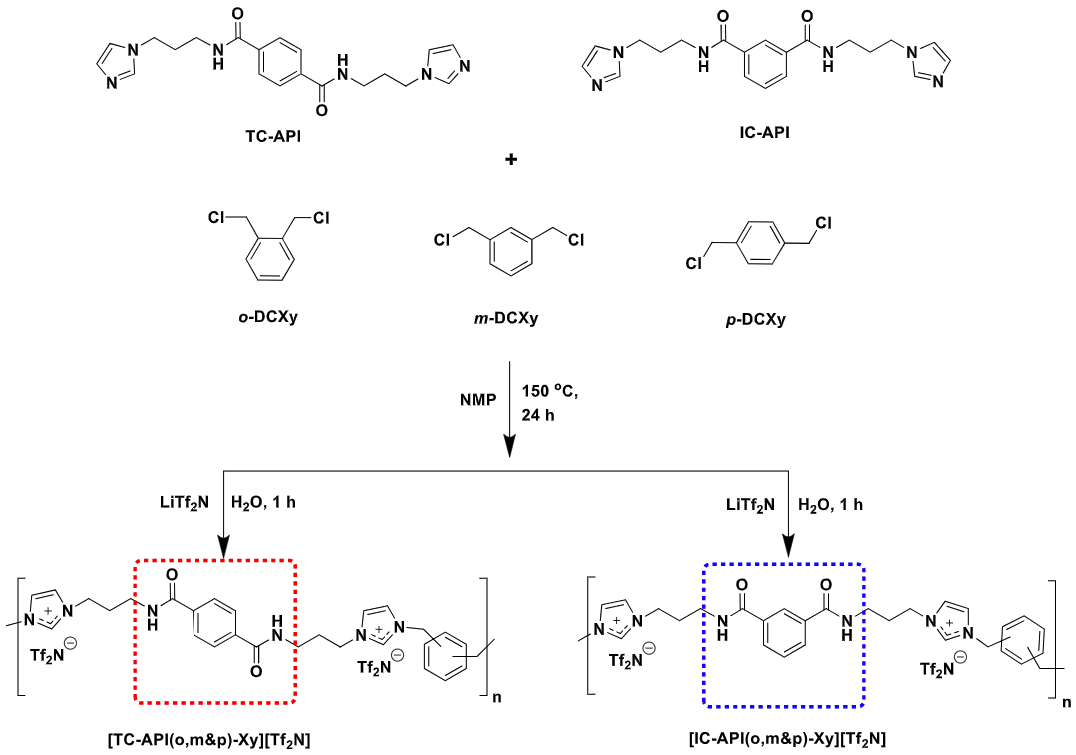

Scheme 6.1. Synthesis of six ionene-polyamides system.

Thus, within the PEG and/or PTMO system, to achieve the elastomer properties with roughly 75 weight percent soft segment, potential options should be available: introducing a hard segment with higher glass trasition temperature or higher interchain

interaction like π-π stacking interaction between different chains and/or H-bonding should be perfect fitting in the system. In this cases, α,α′-Dibromo-p-xylene and bis(4-(bromomethyl)phenyl)methane could be good potential hard segment candidate based on their potentially higher glass transition temperature and π-π stacking interaction between different chains from the aromatic rings within the main chain of the polymer. The synthesis of ionene with α,α′-Dibromo-p-xylene and bis(4-(bromomethyl)phenyl)methane as hard segment within the system were listed below in scheme 6.2. and scheme 6.3.

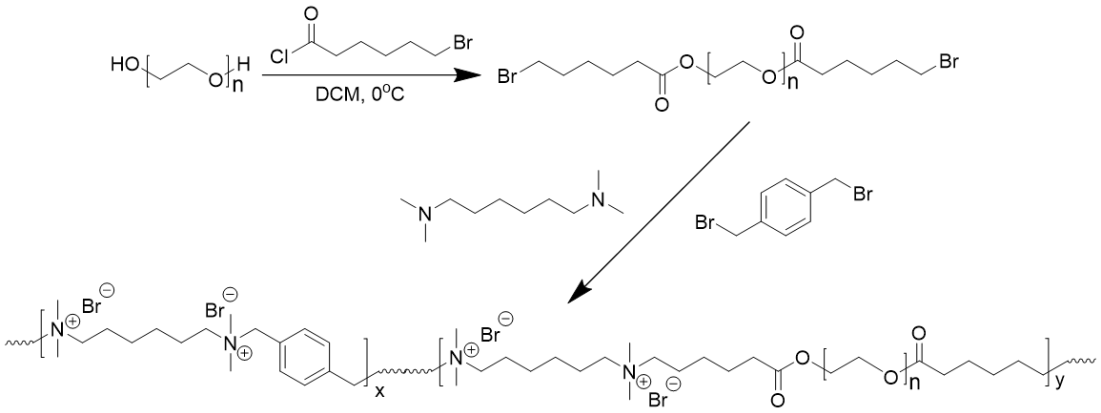

Scheme 6.2. Synthesis of PEG-based ionene with α,α′-Dibromo-p-xylene as the hard segment.

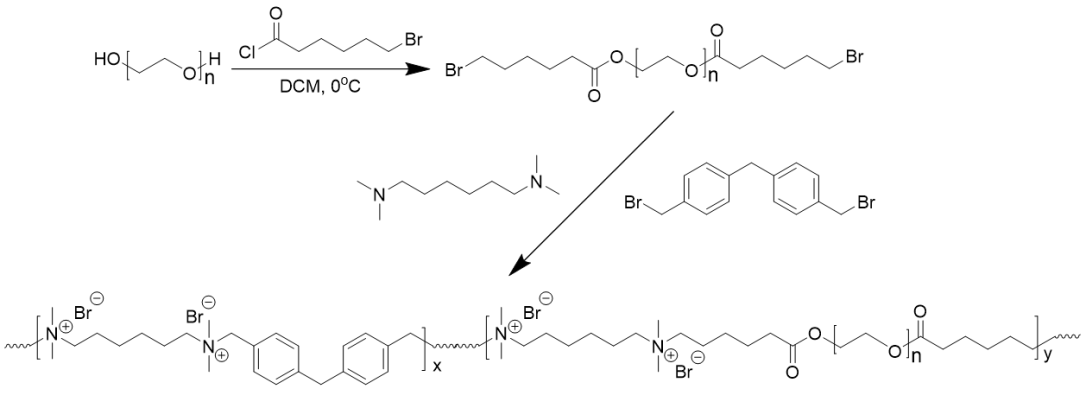

Reference

1. Rao, I. J.; Rajagopal, K. R., A study of strain-induced crystallization of polymers. *International Journal of Solids and Structures* **2001,** *38* (6-7), 1149-1167.

2. Lake, G. J., FATIGUE AND FRACTURE OF ELASTOMERS. *Rubber Chemistry and Technology* **1995,** *68* (3), 435-460.

3. Tanaka, Y.; Tarachiwin, L., RECENT ADVANCES IN STRUCTURAL CHARACTERIZATION OF NATURAL RUBBER. *Rubber Chemistry and Technology* **2009,** *82* (3), 283-314.

4. Katz, J. R., Rontgen spectographic testings on expanded rubber and its possible relevance for the problem of the extension characteristics of this substance. *Naturwissenschaften* **1925,** *13*, 410-416.

5. Ran, S. F.; Wang, Z. G.; Burger, C.; Chu, B.; Hsiao, B. S., Mesophase as the precursor for strain-induced crystallization in amorphous poly(ethylene terephthalate) film. *Macromolecules* **2002,** *35* (27), 10102-10107.

6. Ward, I. M.; Wilding, M. A.; Brody, H., MECHANICAL-PROPERTIES AND STRUCTURE OF POLY(META-METHYLENE TEREPHTHALATE) FIBERS. *Journal of Polymer Science Part B-Polymer Physics* **1976,** *14* (2), 263-274.

7. Jakeways, R.; Ward, I. M.; Wilding, M. A.; Hall, I. H.; Desborough, I. J.; Pass, M. G., CRYSTAL DEFORMATION IN AROMATIC POLYESTERS. *Journal of Polymer Science Part B-Polymer Physics* **1975,** *13* (4), 799-813.

8. Somani, R. H.; Hsiao, B. S.; Nogales, A.; Srinivas, S.; Tsou, A. H.; Sics, I.; Balta-Calleja, F. J.; Ezquerra, T. A., Structure development during shear flow-induced crystallization of i-PP: In-situ small-angle X-ray scattering study. *Macromolecules* **2000,** *33* (25), 9385-9394.

9. Hu, C. L.; Lv, T. X.; Li, J. Q.; Huang, S. Y.; Li, H. F.; Chen, J. Z.; Yu, D. H.; Christiansen, J. D.; Jiang, S. C.; An, L. J., Conformational Energy Settled Crystallization Behaviors of Poly(L-lactic acid). *Acs Applied Polymer Materials* **2019,** *1* (9), 2552-2560.

10. Anastasio, R.; Cardinaels, R.; Peters, G. W. M.; van Breemen, L. C. A., Structure-mechanical property relationships in acrylate networks. *Journal of Applied Polymer Science*.

11. Ikeda, Y.; Yamato, J.; Murakami, T.; Kajiwara, K., Aliphatic poly(oxytetramethylene) ionenes: effect of counter-anion on the properties and

morphology. *Polymer* **2004,** *45* (25), 8367-8375.

12. Avram, E.; Butuc, E.; Luca, C.; Druta, I., Polymers with pendant functional group .3. Polysulfones containing viologen group. *Journal of Macromolecular Science-Pure and Applied Chemistry* **1997,** *A34* (9), 1701-1714.

13. Tao, J. H.; Pan, H. H.; Zeng, Y. W.; Xu, X. R.; Tang, R. K., Roles of amorphous calcium phosphate and biological additives in the assembly of hydroxyapatite nanoparticles. *Journal of Physical Chemistry B* **2007,** *111* (47), 13410-13418.

14. Chen, L. Y.; Xu, J. Q.; Choi, H.; Pozuelo, M.; Ma, X. L.; Bhowmick, S.; Yang, J. M.; Mathaudhu, S.; Li, X. C., Processing and properties of magnesium containing a dense uniform dispersion of nanoparticles. *Nature* **2015,** *528* (7583), 539-+.

15. Kakisawa, H.; Sumitomo, T., The toughening mechanism of nacre and structural materials inspired by nacre. *Science and Technology of Advanced Materials* **2011,** *12* (6).

16. Kammakakam, I.; O'Harra, K. E.; Dennis, G. P.; Jackson, E. M.; Bara, J. E., Self-healing imidazolium-based ionene-polyamide membranes: an experimental study on physical and gas transport properties. *Polymer International* **2019,** *68* (6), 1123-1129.

17. Tamami, M.; Williams, S. R.; Park, J. K.; Moore, R. B.; Long, T. E., Poly(Propylene Glycol)-Based Ammonium Ionenes as Segmented Ion-Containing Block Copolymers. *J Polym Sci Pol Chem* **2010,** *48* (19), 4159-4167.